JOHANNES GUTENBERG UNIVERSITÄT MAINZ

JG|U

Max-Planck-Institut für Polymerforschung

Max Planck Institute for Polymer Research

Energy Transfer in Nanoplatelets – Dye Composites

Master Thesis

David Trieb
Born in Worms

Carried out at the Max Planck Institute for Polymer Research

Submitted to the Department of Chemistry
Johannes Gutenberg-University, Mainz

17. February 2020

Reviewer:

Prof. Dr. Katharina Landfester

Prof. Dr. Thomas Basché

Supervisor:

Dr. Andreas Riedinger

Table of content

Abstract

Organic photocatalysts have become a popular option for catalysis, since they are highly versatile by design and enable us to catalyse reactions using light. However, pure organic catalysts have a glaring disadvantage compared to their metal containing counterparts in their low absorption cross sections. To mitigate this problem, CdSe nanoplatelets (NPLs), a semiconductor nanocrystal with huge absorption cross sections, can be used in a Förster resonant energy transfer (FRET) system where the NPLs act as donor and the photocatalyst dye as acceptor.

The key advantage of using NPLs is that their absorption cross section can be increased by increasing their lateral size. This means that the photocatalyst system could harvest the excitation energy extremely well when using large NPLs. However, recent research shows that the size of an exciton on the surface of the NPLs is very small, around 1.5 nm. Because FRET strongly depends on the distance between donor and acceptor, larger NPLs should lead to a larger average distance between the exciton and the dyes effectively resulting in a loss of FRET efficiency when using large NPLs. The aim of this work is to prove which effect has the most influence towards the energy transfer.

For an optimal spectral overlap between the dye and the NPLs, three monolayer (ML) thick NPLs were used. Because in literature there are no synthesis routes for differently sized three ML NPLs, a new two-step synthesis method was developed. In the first step, laterally small three ML NPLs with a high quantum yield (QY) and narrow size distribution were synthesised. The resulting NPLs were used as seeds for a lateral size extension. The lateral size extension was realised by the addition of cadmium precursor and a less reactive selenium precursor relative to the one used for the seed synthesis. This prevents further nucleation during the size extension. By modifying the amount of precursors added, different lateral sized three ML NPLs were obtained. Using this approach, three different batches of differently lateral sized three ML NPLs were synthesised for the FRET experiments.

The energy transfer experiments confirmed that binding of the dye to the surface of the NPLs leads to an increased photoluminescence of the dye. In addition, the differently sized NPLs lead to different energy transfer rates. In the case where there is a constant amount of dyes per NPL, the energy transfer efficiency is the highest for the small NPLs. This is reasonable, because for small NPLs the average distance between dye and exciton is smaller than for large NPLs. This proves that the distance between exciton and dye is crucial for the energy transfer and is less influenced by the number of absorbed photons. Interestingly, maximum coverage of the NPLs (0.6 dye per nm^2) did not lead to the highest luminescence from the dye. The maximum photoluminescence occurs instead at surface coverage of 0.2 dye per nm^2. At higher coverage the signal appears to decrease likely due to self-quenching between the dyes as a result of energy transfer.

German Summary / Deutsche Zusammenfassung

In der heutigen Zeit spielt das Sparen von Energie eine entscheidende Rolle. Um bei chemischen Reaktionen Energie zu sparen, können Katalysatoren eingesetzt werden. Vor allem organische Photokatalysatoren sind daher Gegenstand aktueller Forschung. Ein häufiger Nachteil aktueller Photokalalysatoren ist allerdings, dass sie einen geringen Absorptionsquerschnitt aufweisen und somit vergleichsweise viel Licht und damit Energie aufgewendet werden muss, um diese Photokatalysatoren zu aktivieren. Daher sollen CdSe-Nanoplättchen (NPLs) mit einem großen Absorptionsquerschnitt eingesetzt werden, um durch einen Energietransfer die von den NPLs absorbierten Photonen zu den Photokatalysatoren zu übertragen und so die Effizienz der Photokatalysatoren zu steigern.

NPLs zeichnen sich unter anderem dadurch aus, dass der Größenquantisierungseffekt nur in einer Dimension - der Dicke - auftritt, welche auf atomarer Skala konstant gehalten werden kann. Allerdings variiert die laterale Größe der NPLs. Mit zunehmender lateraler Größe der NPLs vergrößert sich auch der Absorptionsquerschnitt der NPLs. Dies sollte zu einer Zunahme der Effizienz des Energietransfers führen. Auf der anderen Seite ist die Ausdehnung eines Exzitons mit einem Radius von nur 1,5 nm klein im Vergleich zu der Oberfläche der NPLs. Da die Rate des Energietransfers invers mit der sechsten Potenz des Abstands zwischen NPLs und Photokatalysator verknüpft ist, sollte bei großen NPLs der mittlere Abstand zwischen Exziton und Photokatalysator größer sein und daher die Effizienz des Energietransfers abnehmen. Die Prüfung, welcher der beiden Faktoren entscheidend für den Energietransfer ist, ist Ziel dieser Arbeit.

Um den spektralen Überlapp für den Energietransfer zu maximieren, wurden drei Monolagen (ML) dicke NPLs verwendet. Da in der Literatur für diese NPLs keine Synthesevorschrift existiert, musste eine neue Synthesevorschrift entwickelt werden. Hierzu wurden zuerst drei ML NPLs nach einer bekannten Vorschrift mit einer hohen Quantenausbeute (50%) und einer Kantenlänge von durchschnittlich 12 nm hergestellt. Diese NPLs wiesen eine geringe Größenverteilung auf. Die so hergestellten NPLs wurden in einem zweiten Schritt vergrößert. Zu diesem Zweck wurden zu den NPLs Cadmiumedukte gegeben. Diese Mischung wurde auf 190°C erhitzt und ein Selenedukt mithilfe einer Spritzenpumpe zugetropft. Dies sollte auf der einen Seite dafür sorgen, dass die Nukleation von neuen Partikeln wegen der immer gering gehaltenen Konzentration an Vorläufern nicht stattfindet, und auf der anderen Seite eine bessere Kontrolle über die Größenzunahme der NPLs bewirken. Auf diese Weise standen drei Chargen verschieden großer NPLs zur Verfügung, die für die anschließenden Energietransferexperimente genutzt werden konnten.

Zur Durchführung der Experimente zum Energietransfer zwischen NPLs und Photokatalysator wurden zu den NPLs verschiedene Mengen an Photokatalysator gegeben. Es zeigte sich, dass bei steigender Konzentration des Photokatalysators die Photolumineszenz der NPLs abnimmt. Dabei hängt die Abnahme auch von der Größe der NPLs ab. Ferner wurde festgestellt, dass bei einer konstanten Oberflächenbesetzung der NPLs mit Photokatalysator der Abfall der Photolumineszenz für alle NPLs ähnlich steil ist, während bei einer konstanten Anzahl an NPLs in der Probe der Abfall der Photolumineszenz für die kleinen NPLs am steilsten ist. Daraus kann gefolgert werden, dass bei einer konstanten Oberflächenbesetzung der NPLs die Energietransferrate für alle verschieden großen NPLs ähnlich ist, während bei einer konstanten Anzahl an NPLs in der Probe die Energietransferrate für die kleinsten NPLs am größten ist.

Daneben konnte auch ein Anstieg der Photolumineszenz des Photokatalysators bei steigender Konzentration des Photokatalysators beobachtet werden. Allerdings trat ab einem Oberflächenbesetzung von 0,2 Farbstoffen pro nm^2 Oberfläche der NPLs trotz weiterer Erhöhung der

Photokatalysator-Konzentration eine Abnahme der Photolumineszenz des Photokatalysators auf, welche auf eine Selbstlöschung des Photokatalysators zurückzuführen ist. Auch hier konnte eine Abhängigkeit mit den Größen der NPLs gefunden werden. Bei kleinen NPLs ist die Anzahl der Moleküle des Photokatalysators pro nm^2 Oberfläche der NPLs am größten, bevor die Löschung auftritt. Dies ist vermutlich darin begründet, dass bei kleinen NPLs die Fläche an den Seiten der NPLs verhältnismäßig größer ist als bei großen NPLs und sich somit auch verhältnismäßig mehr Photokatalysatoren an den Seiten der NPLs befinden können, was die Selbstlöschung der Photokatalysatoren erschwert.

Bei Betrachtung der Energietransfereffizienzen kann erneut beobachtet werden, dass bei einer konstanten Oberflächenbesetzung der unterschiedlich NPLs die Steigung der Energietransferrate bei steigender Besetzung der Oberfläche für alle drei NPL-Chargen in etwa konstant ist. Im Unterschied dazu ist bei einer konstanten Menge an Photokatalysator-Molekülen pro NPL deutlich erkennbar, dass die Steigung für die kleinsten NPLs am steilsten ist. Daher kann gefolgert werden, dass für die Energietransfereffizienz der Abstand zwischen Exziton und Photokatalysator ausschlaggebend ist. Da bei kleinen NPLs dieser Abstand im Mittel am geringsten ist, ist bei diesen die Transferrate am größten.

Zusammenfassend kann festgestellt werden, dass es in dieser Arbeit gelungen ist, eine neue Methode zur gezielten Synthese unterschiedlich großer drei Monolagen dicker CdSe NPLs zu entwickeln. Neben der unterschiedlichen Größe zeichnen sich diese NPLs auch durch eine geringe Größenverteilung und durch wohldefinierte optische Eigenschaften aus. Im Bereich des Energietransfers konnte gezeigt werden, dass für die Energietransferrate in NPLs der Abstand zwischen Photokatalysator und NPL maßgeblich verantwortlich ist. Dabei gilt, dass bei kleinen NPLs dieser Abstand im Mittel geringer ist und daher auch die Energietransferrate höher ist. Aufbauend auf dieser Arbeit sollte die verbesserte Effizienz des Photokatalysators bei der Durchführung chemischer Reaktionen untersucht werden. Daneben kann auch durch weitere Verbesserungen der NPL-Synthese eine Steigerung der Effizienz des Photokatalysators angestrebt werden.

1. Introduction

Energy efficiency plays an important role in chemical processes. To save energy, catalysts can be used to lower the activation energy of a chemical reaction. In particular, photocatalysts are interesting because they can incorporate energy supplied by light. The advantage of using light is that it is an abundant energy source and can often supply energy much more efficiently compared to heating. In addition, the energy can be supplied selectively by using excitation wavelengths tailored to the photocatalyst.

A photocatalyst can be judged by how well it uses the light energy to facilitate a chemical reaction[1]. Organic photocatalysts are highly flexible in terms of design, as their properties can be changed by modifying their chemical composition and structures. However, typical organic photocatalysts absorb only in a certain range of wavelengths and they also absorb relatively weakly compared to metal containing counterparts[2]. To improve the absorption of organic photocatalysts, materials with high absorption cross sections can be used to absorb the light and then transduce the energy to the photocatalyst via energy transfer.

One material with particularly large absorption cross section are CdSe nanoplatelets (NPLs)[3]. These NPLs exhibit absorption cross sections up to $10^{-13}\ \mathrm{cm}^2$ [4], larger than materials like quantum dots (QDs) (cross section $10^{-14}\ \mathrm{cm}^2$ [5]) and organic dyes (cross section $10^{-16}\ \mathrm{cm}^2$ [2]).

To be able to design optimised photocatalysts using hybrid semiconductor nanocrystal-dye systems, their energy transfer behaviour has to be studied. For QDs, their energy transfer to organic dyes is well known[6] [7] [8]. For example, Ren et al. showed the energy transfer between dyes and QDs by binding the dye with carboxylic anchors to the surface of the QDs. Their study showed a way to tune the spectral range of such QDs-dye-conjugates and optimised their energy transfer[6]. For CdSe-NPLs, Diroll et al. showed that for four monolayer (ML) thick NPLs and methylviologen dichloride, the electron transfer efficiencies depend on the lateral size of the NPLs[9].

In this work, the goal is to show the influence of the lateral size of NPLs to the Förster resonance energy transfer efficiency, as this is relevant to optimise the NPL-photocatalyst conjugates. According to the Förster theory, the energy transfer rate scales inversely to the power of six with the distance[10] between donor (NPLs) and acceptor (photocatalyst). Hence it is highly advantageous to bind the photocatalyst to the surface of the NPLs. Beside this, to optimise the energy transfer from NPLs to dye, the properties of the NPLs and how they relate to the energy transfer need to be studied. In particular, increasing the size of the NPLs[11] will increase absorption cross section, which should make it easier to harvest light. However, the effect of the size to the energy transfer efficiency has not been studied yet.

The process of a chemical reaction requires breaking and forming chemical bonds. These bonds typically require high energies to break, in the range of blue to UV light. Hence typical photocatalysts rely on energies in that range. Here I conducted the study with the photocatalyst dye 5-(7-(thiophen-2-yl)benzo[c][1,2,5]thiadiazol-4-yl)thiophene-2-carboxylic acid (Th-BT-Th-COOH), provided by the Zhang group at MPIP[12]. This photocatalyst absorbs between 375 nm and 500 nm. Therefore, to conduct this study, I needed to synthesise three ML NPLs (emission wavelength 462 nm) with different lateral sizes. In theory using larger NPLs should lead to a higher absorption cross section[4], so the number of absorbed photons will increase and lead to a higher energy transfer efficiency. But if the NPLs are large, the distance between the exciton located in the NPLs and the photocatalyst becomes larger, which could lead to a decrease in energy transfer efficiency. This is related to the nature of the exciton, which only reaches a lateral expansion of 1 to 1.5 nm[13]. The aim of the work was to test which effect has a larger impact to the energy transfer efficiency.

To enable this study different challenges had to be solved. Firstly, three ML NPLs of different sizes had to be prepared. These NPLs not only had to be highly luminescent, they also had to have a narrow lateral size distribution to make this study meaningful. High quantum yield (QY) will allow the photoluminescent signals from the energy transfer to be more easily detected, while low size distribution makes it easier to investigate the influence of the NPL size to the energy transfer. Existing methods to synthesise three ML NPLs yield either laterally small NPLs with high QYs or large NPLs with very low QYs. Therefore, a new synthesis protocol had to be developed.

For the energy transfer experiments a system of the photocatalyst dye Th-BT-Th-COOH and the NPLs are investigated. To clearly understand how these dyes interact with the NPLs, the nature of the binding must be understood, i.e. we need to know their binding affinity. Also, different concentrations of the dye and NPLs must be tested to obtain systematic results regarding the energy transfer efficiency.

Chapter two of this work contains the theory of the formation of NPLs and the Förster resonance energy transfer. The third chapter includes the materials and methods used in the experiments. This leads to chapter four, where the results of the experiments are discussed. In this section, I showed that that it is possible to produce three ML NPLs in different sizes with an unprecedented narrow size distribution and comparatively high quantum yield (50%). In a second part of chapter four, the energy transfer of these NPLs with the photocatalyst is discussed, to test the hypothesis established before. The results are summarized in chapter five.

2. Theoretical background

2.1. Principles of synthesis for nanocrystals

Introduction to nanocrystal synthesis

To obtain nanomaterials, two main approaches are available: the top-down and the bottom-up approach. While the top down method starts with bulk material crushed to nanoscale, the bottom up method starts from small precursor molecules, which form nuclei and then grow[14]. The NPLs we intent to study in conjunction with dyes are produced by the bottom up method.

The mechanism of the traditional bottom-up method for nanoparticles with narrow size distributions is described by the LaMer model[15], shown in Figure 1.

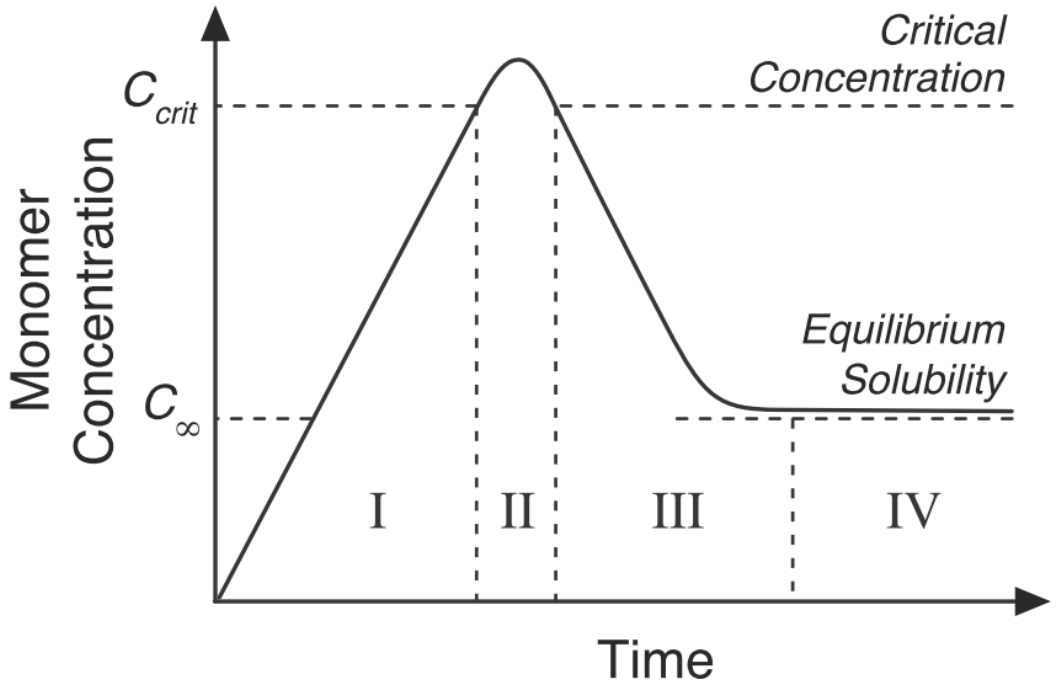

Figure 1: LaMer plot showing the different phases of synthesis of nanoparticles over time depending on the monomer concentration, adapted from [16].

The classical LaMer model describes the formation of nanocrystals with low size dispersion in three phases, which can be further grown by Ostwald ripening as fourth phase[16]. The four phases are described as follows:

- In phase I, the precursors react and form monomers. Thus, the monomer concentration is increased over time until a critical concentration C_{crit} is reached.
- Above this critical concentration, nucleation starts due to the aggregation of monomers, forming nuclei (phase II). The nucleation consumes monomers, thus lowering the monomer concentration over time. Nucleation stops when the concentration of monomers drops below the critical concentration. This marks the beginning of phase III.
- In phase III, the newly emerged particles are growing, as long as the concentration of the monomers stays above C_∞. This is feasible if the precursor reaction to monomers is slower than the nucleation rate so that in phase III there is still supply of free monomers.

- After some time, the precursor reservoir is depleted and no new monomers can be formed. Therefore, the monomers concentration reaches the solubility limit of the system (phase IV). In this phase the particles can grow further by Ostwald ripening. This means that the average size of particles increases by growth of larger particles by mass transfer of monomers from smaller, dissolving particles, until the small particles disappear. Since this usually increases the size distribution, nanocrystal syntheses are commonly stopped before the system enters phase IV.

The whole process is driven by the Gibbs free energy ΔG[17]. This energy is composed of two terms, the free surface energy of the nanoparticles ΔG_S and the volume energy of the material ΔG_V. The free surface energy depends on the surface energy γ and of the square radius r of the nanoparticles. The volume energy ΔG_V depends on the radius r of the nanoparticles to the power of three and on the bulk volume energy $\Delta G_{V,Bulk}$, which is shown in equation 1.

$$\Delta G_{V,Bulk} = \frac{-k_B T \ln(S)}{V} \tag{1}$$

In this equation k_B is the Boltzmann constant, T the temperature, S the supersaturation of the solution and V the molar volume. This leads to the following equation of the free energy for nanocrystals.

$$\Delta G = \Delta G_S + \Delta G_V = 4\pi r^2 \gamma + \frac{4}{3}\pi r^3 \Delta G_{V,Bulk} \tag{2}$$

This equation shows the components of the free energy for the synthesis of particles. A schematic plot of this free energy against the radius of the particles is shown in Figure 2.

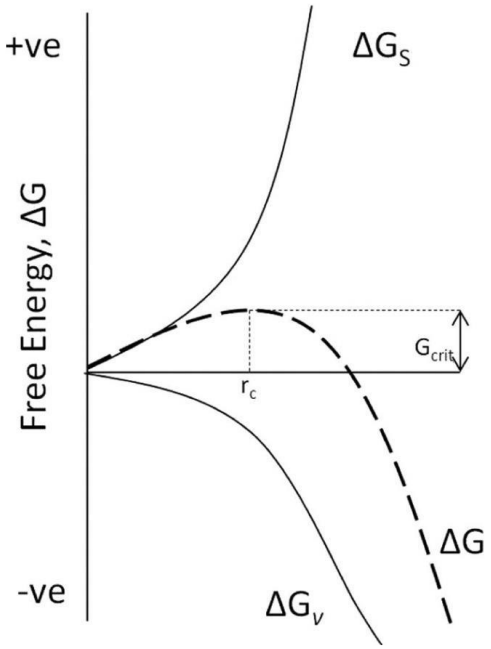

Figure 2: Behaviour of the free energy and their components with increasing the size of the nanoparticles, adapted from[18].

As shown in Figure 2, the surface energy ΔG_S is positive. On the other hand, the volume energy ΔG_V is negative. At the start of the synthesis, the surface energy has a stronger influence on the free energy than the volume energy. For this reason, the free energy goes up in the first part of the synthesis. Because the volume energy scales to the power of three to the radius, while the surface energy only scales with the square of the radius, the free energy reaches a maximum at a critical radius r_C and then goes down. For this reason, the nuclei have to overcome radius r_C to gain the thermodynamic driving force for growth. If the nuclei do not overcome this radius r_C, they will dissolve again. For this reason,

once the size of the nuclei becomes large enough, the growth of nanocrystals is energetically advantageous.

In practical applications, there are two ways of doing this bottom-up synthesis. One is to do the nucleation and the growth in one flask[19], while the other forms the nuclei first and then introduce them to a growth solution[20]. Both methods are used in this work. The first one is used for direct synthesis of NPLs, the second one for the size extension of existing NPLs.

Mechanism of the anisotropic growth

The LaMer model described in the previous section predicted that nanoparticles from a material with a cubic crystal structure grow in all three dimensions at the same speed. For this reason at the end of growth, a quasi-spherical shape (truncated cube) is expected to minimize the surface energy. However, the model did not predict the possibility of materials with an isotropic cubic crystal structure like zinc blende CdSe[21] to form anisotropic nanocrystals. To understand how NPLs can be formed at all, we have to look closer to the actual synthetic conditions where NPLs are formed.

The starting point of the anisotropic growth is a stochastic symmetry breaking event during nucleation according to the model described by Riedinger et al.[22]. In the model described by LaMer[15], diffusion is the limiting factor of the growth. However, in the synthesis of NPLs, $Cd(OAc)_2$ and $Cd(myr)_2$ are used. These two cadmium precursors react with each other to form an insoluble coordination polymer. This ensures that the solubility of cadmium is very low. For this reason, within the cadmium coordination polymer the local cadmium concentration is extremely high. Therefore, the growth within these coordination polymers is not diffusion limited but is instead limited by the reaction of monomers with the surfaces. As a result, the nucleation of new island on facets of the primary particles becomes the rate-limiting factor for the growth of NPL. On a symmetry-broken primary particle two places for the nucleation of a new island are possible (Figure 3A), one on the wide facet or one on the narrow facet.

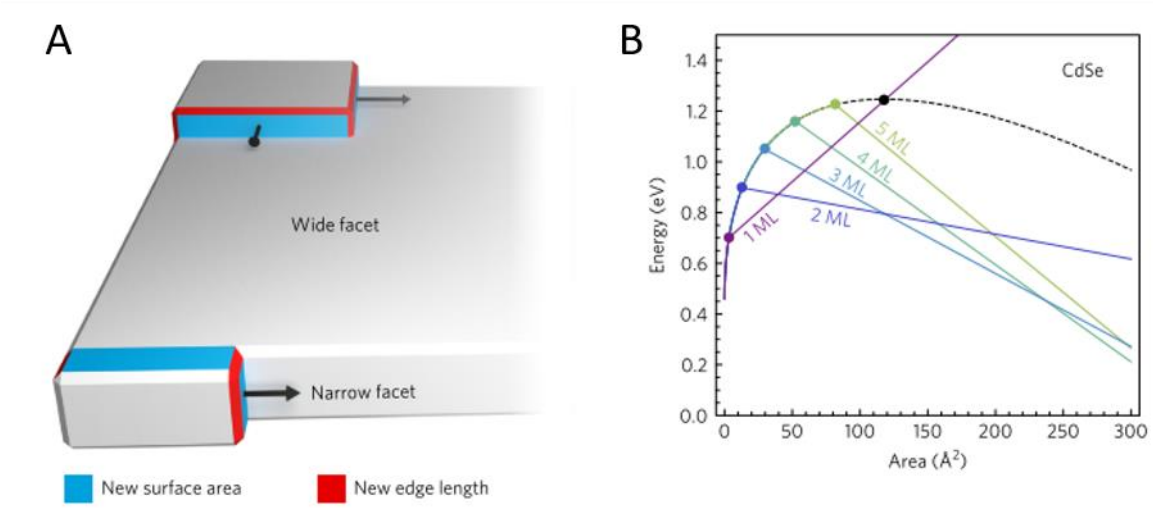

Figure 3: (A) Scheme showing the different options of creating new layers of NPL. (B) Nucleation barrier depending on the area for the different facets of a NPL. Dotted line for the wide facets, coloured lines for the narrow facets of the different ML of NPLs, adapted from[22].

For a new layer to form, first a new island has to nucleate on one of the facets. In analogy to the traditional nanocrystal synthesis, described in the previous section, these islands have to overcome a critical size. If this does not happen, the islands dissolve again. Only if the islands become larger than this critical size, a new layer can grow. If the critical size is larger than the size of a narrow facets the

nucleation barrier is lower than the one for wide facets. For this reason, small facets grow much faster, and a very thin NPL with an anisotropic shape can be obtained (see Figure 3A).

The energetics of this growth mode can be described as follows. Three terms of energy influence the energy of the whole island ΔE, namely the volume energy E_V, the surface energy E_A and the edge energy E_L. These terms of energy are depending on the change of the volume ΔV, the area ΔA and the edge length ΔL. Therefore, the island energy can be described as shown in equation 3.

$$\Delta E = \Delta V E_V + \Delta A E_A + \Delta L E_L \tag{3}$$

Similar to classical nucleation theory, the volume energy E_V is always positive, while the surface energy E_A and the edge energy E_L are always negative. The position of the island influences the energy level of the island. If the location is on the narrow facet that is smaller than the critical island size, it leads to a smaller ΔL. If the location is on the wide facet, ΔL is larger. Because ΔL scales with the negative edge energy E_L, the influence on the wide facet is larger. Therefore, nucleation and growth of new islands on the wide facets is disadvantageous for the system. This is also shown in Figure 3B. Here the dotted line represents the energy needed for the wide facets. It is obvious, that, at a certain area, less energy is required for the narrow facets (coloured dots in Figure 3B) than for the wide facets. The maximum represents the critical island size. If the primary particle has facets smaller than this size, the nucleation barrier is reduced and anisotropic NPLs can be synthesised even from isotropic materials like CdSe if the growth rate is surface-reaction limited rather than diffusion limited[22].

Figure 3B shows that the nucleation barrier for a new island on the differently sized facets differs, as shown with the different coloured point. To obtain only NPLs in one thickness, the reaction conditions, like the temperature and the reactivity of the precursors, have to be adjusted. If the conditions are selected correctly, only one thickness will form favourably resulting in a precise control of the product[22].

2.2. Properties of nanocrystals

Principles of quantum confinement for spherical nanocrystals

Nanoparticles behave differently to the corresponding bulk material, particularly regarding their electronic and optical properties. The reason for the different properties of nanocrystals is discussed in this section. Therefore, a scheme of the electronic states for different kinds of materials and a scheme of the particle in the box model are shown in Figure 4.

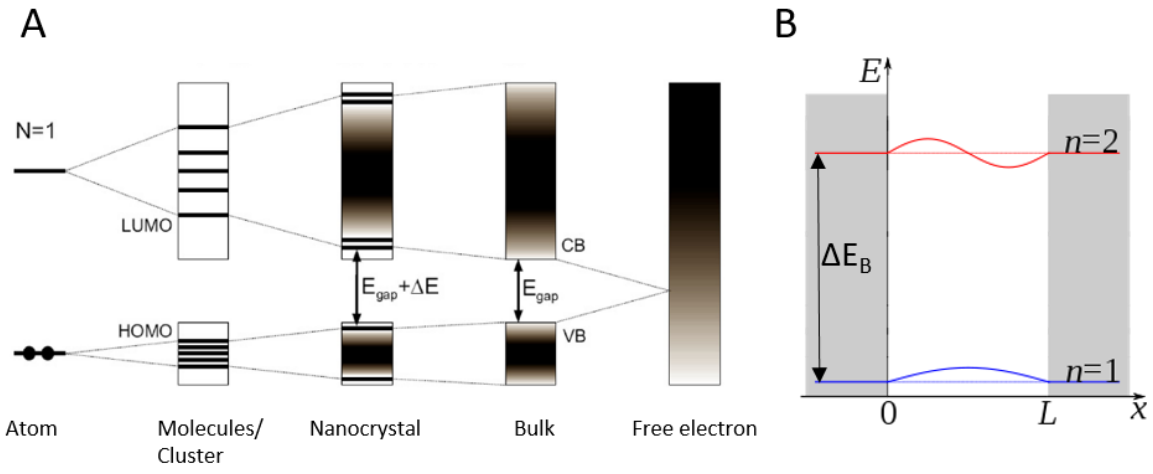

Figure 4: (A) Electronic states for different materials, adapted from[23] and adjusted. (B) Scheme of the particle in the box model, adapted from[24] and adjusted.

As shown in Figure 4 A, the gap between the highest occupied state and the lowest unoccupied state is different for the different materials with different numbers of atoms N. For one atom (N = 1) the absorption takes place between two well defined electronic states. For molecules or clusters with up to 100 atoms, the number of electronic states is much higher, but the distance between the highest occupied molecular orbital (HOMO) and the lowest unoccupied molecular orbital (LUMO) is still well defined. For bulk materials with a theoretically infinite number of atoms, the electronic states are not well defined as orbitals anymore. Due to interactions of the atoms with each other within the lattice of the bulk material, the number of energy levels increases. This results in many possible states. States with a nearly equal energy form one band. For semiconductor materials, the band occupied by electron with the highest energy is called valence band (VB) and the band at the lowest energy, which is unoccupied is called conduction band (CB)[25]. To excite the bulk material, the energy needed would have to be at least the energy equal to the gap energy E_{gap} between VB and CB.

From the electronic point of view, nanocrystals are between cluster and bulk material[21]. Their number of atoms is finite, but the number is so high (up to 10,000) that the orbitals can be summed up as bands. This works fine for the middle of the band, but at the edges of the band, the density of states is lower than in the bulk band. This means that the energy levels at the band edges are discrete. If the dimension(s) of the crystal is smaller than the Bohr radius, the energy levels of this discrete states depend on the size of the nanocrystals. The energy can be described by the particle in the box model, shown as scheme in Figure 4 B. For small particles, L is small. If L is small, the energy difference between the first and the second harmonic oscillation ΔE_B becomes large. If ΔE_B is large, the energy for the luminescence becomes large and the crystal will emit at shorter wavelengths. For larger nanocrystals, they will have a larger L and therefore a smaller ΔE_B[21].

Properties of anisotropic NPLs

Absorption and photoluminescence spectra for NPLs with different MLs are shown in Figure 5.

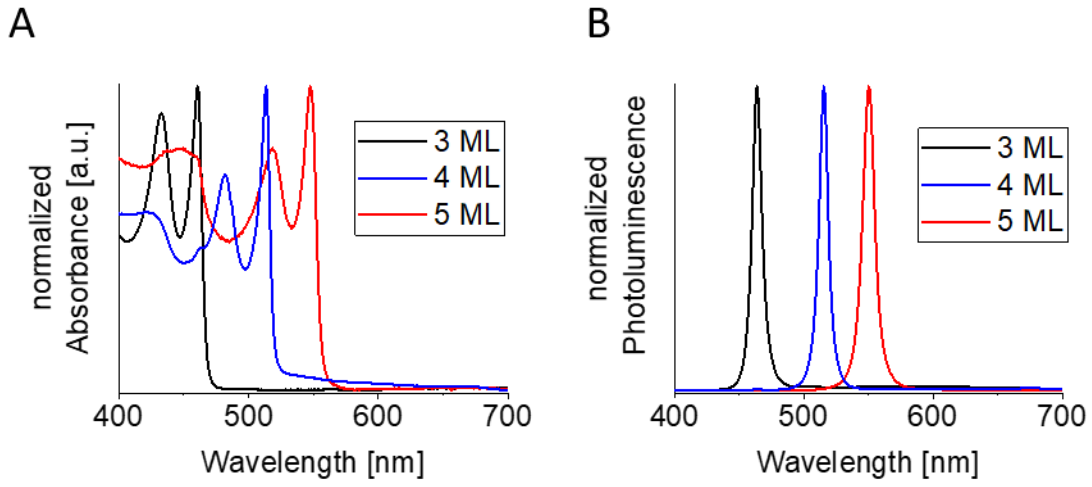

Figure 5: (A) Normalized absorption spectra for 3, 5 and 5 ML NPLs. (B) Normalized photoluminescence spectra for 3, 4 and 5 ML NPL. Data for both figures obtained from Henry Halim.

In the absorption spectra in Figure 5A, two maxima for each NPL ML can be seen. These maxima correspond to the light hole transition at shorter wavelengths and the heavy hole transition at longer wavelengths[26]. With increasing number of monolayers, a red shift in the absorption peaks is observable. This shift is also observable for the photoluminescence of the NPL, shown in Figure 5 B. The linewidth of the absorption bands and the photoluminescence is very sharp for all NPLs, with FWHM around 10 nm. These properties are a result of the electronic structure of the NPLs.

The wavelength of the NPLs photoluminescence only depends on the thickness. This is because the thickness of the NPLs is smaller than the Bohr radius of CdSe (5.4 nm)[27], while the lateral dimensions are larger. So NPLs only have a one-dimensional quantum confinement in contrast to QDs, where quantum confinement occurs in three dimensions.

Because the thickness of the NPL is atomically precise and responsible for the photoluminescence, the FWHM is very small. For normal QDs ensembles however, the FWHM is larger since each QD will emit slightly differently due to the size distribution of the QDs resulting from the colloidal synthesis (inhomogeneous broadening). For NPLs, the lateral size distribution is not relevant for the wavelength of the photoluminescence, if the lateral size is larger than the Bohr radius. Since the thickness of the NPLs can be adjusted in an atomically precise manner, the luminescence of the NPLs is homogeneous[28].

Another property of NPLs that is different to standard spherical nanoparticles is their stronger tendency to agglomerate or stack. Stacking means, that NPLs are strictly ordered. This results from the strong depletion attraction force between NPLs. This force for NPLs is higher as for QDs because of the shape of the NPLs. The depletion attraction force results from the excluded volume between nanoparticles. Resulting from the shape, this excluded volume is larger for flat particles compared to spherical particles. By increasing the excluded volume, the strength of the depletion attraction forces increases[29]. Thus stacking is more favoured, if the size distribution of the NPL is narrow and the NPLs are regular formed (square/rectangular)[30]. Taking this into account makes it possible to roughly judge the size distribution of the NPLs in the transmission electron microscope.

2.3. Theory of Förster resonance energy transfer

The theory of Förster resonance energy transfer (FRET) explains the non-radiative energy transfer from a donor to an acceptor. In this work, the donors are the NPLs and the acceptors are photocatalyst dyes.

The electronic principles of the energy transfer are shown in the Jablonski diagram in Figure 6.

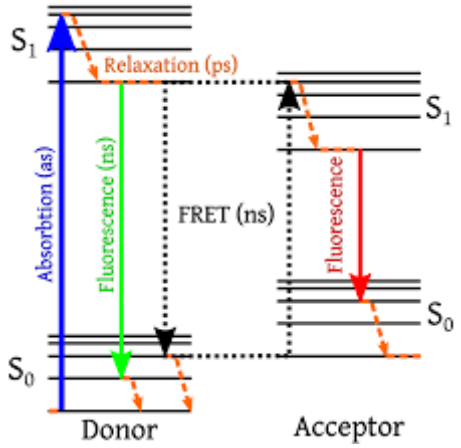

Figure 6: Jablonski diagram showing the electronic principles of Förster resonance energy transfer, adapted from[31].

This diagram shows the relevant electronic states of a donor and an acceptor. If the ground state S_0 of the donor is excited by light, an electron reaches an excited state S_1 of the donor (blue line in Figure 6). After the vibrational relaxation to the vibrational ground state of the S_1 state, there are two possibilities for the S_1 state of the donor to relax to the ground state S_0. This can happen by normal fluorescence (green line in Figure 6) or by energy transfer, if there is an acceptor. If the energy transfer occurs, the electron in the excited state S_1 of the donor relaxes without the emission of radiation to the ground state S_0. Simultaneously an electron in the acceptor gets into a vibrational state of the excited state S_1. The energy between the states of the energy transfer must be equal in order to ensure

energy conservation[32]. In the acceptor, the vibrational relaxation happens after the energy transfer. Afterwards the acceptor undergoes fluorescence (red line in Figure 6).

The interaction described in this way arises due to dipole-dipole interaction between donor and acceptor and requires different conditions: the orientation factor, the distance between donor and acceptor (Förster radius) and the spectral overlap. These conditions will be discussed in the following three sections.

Orientation factor

From quantum mechanics it is known that electronic states can only interact with each other if their transition dipoles are not orthogonal. Therefore, to do the energy transfer, the orientation of the transition dipoles of the donor and the acceptor must be evaluated, to see if they are orthogonal or not. To do this, the so-called orientation factor κ^2 is used. This factor contains the vector for the transition dipole of the donor $\hat{p}_D$ and of the acceptor $\hat{p}_A$. These two vectors relate to each other by a connection vector $\vec{r}$. The angles between the vectors of the transition dipoles and the connection vector $\vec{r}$ are θ_A respectively θ_D. The angle between the transition dipoles is called ϕ_{DA}. All vectors and angles and their connections are shown in the scheme in Figure 7.

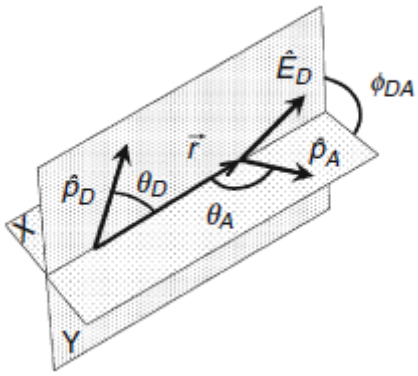

Figure 7: Schematic drawing of the relation between the transition dipoles of donor and acceptor ($\hat{p}_D$ and $\hat{p}_A$), the connection between both ($\vec{r}$), the angles between r and $\hat{p}_D$ and $\hat{p}_A$ (θ_D and θ_a) and the angles between the transition dipole moments ϕ_{DA}. $\hat{E}_D$ represents the unit vector, adapted from[32].

To calculate κ^2 the following formula can be used:

$$\kappa^2 = (\cos \phi_{DA} - 3 \cos\theta_D \cos\theta_A)^2 \quad (4)$$

κ^2 can range between 0 and 4: If all the vectors are parallel and all angles have a value of 0°, then κ^2 is 4. In terms of orientation factor, the energy transfer is ideal in this case. If all the vectors are orthogonal (all the angles have a value of 90°), then κ^2 is 0. In this case, energy transfer is forbidden.

In typical FRET experiments, the donors and the acceptors are completely free in solution, so a statistical value for $\kappa^2 = 2/3$ can be used[32]. However, for systems where the donor and acceptor are fixed to each other like in the case of small molecules bound to the surface of nanocrystals, a value for the orientation factor κ^2 can be estimated based on "geometrical" considerations[33].

Förster radius

Besides the orientation factor, the distance between donor and acceptor is critical for the energy transfer. The energy transfer efficiency *E* depends inversely to the power of six on the distance between donor and acceptor *R*, as the following equation shows.

$$E = \frac{R_0^6}{R_0^6 + R^6} \quad (5)$$

In this equation R_0 is the Förster radius, defined as distance between donor and acceptor where FRET efficiency = 0.5[34]. To show how strong the radius R influences the transfer efficiency, the efficiency is plotted against the normalized radius in Figure 8.

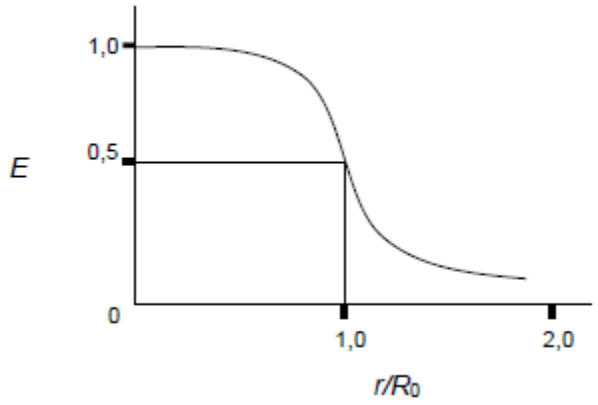

Figure 8: Energy transfer efficiency and the dependence to the distance between donor and acceptor r, normalized to R_0, adapted from[35].

The steep drop in Figure 8 shows that a small change in distance between the donor and the acceptor can have a large influence on the efficiency of the energy transfer when the distances are close to the Förster radius. The Förster radius depends on the donor-acceptor combination and is typically in the range of a few nanometres[32].

Spectral overlap

The third condition for the energy transfer is a spectral overlap between the donor and the acceptor. As shown in Figure 6, energy transfer is an isoenergetic process in which energy goes from the excited state of the donor to an acceptor. Therefore, donor and acceptor must have certain optical properties, which are shown as scheme in Figure 9.

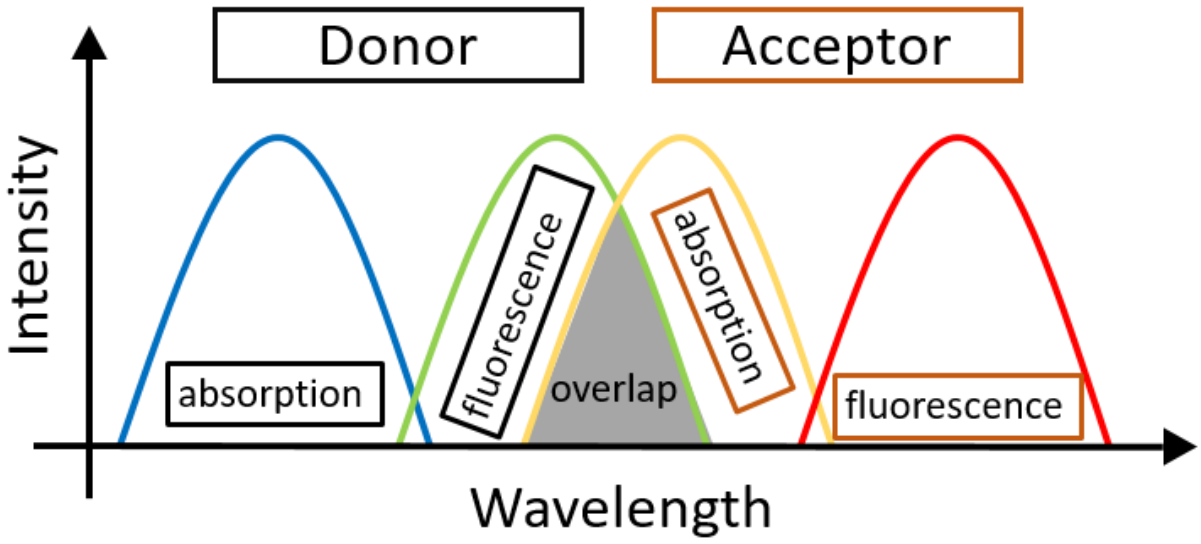

Figure 9: Scheme of the spectral overlap required for energy transfer.

As shown in Figure 9, the emission of donor (green line) and the absorption band of the acceptor (yellow line) overlap, shown by the grey area. This overlap is required for energy transfer. A large overlap leads to a higher energy transfer efficiency[34]. If there is no overlap between the emission of the donor and the excitation of the acceptor, energy transfer cannot take place[32].

Influences of the energy transfer to luminescence intensity and lifetime

Energy transfer can be evaluated either by photoluminescence or photoluminescence lifetimes. With increasing efficiency of the energy transfer, the luminescence of the donor decreases. The opposite happens to the acceptor, whose luminescence increases with increasing energy transfer efficiency. Meanwhile, the lifetime of the donor decreases with a higher FRET efficiency, while the lifetime of the acceptor increases with a higher FRET efficiency[32].

3. Experimental section

3.1. Chemicals

In Table 1 the chemicals, the abbreviation, the chemical formula, the manufacturer and the purity of the chemicals used in this work are listed.

Table 1: List of used chemicals with their abbreviation, sum formula, manufacturing company and purity.

Chemical	Abbreviation	Sum formula	Manufacturing company	Purity / %
Hexane		C_6H_{14}	Fischer scientific	95
Methyl acetate		$C_3H_5O_2$	Merck KGaA	99
1-Octadecene	ODE	$C_{18}H_{38}$	Acros organics	90
Cadmium acetate - dihydrate	$Cd(OAc)_2 \cdot 2\ H_2O$	$Cd(CH_3COO)_2 \cdot 2\ H_2O$	Acros organics	98
Selenium		Se	Alfa Aesar	99.999
Ethanol	EtOH	C_2H_6O	Sigma-Aldrich	99.8
Toluene		C_7H_8	VWR chemicals	99.8
9,10-Diphenylanthracene	DPA 1	$C_{26}H_{18}$	Fischer scientific	98
9,10-Diphenylanthracene	DPA 2	$C_{26}H_{18}$	Acros organics	97.5
Toluene dry		C_7H_8	Acros organics	99.85
Rhodamine 6G		$C_{28}H_{31}N_2O_3Cl$	*)	*)
Perylene		$C_{20}H_{12}$	Fluka	99.7
Bis(steaoryl)selenide		$C_{36}H_{70}O_2Se$	Synthesised by A. Manhart	*)
Cadmium myristate	$Cd(myr)_2$	$Cd(C_{14}H_{27}O_2)_2$	Synthesised by P. Kolpakov	*)
Oleic Acid		$C_{18}H_{34}O_2$	Sigma-Aldrich	90
Trioctylphosphine	TOP	$C_{24}H_{51}P$	Sigma-Aldrich	97

*) chemicals in house

3.2. Synthesis of nanoplatelets

Synthesis of NPL with TOP-Se at 240 °C [36]

Before the synthesis, the precursor solutions were prepared.

For the cadmium precursor solution, 0.1344 g (0.05 mmol) $Cd(OAc)_2 \cdot 2\ H_2O$ in 1.4 mL ethanol was dissolved under heating to 40 °C. Then 53.2 µL of oleic acid was added. Afterwards the solution was transferred to a syringe.

For the selenium precursor solution, a trioctylphosphineselenium (TOP-Se) stock solution was prepared with 0.180 g (2.28 mmol) Se and 1.016 mL (2.28 mmol) TOP, which were mixed in a glovebox. 266 µL of this TOP-Se stock solution was diluted with 1134 µL of ODE and transferred in a second syringe.

15 mL of ODE was filled in a three-necked flask and degassed under vacuum at 100 °C for 15 min. Afterwards the flask was heated to 240 °C under argon in 30 min. After reaching this temperature the precursor solutions were simultaneously added using a dual syringe pump over a period of 12 min at a speed of 84 µL/min. During the addition, the colour of the solution changed from colourless to yellow. Aliquots were taken after 3 min, 6 min and 9 min. After the addition of the precursors, 1 mL of oleic

acid was added. Then the solution was cooled down to room temperature, diluted with 5 mL hexane and centrifuged at 5000 rpm for 10 min. The precipitate containing the NPLs was re-dispersed in hexane. Aliquots taken during the reaction were treated analogously.

Synthesis of NPL with TOP-Se at 170 °C [37]

To prepare the selenium precursor from the TOP-Se stock solution (described in the previous section) 6.7 µL were diluted with 143 µL ODE and placed in a syringe. In a three necked flask, 240 mg (0.9 mmol) $Cd(OAc)_2 \cdot 2\ H_2O$ were mixed with 15 mL of ODE and 150 µL of oleic acid. The mixture was heated up to 100 °C for degassing under vacuum during 15 min. Afterwards, the mixture was heated up to 170 °C under argon and the selenium precursor was added. Aliquots were taken 2.5 min, 5 min and 7.5 min after the addition of the selenium precursor. The reaction was stopped after 10 min by cooling to room temperature. Then the mixture was centrifuged at 8000 rpm. The precipitate contains the NPLs and was re-dispersed in hexane. Aliquots taken during the reaction were treated analogously.

Low temperature synthesis (140 °C)[19]

In a three necked flask, 127.5 mg (0.225 mmol) of $Cd(myr)_2$ and 17.3 mg (0.065 mmol) of $Cd(OAc)_2 \cdot 2\ H_2O$ were dissolved in 15 mL ODE. This mixture was heated up to 100 °C and degassed under vacuum during 15 min. Afterwards the mixture was heated up to 140 °C under argon. At this temperature, a mixture of 45.8 mg (0.075 mmol) of bis(steaoryl)selenide dissolved in 1 mL of water free toluene was added with a syringe. One minute later, 52 mg (0.195 mmol) $Cd(OAc)_2 \cdot 2\ H_2O$ was added. The mixture was kept at 140 °C for five days. After five days, the mixture was cooled down to room temperature. Then 0.5 mL oleic acid was added. The reaction mixture was transferred to a centrifuge tube, the volume was filled up to 15 mL with hexane and the mixture was centrifuged at 5000 rpm for 10 min. The supernatant of this centrifugation was diluted with 15 mL of methyl acetate and centrifuged again at 8000 rpm for 10 min. The precipitate of this centrifugation was re-dispersed in 5 mL hexane. The resulting solution was clear yellow and contained pure 3 ML NPLs.

The reaction was repeated 4 times. The exact masses of the chemicals are listed in Table 2.

Table 2: Exact masses of the chemicals used for the different batches of synthesis of NPL with the low temperature method.

	$Cd(myr)_2$ / mg	$Cd(OAc)_2 \cdot 2\ H_2O$ first time / mg	Bis(steaoryl)selenide /mg	$Cd(OAc)_2 \cdot 2\ H_2O$ second time / mg
Batch 1	129.1	20.5	49.0	52.9
Batch 2	128.5	18.4	46.2	52.5
Batch 3	127.5	17.3	45.8	52.0
Batch 4	128.3	17.9	48.7	53.2

Preparation of Se-ODE[36]

To prepare the Se-ODE, 46.5 mL of ODE was introduced to a three necked flask and degassed under vacuum for 15 min at 100 °C. Afterwards, the ODE was heated up to 180 °C under argon and 393 mg (4.976 mmol) selenium dissolved in 3.3 mL toluene was added. The reaction mixture was heated up to 205 °C during 25 min. During this period, the colour of the mixture changed from grey to yellow. Then mixture was kept at 205 °C for 30 min. Then the solution was cooled to room temperature and transferred to a glovebox. The concentration of Se-ODE in this solution was approached to 0.1 mol/l.

Lateral size extension of NPLs

The size extension was performed five times. The exact amounts of used chemicals, the reaction temperature and the frequency of aliquots for each attempt are listed in Table 3.

5 mL ODE, a certain amount of seeds, $Cd(myr)_2$ and $Cd(OAc)_2 \cdot 2\ H_2O$ were degassed at 100 °C for 15 min. Then the solution was heated up to the desired temperature under argon. The Se-ODE was introduced using a syringe pump at speed of 50 µL/min. Aliquots were taken after adding a certain amount of Se-ODE. The reaction was stopped by cooling down with a water bath. As the reaction was cooling, the syringe pump was stopped at 100 °C and 1 mL of oleic acid was added at 60 °C. After reaching room temperature, the reaction mixture was diluted with 5 mL methyl acetate and centrifuged at 8000 rpm for 10 min. The precipitate was re-dispersed with 5 mL hexane.

For the aliquots, 250 µL of oleic acid and 500 µL of methyl acetate were added instead. They were centrifuged at 8000 rpm for 10 min and re-dispersed in 1 mL hexane. The resulting solution was yellow and contained the size extended NPL.

Table 3: Reaction temperature, used amounts of chemicals and number of batches of seeds for the different attempts to obtain size extended NPLs.

Exper-iment	Reaction temperature / °C	$Cd(myr)_2$ / mg	$Cd(OAc)_2 \cdot 2\ H_2O$ / mg	Batch seeds	Volume seeds / mL	Added Se-ODE / mL	Aliquots taken after adding Se-ODE / mL
SG 1	140	11	7	3	1	1.2	0.6
SG 2	140	11.6	7.7	4	0.51	4	0.6, 1.2, 2
SG 3	180	11.2	8.1	4	0.51	4	0.6, 1.2, 2
SG 4	190	12.8	8.5	1	1	4	0.6, 1.2, 2
SG 5	200	12.8	8.2	1	1	4	0.6, 1.2, 2

Synthesis of the final stock solutions for the energy transfer experiments

To prepare the seeds for the synthesis of the final NPLs, a new batch of seeds was synthesised with the low temperature method in a double scale. Therefore, in a three necked flask, 255.7 mg (0.451 mmol) of $Cd(myr)_2$ and 33.8 mg (0127 mmol) of $Cd(OAc)_2 \cdot 2\ H_2O$ were dissolved in 30 mL ODE. This mixture was heated up to 100 °C and degassed under vacuum during 15 min. Afterwards the mixture was heated up to 140 °C under argon. At this temperature, a mixture of 91.6 mg (0.151 mmol) of bis(steaoryl)selenide dissolved in 2 mL of water-free toluene was added with a syringe. One minute later, 105.2 mg (0.395 mmol) $Cd(OAc)_2 \cdot 2\ H_2O$ was added. The mixture was kept at 140 °C for five days. After five days, the mixture was cooled down to room temperature. Then 1 mL oleic acid was added. The reaction mixture was transferred to a centrifuge tube, the volume was filled up to 30 mL with hexane and the mixture was centrifuged at 5000 rpm for 10 min. The supernatant of this centrifugation was diluted with 30 mL of methyl acetate and centrifuged again at 8000 rpm for 10 min. The precipitate of this centrifugation was re-dispersed in 10 mL hexane. The resulting solution was clear yellow and contained pure 3 ML NPLs. The resulting NPLs are labelled with NPL A in this work.

The three batches of size extended NPL were synthesised at 190 °C following the protocol for size extension of the NPL in the section before. Therefore, 2 mL seeds of NPL A are used for each size extension. In Table 4 the exact amounts of used chemicals are listed.

Table 4: exact amounts of used chemicals for the size extension of the final NPL batches.

	$Cd(myr)_2$ / mg	$Cd(OAc)_2 \cdot 2\ H_2O$ / mg	Added Se-ODE / mL
NPL B	12.8	8.3	0.526
NPL C	12.7	8.2	1.029
NPL D	12.2	8.2	1.531

TEM imaging of the NPL

To provide the TEM images of the NPLs, 10 µL of a sample was diluted with hexane and dropped to a carbon coated copper TEM-grid. Within one minute, the hexane was evaporated. Afterwards the sample was analysed with a JEOL JEM-1400 TEM, having an acceleration voltage of 120 kV. The sizes of the NPLs were measured from the TEM-images with the ImageJ-software. For the measurements it was approached, that the NPLs are square. For a typical size determination, 100 to 200 NPLs were measured.

3.3. Energy transfer experiments

A stock solution of the dye Th-BT-Th-COOH was prepared by dissolving 1.6 mg of the pure powder in 8.445 mL toluene (Concentration = $5.5 \cdot 10^{-4}\ \frac{\mathrm{mol}}{\mathrm{L}}$). For the energy transfer experiments, this stock solution was diluted to a concentration of $1.375 \cdot 10^{-4}\ \frac{\mathrm{mol}}{\mathrm{L}}$.

Two different spectrometers were used to record the absorption. Either an Avantes spectrometer or a Cary 60 spectrometer (Agilent technologies) was used. The Avantes spectrometer was used for all experiments except for the experiments to determine the QY and the comparison between one and many cuvette method.

Photoluminescence spectra were measured with an Avantes spectrometer. The sample was excited with a LED (Prizmatix) in a 90° angle. Excitation wavelength = 369 nm.

The lifetime measurements were measured with a PicoQuant time correlation single photon counting (TCSPC) setup. The excitation laser emits with a wavelength of 380 nm, a repetition rate of 5 MHz and a pulse duration of 44 ps. The duration of the measurement was set for 1 minute for the lifetime of the NPL (462 nm) and 7:30 minutes for the lifetime of the dye (565 nm).

Preparation of the samples for the comparison between one cuvette and many cuvettes

34.83 µL of NPL A and 600 µL of toluene were added in the cuvette(s). For the “many cuvette method”, 0, 1, 2, 4 or 6 µL of dye solution was added to the different cuvettes. The absorption and the photoluminescence were recorded after mixing. For the “one cuvette method”, the NPLs were measured without dye and after sequentially adding the dye ($c = 1.375 \cdot 10^{-4}\ \frac{\mathrm{mol}}{\mathrm{L}}$) to this sample, that the cumulative amount of dye is identical to the “many cuvette method”.

Preparation of the samples for the kinetic measurements

A certain amount of NPL was diluted with a certain amount of toluene in a cuvette (Table 5). Then absorption and photoluminescence spectra were recorded. After that, a certain amount of dye was added and the photoluminescence peak for the dye (at 565 nm) and the NPL (at 462 nm) were recorded every second over a period of 10 min. After recording of the time trace, a whole absorption and photoluminescence spectra were recorded. Two attempts of this experiment were done.

Table 5: Used volumes of NPL, toluene and dye for the kinetic experiments.

Sample	V NPL / µL	n NPL / 10^{-11} M	V toluene / µL	V dye / µL	n dye / 10^{-9} M
NPL A	139	11.7	461	50.69	6.97
NPL C	94.8	2.9	505	44.35	6.10
NPL D	61.6	2.4	538	31.69	4.36

Preparation of the samples with constant concentration of NPLs

For the sample preparation, a certain amount of NPLs and toluene were introduced to a cuvette (Table 6). Absorption and photoluminescence spectra were recorded before adding the dye. Then both spectra were recorded in steps after sequentially adding 1 µL of dye ($c = 1.375 \cdot 10^{-4}\ \frac{mol}{L}$) until a cumulative volume of 2 µL of dye. Then the same was done in 2 µL steps until a cumulative volume of 30 µL of dye and thereafter in 5 µL steps until a cumulative volume of 60 µL for NPL A (150 µL for NPL C and NPL D). The data of this experiment are labelled with Exp. con. 1.

Table 6: Used volumes of NPLs and toluene for the experiments with constant concentration of NPLs.

Sample	V NPL / µL	n NPL / 10^{-11} M	V toluene / µL
NPL A	36.9	3.1	600
NPL C	100	3.1	534
NPL D	77.5	3.1	557

This experiment was repeated, using the same mixing procedure as before and the same volumes, as listed in Table 6. However, this time the dye was added until cumulative volume of 150 µL for NPL A. Also, in this case the lifetime of NPL and dye was measured, but not at every concentration due to convenience. The cumulative volume of dye for each sample, at which the lifetime was measured is displayed in Table 7. The data from this experiment are labelled with Exp con. 2.

Table 7: Cumulative amount of dye ($c = 1.375 \cdot 10^{-4}\ \frac{\mathrm{mol}}{\mathrm{L}}$), at which the lifetime of NPL and dye was measured for the experiments with constant concentration.

Sample	Cumulative volumes of dye, at which lifetime was measured / µL
NPL A	0, 6, 10, 14, 18, 22, 26, 30, 50, 75, 100, 125, 150
NPL C	0, 6, 14, 18, 22, 26, 30, 40, 50, 60, 70, 85, 100, 125, 150
NPL D	0, 6, 14, 20, 26, 30, 40, 50, 60, 70, 80, 90, 100, 125, 150

Experiments with constant absorption of the NPL samples

For the experiments with constant absorption of NPLs, a certain amount of NPLs and toluene was filled to a cuvette and the absorption and photoluminescence spectra recorded. The exact volumes of NPLs and toluene are located in Table 8. Then, 12.67 µL of dye ($c = 1.375 \cdot 10^{-4}\ \frac{\mathrm{mol}}{\mathrm{L}}$) was added for the first two measurements. 6.34 µL of dye was added for the last eight measurements. The lifetime was recorded every time during the experiment. The data from this experiment are labelled with Exp. abs.

Table 8: Volumes of NPLs and toluene for the sample of the experiments with constant absorption of the samples.

Sample	V NPL / µL	n NPL / 10^{-11} M	V toluene / µL
NPL A	139	11.7	461
NPL C	94.8	2.9	505
NPL D	61.6	2.4	538

4. Results and discussion

4.1. Nanoplatelet synthesis

This part of the project takes aim to identify a method that allows the synthesis of three ML NPLs with different lateral sizes and high quantum yield. It would be ideal to have different sized NPLs edge length between 10 nm to 50 nm to systematically test the influence of the spacing between the photocatalyst and the excitons in NPLs, which have a size of 1.5 nm[13]. In this project three different methods were attempted in order to know which method leads to NPLs with the most desired properties. After the synthesis the NPLs are characterised to obtain their size and spectral properties.

The following synthesis were done:

- Direct Synthesis with TOP-Se as Se-precursor at different temperatures.
  Experiments called DS 1 – DS 3 (section 4.1.1.)
- Low temperature synthesis with bis(stearoyl)selenide as Se-precursor.
  Experiments called Batch 1 – Batch 4 (section 4.1.2.)
- Seeded growth of NPLs at different temperatures with Se-ODE as Se-precursor and NPLs from Batch 1 – Batch 4 as seeds. Experiments called SG 1 – SG 5 (section 4.1.3.)
- Synthesis of the NPLs with optimised conditions for temperature and precursor.
  Experiments called NPL A – NPL D (section 4.1.4.)

4.1.1. Direct synthesis

In a first step two direct synthesis protocols found in literature were approved. An overview of the synthesis is given in Table 9.

Table 9: Summary of experiments discussed in section 4.1.1.

Experiment	Temperature	Seeds	Se-Precursor	Figure
DS 1	240 °C	-	TOP-Se	Figure 10
DS 2	240 °C	-	TOP-Se	Figure 11
DS 3	170 °C	-	TOP-Se	Figure 12

Using TOP-Se as selenium precursor at high temperatures (240 °C)

In literature, there is described a synthesis procedure, which leads to laterally large NPLs. These NPLs can have a lateral size up to 700 nm [36]. For the synthesis TOP-Se at 240 °C was used. The literature synthesis protocol was reproduced as proven by TEM images, absorption and photoluminescence spectra (shown in Figure 10).

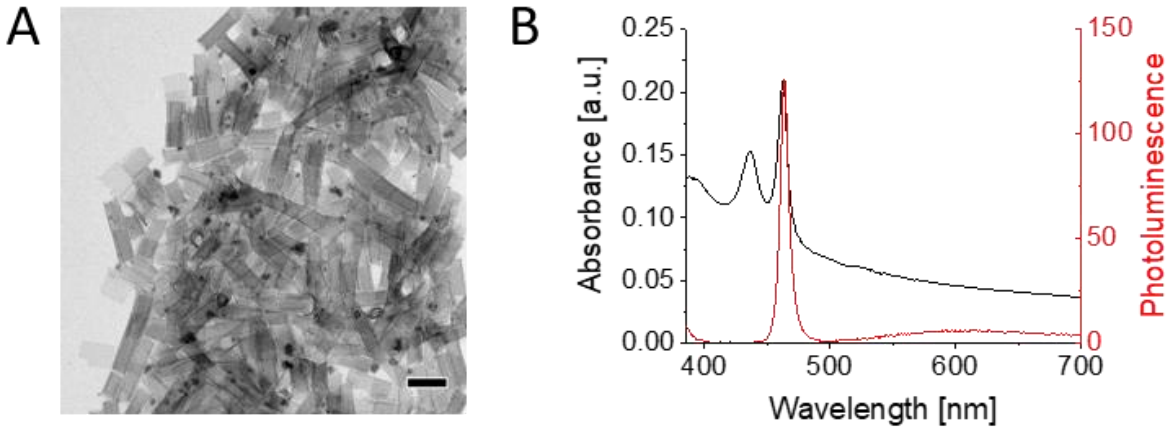

Figure 10: Synthesis of 3 ML NPLs using TOP-Se as selenium source at 240 °C reaction temperature (DS 1). (A) TEM image of the obtained NPLs. The scalebar in the TEM image corresponds to 100 nm. (B) Absorption and photoluminescence spectra of the sample.

The results of this experiment (DS 1) are shown in Figure 10 and agree with the literature, hence the literature is reproducible[36]. However, the results of this first experiment show several problems with this method for the further applications of the NPLs. First of all, the NPLs are very large, around 126 ± 39 nm. This shows also a large size distribution for the obtained NPLs. Secondly, as seen in the TEM image (Figure 10 A), these large NPLs roll up, agreeing to the observation reported in literature[36]. The rolling needs to be avoided for the later energy transfer experiments, because rolling reduces the effective surface area, where the photocatalyst ligand can bind to.

In the absorption spectra (black line, Figure 10 B), non-zero absorption after the maximum at 462 nm indicates scattering of the rolled-up and agglomerated NPLs. Therefore, this synthesise method should be modified for the study. A possible modification to this method is to shorten the reaction times to obtain smaller NPLs, ideally with edge lengths of at most around 50 nm. NPLs of that size should have a lower tendency to roll up.

To find the ideal reaction time for NPLs of such size, aliquots were taken at different time points: three, six, nine and twelve minutes after the start of adding the precursors. The sample obtained after twelve minutes is shown in Figure 10. The spectra and the TEM images of the other aliquots are shown in Figure 11.

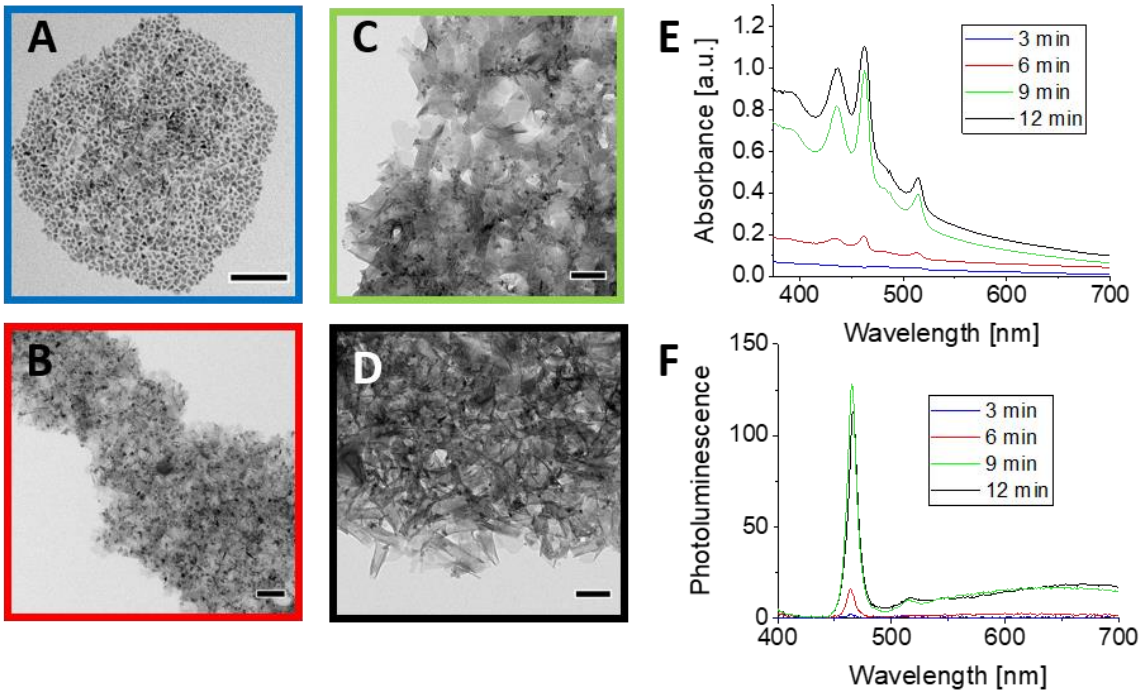

Figure 11: Results of the direct synthesis of the large NPLs with taking aliquots (DS 2). TEM images of the obtained products after (A) 3 min, (B) 6 min, (C) 9 min, and (D) 12 min. The scalebar in the TEM images corresponds to 100 nm. (E) Absorption spectra and (F) photoluminescence spectra of the obtained products.

In the absorption spectra of the first two aliquots, only a very weak peak around 431 and 461 nm, corresponding to the formation of NPLs, is observable (blue respectively red line in Figure 11 E). Because these peaks did not stand out from the background very well, the development of NPLs starts slowly. In addition, the shape of the NPLs in these two samples is very irregular (Figure 11 A and B). This is especially notable for the particles formed after 3 min, as their shapes deviate far from the expected rectangular form and are very small, with an average size of 10.5 nm.

In the second aliquot, NPLs with an average size of 28 nm can be found. However, other side products are also visible in the TEM and the absorption spectra show scattering after the maximum at 462 nm. The size distribution of the particles is also very broad.

The NPLs obtained in the aliquots after 9 and 12 min are very large and have a wide size distribution. That NPLs are obtained is visible in the absorption spectra (green and black line in Figure 11 E) and in the TEM images (Figure 11 C and D). The size of the NPL is measured to 59 nm after 9 min and 129 nm after 12 min. This large sizes of the NPL may lead to agglomeration and thus to the Rayleigh scattering, observable in the absorption spectra. Beside this, a wide size distribution is found, and it is observed that the NPL obtained after 12 min tend to roll up. In the TEM images of both samples, also side products can be found, visible through the black spots. This indicates, that these NPLs are not ideally suitable for our energy transfer experiments.

Judging from the photoluminescence spectra (Figure 11 F), the quantum yield of these NPLs are very low. The measured quantum yield is around 1.25% for the sample after twelve minutes. These results show that this method is not suitable for our purpose.

Using TOP-Se as selenium precursor at lower temperatures (170 °C)

Decreasing the reaction temperature should lead to smaller NPLs and prevent rolling[37]. Here the reaction temperature was decreased to 170 °C. Again, aliquots were taken during the reaction to get different sized NPLs. The results of these syntheses (DS 3) are shown in Figure 12.

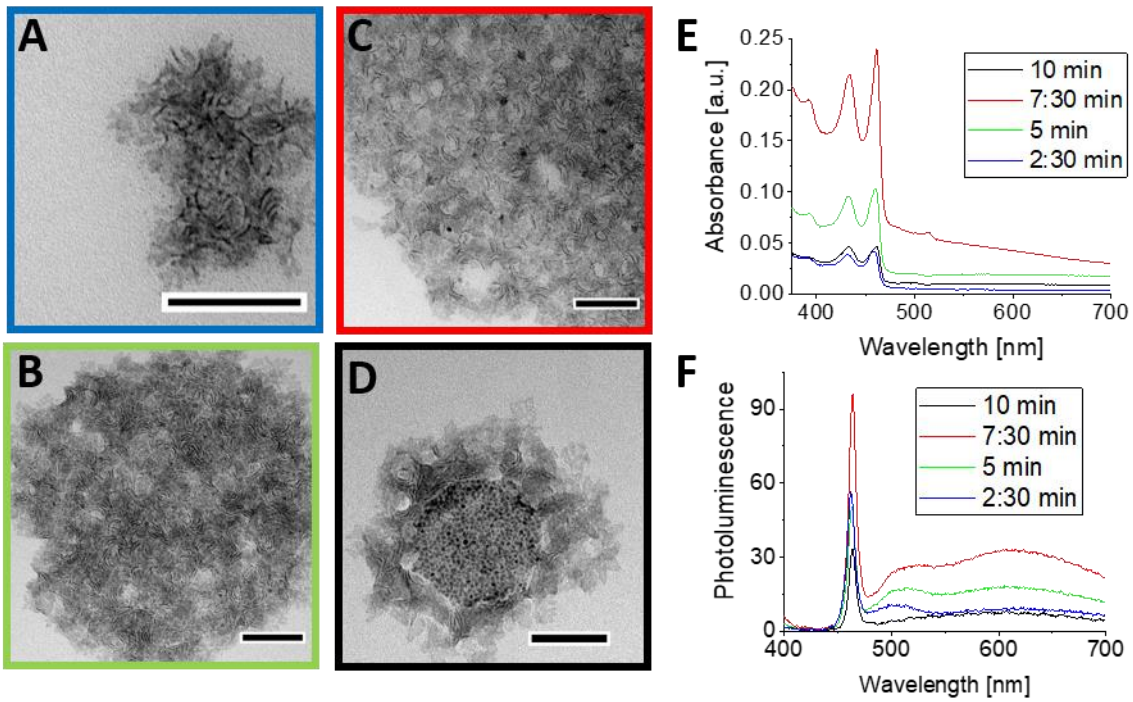

Figure 12: Obtained products after the synthesis of the synthesis at 170 °C using TOP-Se with aliquots (DS 3). TEM images of the samples received after (A) 2:30 min, (B) after 5 min, (C) after 7:30 min and (D) after 10 min. The scalebar in the TEM images corresponds to 100 nm. (E) Absorption spectra and (F) photoluminescence spectra of the samples.

The synthesis yields NPLs of different sizes as observed in the TEM pictures (Figure 12 A, B, C and D). The sample after 2.5 min has an average size of 14 ± 3 nm, which increases to 19 ± 3 nm after 5 min and then to 25 ± 4 nm after 7.5 min. For the final sample obtained after 10 min, the size cannot be properly measured, because the shape of the NPLs are highly irregular and often folded.

Despite having decent sizes suitable for the experiments, the samples have quite a wide size distribution. This is noticeable because there is no stacking of the NPLs observed in any of the TEM images. The stacking of the NPLs is a hint for a low size distribution, since regularly sized NPLs favour stacking[30].

Based on the absorption spectra (Figure 12 E), all samples show the characteristic peak at 462 nm, indicating the formation of 3 ML NPLs. The scattering signals from these samples are also much less apparent compared to the samples in the previous section. Unlike the previous synthesis, even the first aliquot clearly shows the optical features of 3ML NPLs. The absorption of the aliquot after 10 min may be quite low (black line in Figure 12 E), but this is reasonable due to the higher dilution of this sample.

Looking at the photoluminescence spectra, a second problem arising from this synthesis becomes apparent. The presence of a broad peak centred at 600 nm (Figure 12 F) indicates the presence of surface trap states on the NPLs[38]. This hints to the existence of electronic states located in the bandgap of the NPLs[39]. These trap states result from surface defects which were formed during the synthesis[40].

4.1.2. Low temperature (140 °C) nanoplatelet synthesis

The two methods described in the previous section show several problems. Both methods lead to NPLs with a wide size distribution and NPLs with very low quantum yields. For these reasons, a new approach for the synthesis of the NPLs was needed. Instead of directly forming the NPLs with different sizes, the idea was to synthesise small, high quality NPLs with a low size distribution and high QY and then extend their lateral size in the second step. Therefore, another method to synthesise three ML NPLs was chosen[19]. This method leads to NPLs with a high QY and narrow lateral size distribution. For this synthesis, a highly reactive selenium precursor, bis(stearoyl)selenide, was used.

The experiment was repeated four times in order to get enough three ML NPLs for the later size extension experiments, listed in Table 10.

Table 10: Summary of the experiments described in section 4.1.2.

Experiment	Temperature	Seeds	Se-Precursor	Figure
Batch 1	140 °C	-	bis(stearoyl)selenide	Figure 14 A/E-F
Batch 2	140 °C	-	bis(stearoyl)selenide	Figure 14 B/E-F
Batch 3	140 °C	-	bis(stearoyl)selenide	Figure 14 C/E-F
Batch 4	140 °C	-	bis(stearoyl)selenide	Figure 14 D/E-F

The higher reactivity of the selenium precursor allows the formation of NPLs at low temperature. Previous studies found that the quantum yield is higher when the reaction temperature is lower, which favours the formation of more perfect NPLs[19]. Spectra of NPLs synthesised with this method are shown in Figure 13.

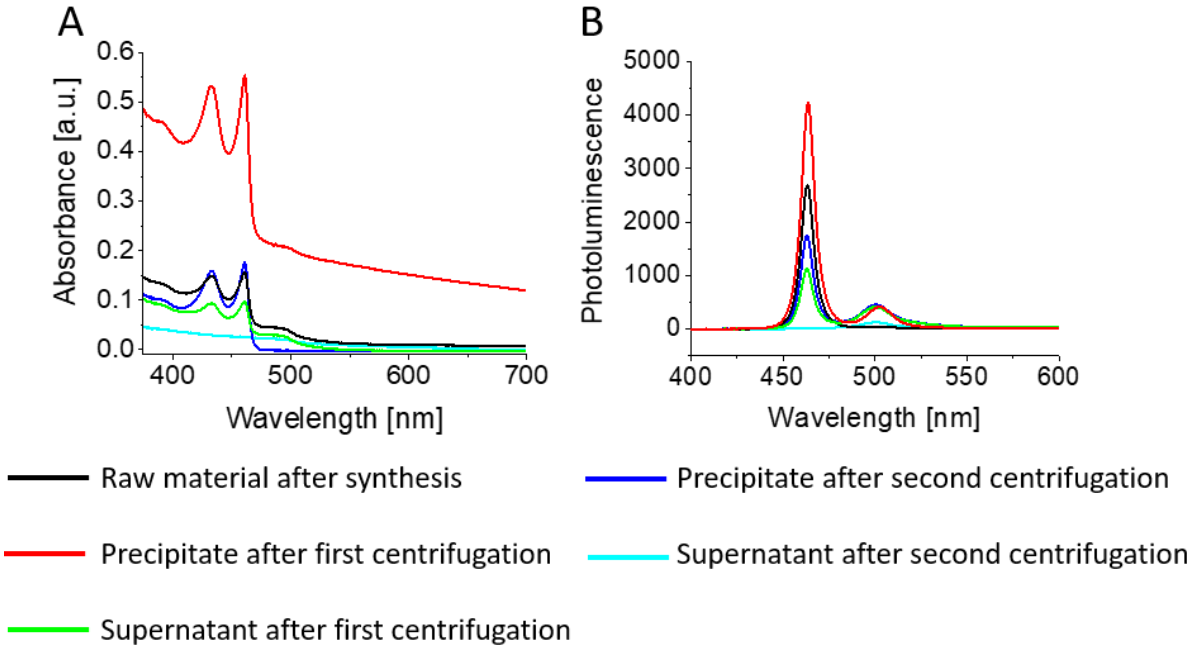

Figure 13: Purification steps of the 3 ML NPLs after the low temperature synthesis for the NPLs of batch 2. (A) Absorption spectra and (B) photoluminescence spectra of the batch for the different purification steps.

The spectra of the raw material after the reaction are shown in the black line in Figure 13. Three major peaks at the absorption spectra (Figure 13 A) can be found. The peaks at 462 nm and at 432 nm stem

from the heavy-hole and light-hole transition in three ML NPLs as expected, while the peak at 510 nm results from quantum dots (QDs), which are a side product of this reaction.

To get rid of unreacted cadmium precursors, the NPLs were centrifuged at 5000 rpm. At this speed, only the unreacted cadmium precursor precipitates. The spectra of the sample after the first centrifugation show this fact. In the precipitate (Figure 13, red line) the absorption signal never reaches the base line which indicates the presence of large scattering particles. These large particles indicate the presence of agglomerated precursors. But in the supernatant (green line in Figure 13) this scattering signal from the sample disappears, indicating good removal of unreacted precursors.

To extract the NPLs out from the mixture, a second centrifugation was performed at 8000 rpm. Before this centrifugation, methyl acetate was added as an antisolvent. This makes it easier for the nanoparticles to agglomerate and to precipitate. By adding an appropriate amount of antisolvent the two species, QDs and NPLs can be separated. The result of this separation is visible in the spectra. The precipitate of the second centrifugation contains the NPLs (blue line in Figure 13) and less QDs than before. In the spectra of the supernatant of the second centrifugation (turquoise line in Figure 13), no NPLs are observed, while some QDs remain. This shows that a clean NPL sample is obtained as precipitate of the second centrifugation.

For the following experiments, several batches of NPLs were synthesised with this method. TEM pictures and spectral data of these NPLs after purification are shown in Figure 14.

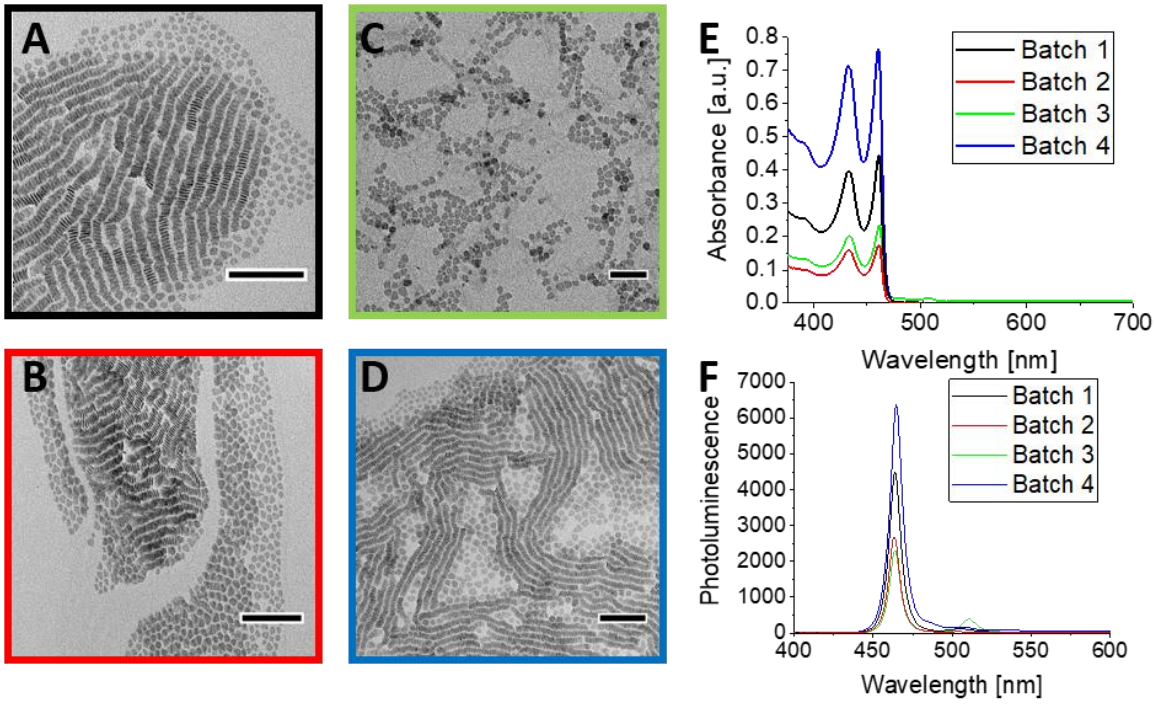

Figure 14: Different batches of 3 ML NPLs synthesis with the low temperature method. TEM images of the different batches. (A) Batch 1, (B) batch 2, (C) batch 3 and (D) batch 4. The scalebar in the TEM images corresponds to 100 nm. (E) Absorption spectra and (F) photoluminescence spectra for all batches.

Once purified, QD peaks are no longer observed in the absorption spectra (Figure 14 E). The sharp peak with a maximum at 460 nm shows the formation of three ML NPLs and no other fluorescent nanoparticles. The photoluminescence spectrum confirm this observation (Figure 14 F) as only a narrow peak at 462 nm is visible. At higher wavelengths, the photoluminescence for all batches of NPLs is close to zero unlike the previous sections. This signals the absence of trap states.

In the TEM images (Figure 14 A, B, C and D), the NPLs are stacked in rows. This is a hint for the narrow size distribution of the NPLs. The average sizes of the NPLs synthesised in the different batches also do not vary much. The typical edge size for the NPLs synthesised by this method is 12 nm. The NPL sizes from the different batches can be found in Table 11.

Table 11: Edge size and standard deviation for the NPLs batches obtained with the low temperature method.

NPLs	Batch 1	Batch 2	Batch 3	Batch 4
Edge size / nm	10.5 ± 2.1	11.7 ± 2.1	16.1 ± 2.6	11.9 ± 1.9

Because of the long synthesis period of five days and the slow growth of the NPLs, it is not feasible to get significantly larger or smaller NPLs by changing the growth time. For this reason, these small NPLs are used as seeds for a seeded growth synthesis. The seeded growth synthesis aims to extend the lateral size of the NPLs to get even larger NPLs while keeping the properties of these NPLs. The development of this synthesis will be described in the next chapter.

4.1.3. Extending the lateral size of nanoplatelets with seeded growth

To extend the lateral sizes of three ML NPLs with the seeded growth method, a new procedure has to be developed based on an existing method applied to four ML NPLs[37]. In this method, $Cd(OAc)_2 \cdot 2\ H_2O$ and Se-ODE are used as precursors for the size extension. For the synthesis of three ML NPLs, $Cd(OAc)_2 \cdot 2\ H_2O$ and $Cd(myr)_2$ are used as cadmium precursors because both are used in the seed synthesis.

The key for successful lateral growth is to avoid the formation of new nanoparticles. Therefore, several precautions were taken to develop this method. Firstly, a less reactive Se precursor (Se-ODE) was used for the growth process. Since Se-ODE is less reactive than the bis(stearoyl)selenide, the likelihood of nucleation of new nanocrystals should be reduced. Secondly, Se-ODE was added slowly with a syringe pump. This is necessary for a slow growth of the NPLs to get a narrow size distribution and to avoid the nucleation of new particles. Nucleation of new particles can be avoided if the concentration of available precursor is always below the critical concentration. The use of a syringe pump also allows a better control over the final size of the NPLs, depending on the amount of precursor added.

Table 12 gives an overview over the performed experiments.

Table 12: Summary of the experiments discussed in section 4.1.3.

Experiment	Temperature	Seeds	Se-Precursor	Figure
SG 1	140 °C	Batch 3	Se-ODE	Figure 15
SG 2	140 °C	Batch 4	Se-ODE	Figure 16
SG 3	180 °C	Batch 4	Se-ODE	Figure 17
SG 4	190 °C	Batch 4	Se-ODE	Figure 18
SG 5	200 °C	Batch 1	Se-ODE	Figure 19

Seeded growth at 140 °C

The first experiment (SG 1) of the lateral size extension of the NPLs was performed at 140 °C. The results are shown in Figure 15.

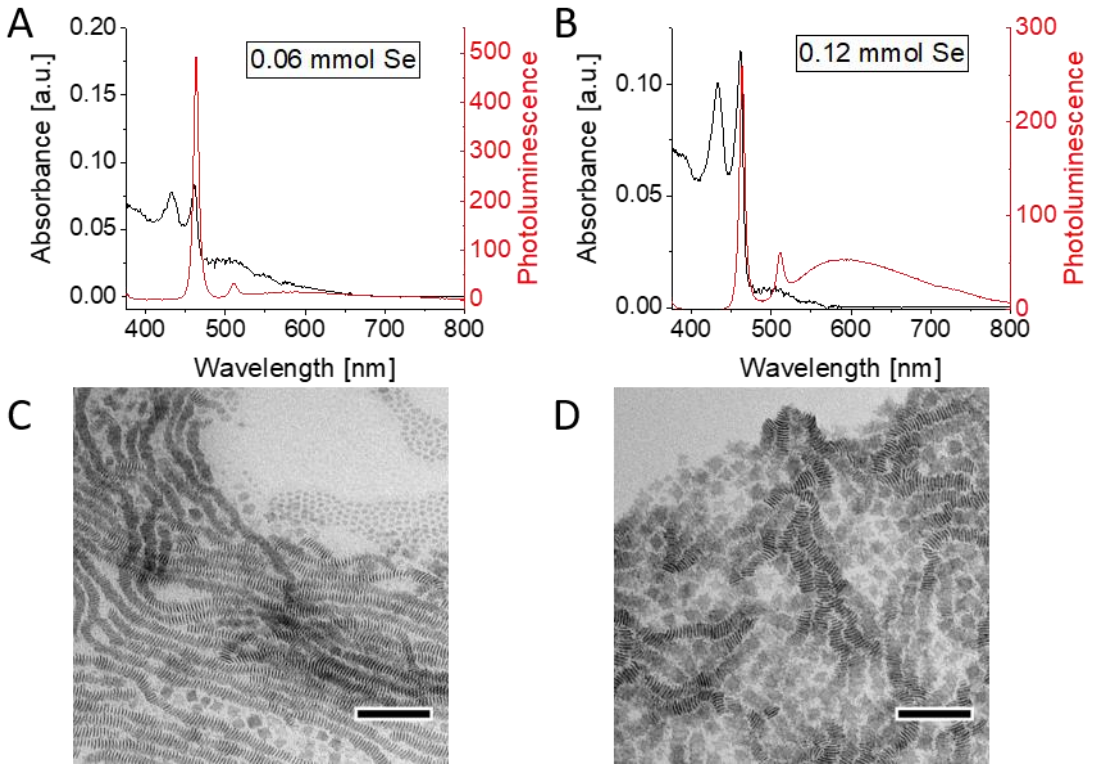

Figure 15: Proof of principle to get size extended 3 ML NPLs by seeded growth (SG 1). (A) Absorption and photoluminescence spectra of the sample after adding 0.06 mmol Se-ODE. (B) Absorption and photoluminescence spectra of the sample after adding 0.06 mmol Se-ODE. (C) TEM image of the sample obtained after adding 0.06 mmol Se. (D) TEM image of the sample obtained after adding 0.06 mmol Se. The scalebar in the TEM images corresponds to 100 nm.

Two samples from this experiment (SG 1) were obtained, one after adding 0.06 mmol Se-ODE and the other one after adding 0.12 mmol Se-ODE. As seen from the absorption spectra (black line in Figure 15 A and B), it was possible to avoid the formation of new unwanted side products. The TEM images confirm this (Figure 15 C and D), as the obtained NPLs are stacked in the same way as the seeds, hinting a narrow size distribution of the NPLs. The measured size of the NPLs is 13.3 ± 1.8 nm for the sample after adding 0.06 mmol Se and 20.3 ± 2.5 nm after adding the 0.12 mmol Se. Comparing these sizes to the size of the seeds (16 nm, see Table 11), it seems that the size of the NPLs decreases after adding 0.06 mmol Se, but increases by 4 nm after adding 0.12 mmol Se. This result shows, that in principle it is possible to change the lateral size of the seeds with this method.

By increasing the amount of Se-ODE the quality of the NPLs becomes slightly worse. In photoluminescence spectra (red line in Figure 15 A and B) the broad peak around 600 nm becomes more intense, especially in the sample where 0.12 mmol Se is added. This suggests that the amount of trap sates has increased. The lower quality of NPLs is also visible in the TEM images of this sample where the edge of the NPLs start to fray. In contrast, the TEM of the seeds (Figure 14 C) shows straighter edges without fray.

To verify the findings from this experiment, the experiment was repeated with another batch of NPLs (batch 4). The duration of the experiment was extended and more Se-ODE was added in order to see a lager difference in size, but the pump speed was kept in the same speed. The result of this experiment (SG 2) is shown in Figure 16.

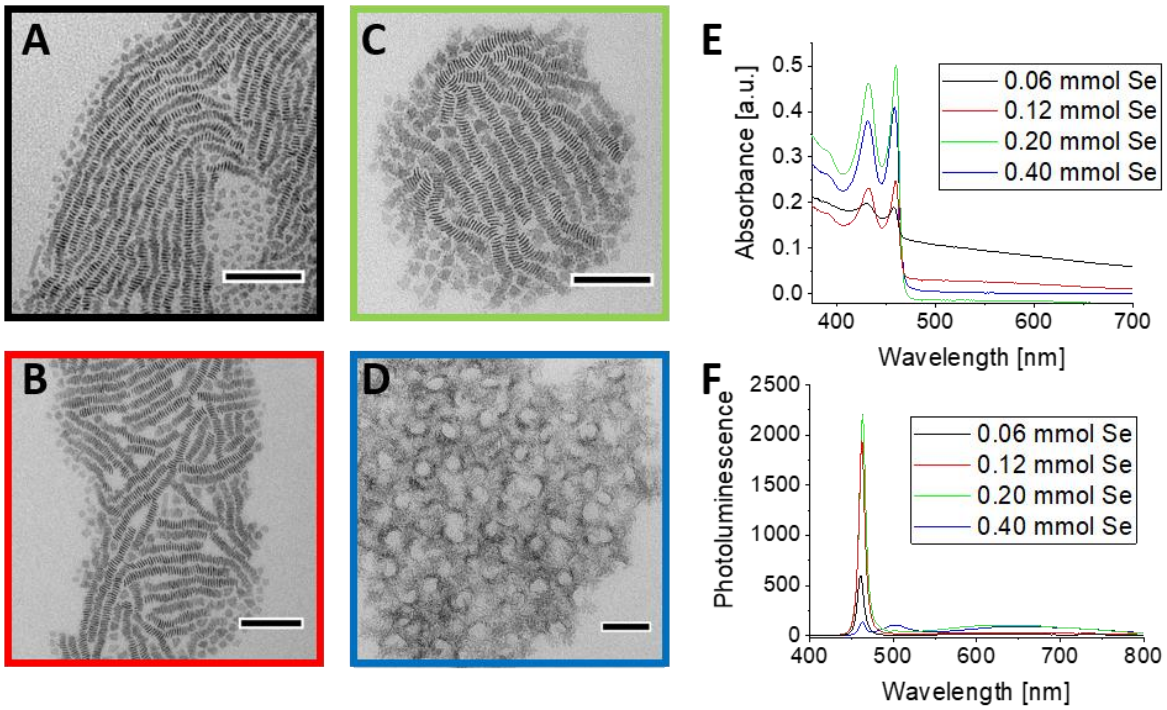

Figure 16: Size extension for the 3 ML NPLs using seeded growth method (SG 2). TEM images of the obtained samples after adding (A) 0.06 mmol Se, (B) 0.12 mmol Se, (C) 0.20 mmol Se and (D) 0.40 mmol Se. The scalebar in the TEM images corresponds to 100 nm. (E) Absorption spectra and (F) Photoluminescence spectra of the samples.

The results of this experiment (SG 2, Figure 16) appear to be similar to the previous experiment. The NPLs in the sample obtained after adding 0.06 mmol Se have a size 11.5 ± 1.5 nm (Figure 16 A), slightly smaller than the seeds with the starting size of 11.9 nm. In the second sample a size of 14.1 ± 1.8 nm is measured (Figure 16 B), an increase of 2 nm with respect to the seeds. By increasing the amount of Se-ODE further, the size can be further extended. In the third sample, after adding 0.2 mmol Se (Figure 16 C), an average size of 16.6 ± 2.1 nm is measured and the final sample has a size of 31 ± 4 nm (Figure 16 D).

The purity of the product appears quite good as seen in the absorption spectra (Figure 16 E) where no peaks are observed after the three ML NPL maximum at 462 nm. In other words, there was an absence of nucleation of new nanocrystals or other side products during the size extension. But there are also some problems with the obtained NPLs. The amount of trap states increases with the added amount of Se-ODE, visible in the photoluminescence spectra (Figure 16 F). The photoluminescence of the NPLs at 462 nm also decreases significantly when the size increases. These two effects are strongly seen in the final sample after adding 0.40 mmol Se (blue line), where the peak height at 462 nm and at 650 nm becomes effectively the same.

The absorption of the NPLs here increases with the size of the NPLs, while the photoluminescence decreases. As a result, the quantum yield gets lower and lower with increasing size extension. This decrease can be explained by the fraying of the NPLs' edges seen in the TEM pictures. The first sample after adding 0.06 mmol Se shows nicely stacked NPLs with sharp edges (Figure 16 A). As more as Se-ODE is added the shape becomes less regular. In the final TEM picture after adding 0.40 mmol Se (Figure 16 D), the shape of the NPLs have become quite irregular, with no sharp edges nor stacking. Furthermore, they also seem to start to roll up due to their large size. Hence, adding more Se-ODE to get larger NPLs may not be the best method to proceed, because the NPLs fray out and lose their optical properties.

A reason for the NPLs fraying could be due to the reaction temperature. One hypothesis is that when the precursors react with the NPLs, they remain in a kinetic minimum instead reaching the thermodynamic one, since there is a lack of energy to rearrange the atoms. It may be possible to provide more energy to the system by simply increasing the reaction temperature and bring the precursors to the thermodynamic minimum. This way NPLs with sharper edges and better optical properties could be obtained.

Seeded growth at higher temperatures (180 °C, 190 °C, 200 °C)

To avoid fraying at the edges, the synthesis was repeated at higher temperatures. To find the optimal temperature, 180 °C (SG 3), 190 °C (SG 4) and 200 °C (SG 5) were tested. The experiment at 180 °C used NPLs from batch 4 as seeds while the experiments at 190 °C and 200 °C were performed with seeds from batch 1. Results of these experiments are shown in Figure 17, Figure 18 and Figure 19.

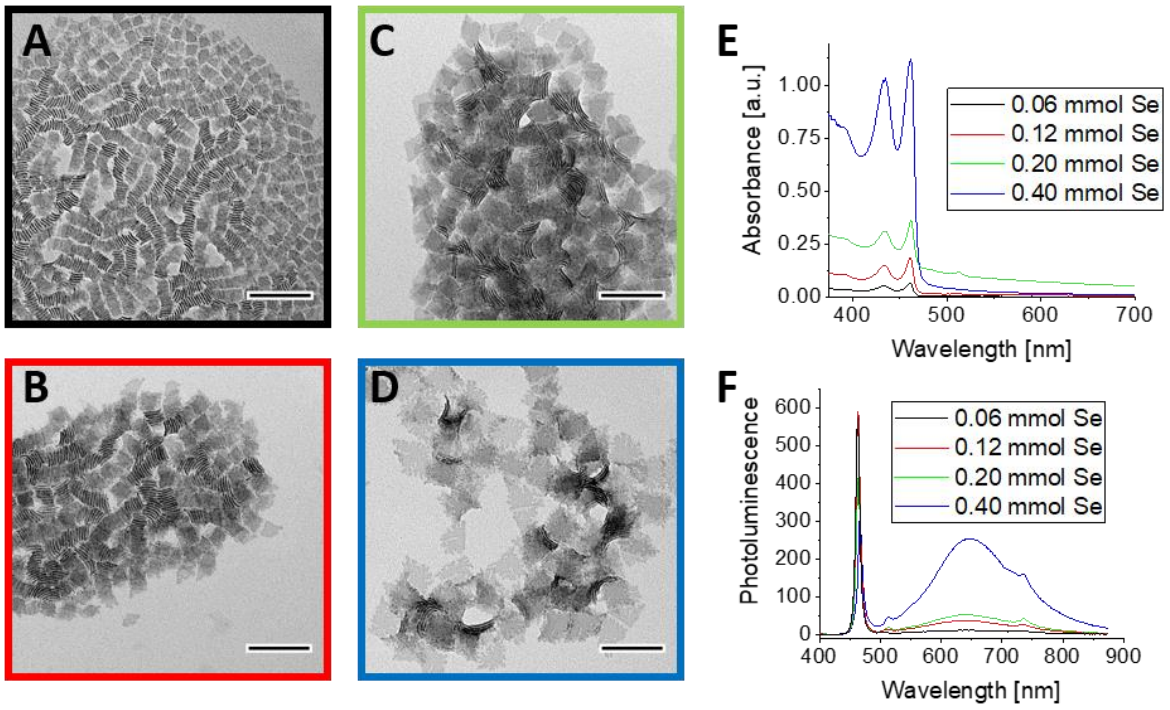

Figure 17: Size extension using seeded growth of the 3 ML NPLs performed at 180 °C (SG 3). TEM images of the sample, obtained after adding (A) 0.06 mmol Se, (B) 0.12 mmol Se, (C) 0.20 mmol Se and (D) 0.40 mmol Se. The scalebar in the TEM images corresponds to 100 nm. (E) Absorption spectra and (F) photoluminescence spectra of the obtained samples.

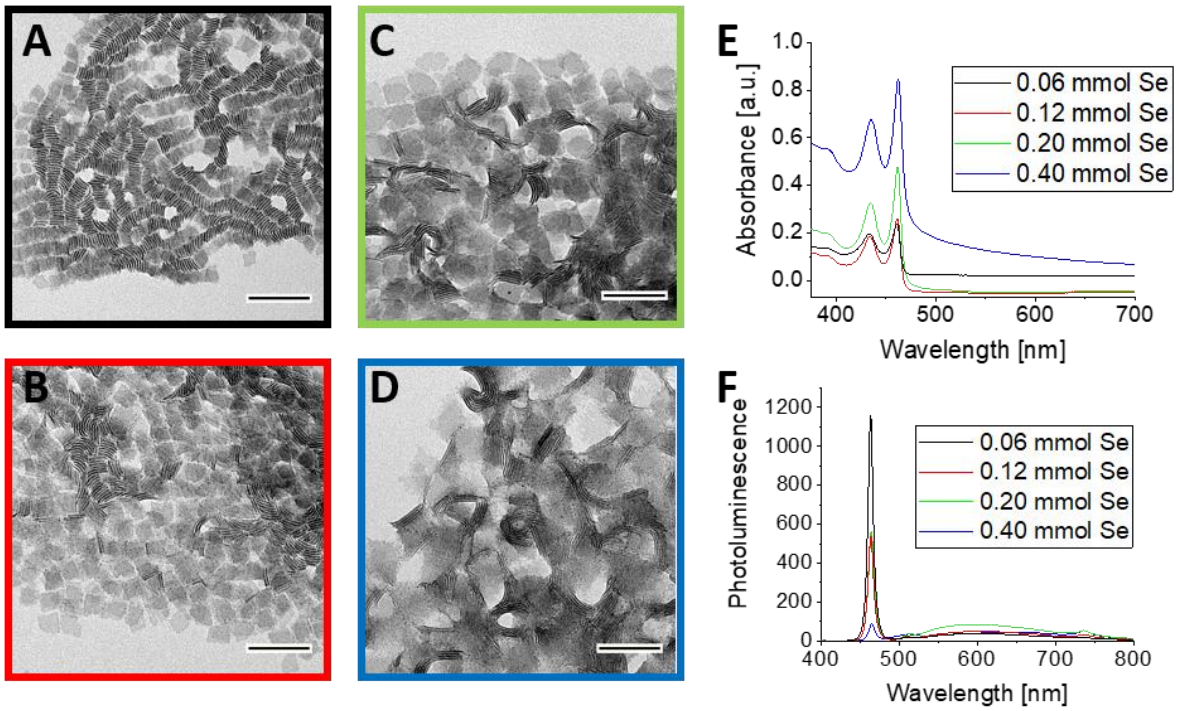

Figure 18: Size extension using seeded growth of the 3 ML NPLs performed at 190 °C (SG 4). TEM images of the sample, obtained after adding (A) 0.06 mmol Se, (B) 0.12 mmol Se, (C) 0.20 mmol Se and (D) 0.40 mmol Se. The scalebar in the TEM images corresponds to 100 nm. (E) Absorption spectra and (F) photoluminescence spectra of the obtained samples.

The NPLs obtained in the experiment at 180 °C (SG 3) show a much larger size extension compared to the ones obtained at 140 °C. For example, the NPLs obtained after adding 0.06 mmol Se have a size of 18.4 ± 2.1 nm (Figure 17 A), significantly larger than the seeds (11.9 ± 1.9 nm). The stacking of the NPLs is once again observed, especially for the first two samples. This indicates that the NPLs have a regular shape and a narrow size distribution. For all samples the size was measured from the TEM pictures. The results are shown in Table 13.

Table 13: Sizes of the NPLs obtained with seeded growth at 180 °C (SG 3).

TEM picture	Figure 17 A	Figure 17 B	Figure 17 C	Figure 17 D
Size / nm	18.4 ± 2.1	25.8 ± 3.5	35.5 ± 5.7	51.1 ± 6.7

Assuming no formation of new nuclei, the size extension can also be observed in the absorption spectra (Figure 17 E). As the size becomes larger, the absorption cross section of the NPLs increase, which is reflected in the spectra as an increase in absorbance. The absorption spectra together with the TEM images support this assumption indicating that the NPLs are just becoming larger during the synthesis as planned.

However the quality of the NPLs is still not ideal since the edges are frayed (Figure 17 F) and the photoluminescence spectra show a high amount of trap states, especially in the sample obtained after adding 0.40 mmol Se (blue line in Figure 17 F). By conducting the experiment 190 °C (SG 4), the same trends found at 180 °C can reproduced but at a higher quality. Sizes are slightly larger compared to 180 °C case, as shown in Table 14.

Table 14: Sizes of the NPLs obtained with seeded growth at 190 °C (SG 4).

TEM picture	Figure 18 A	Figure 18 B	Figure 18	Figure 18 D
Size / nm	21.2 ± 3.0	29.1 ± 4.9	38.0 ± 6.5	42.1 ± 8.9

The size increase can again be observed in the absorption spectra (Figure 18 E). Notably, the photoluminescence spectra show that the amount of trap states in this case is lower compared to the previous experiment at 180 °C (Figure 18 F), which supports the hypothesis that increasing the temperature can provide enough energy for atoms to rearrange and form more perfect crystals.

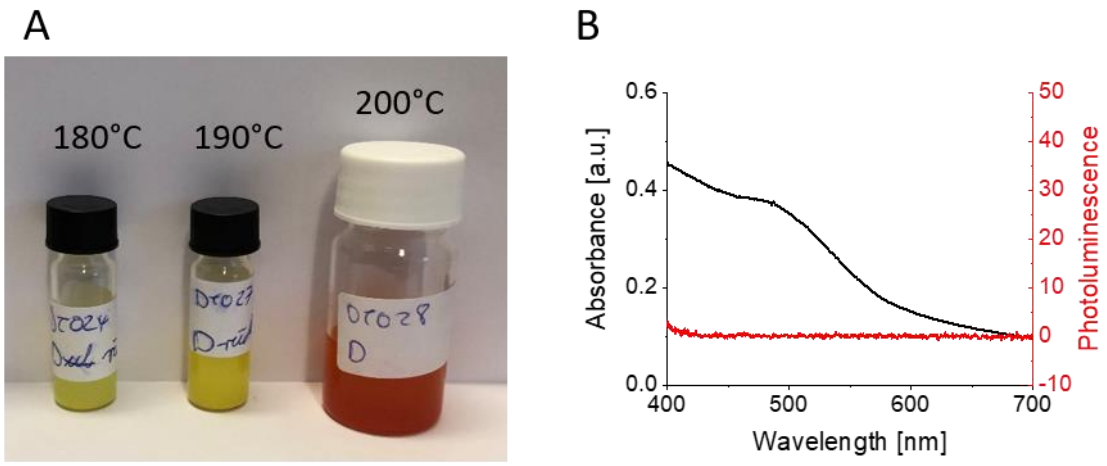

Figure 19: (A) Photography of the samples after adding 0.40 mmol Se at 180 °C (SG 3, left), 190 °C (SG 4, middle) and 200°C (SG 5, right). (B) Absorption and photoluminescence spectra of the sample obtained at 200 °C (SG 5).

However, this approach has a limit since the NPLs degrade when the temperature is too high. Normally, the obtained NPLs are yellow after the synthesis at 180 °C and 190 °C. At 200 °C (SG 5), the reaction mixture changes from yellow to red, as shown in Figure 19 A. This change can be seen in the absorption spectra (black line in Figure 19 B) of the sample at 200 °C, where no peaks of the NPLs ca be found. In addition, the photoluminescence spectra of this sample (red line Figure 19 B), is totally flat. This shows the lack of photoluminescent particles in the sample and indicates that the seeds are destroyed.

As result, it is the case that 190 °C is the optimal temperature to extend the size of three ML NPLs. At this temperature, there is a large size extension and regular formed NPLs with sharp edges and less trap states are obtained.

4.1.4. Synthesis and characterisation of nanoplatelets for energy transfer experiments

4.1.4.1. Synthesis of the stock solutions containing NPLs with different lateral sizes

After finding the ideal reaction parameters, the stock solutions of the NPLs for the later FRET experiments were prepared. All performed NPLs synthesis which are described in this section are listed in Table 15.

Table 15: Summary of the NPLs discussed in section 4.1.4.

Experiment	Temperature	Seeds	Se-Precursor	Figure
NPL A	140 °C	-	Bis(stearoyl)selenide	Figure 20
NPL B	190 °C	NPL A	Se-ODE	Figure 21
NPL C	190 °C	NPL A	Se-ODE	Figure 22
NPL D	190 °C	NPL A	Se-ODE	Figure 23

To start with, a new batch of seeds is synthesised (NPL A). These seeds are used for the raw material for size extension and represent the smallest size NPLs for the energy transfer experiments. Spectra and TEM images of these seeds are shown in Figure 20.

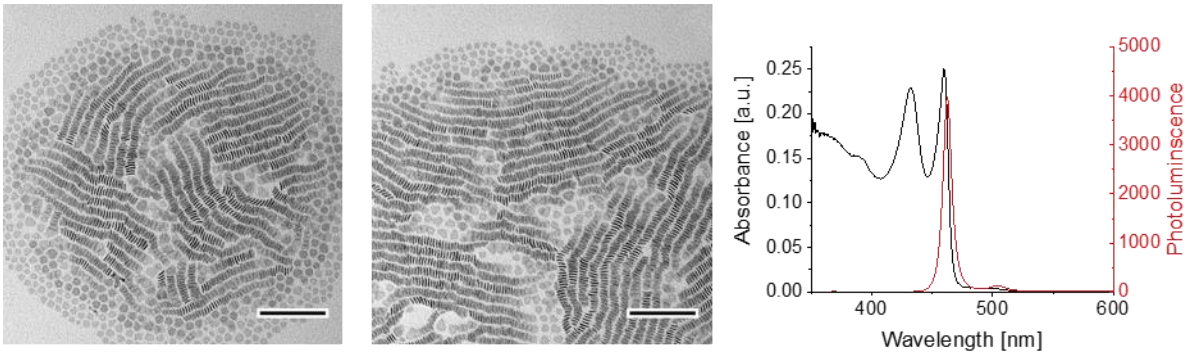

Figure 20: TEM images and spectral data of the seeds used for the synthesis of the final NPLs batches. In the following, they are named with NPL A. The scale bar in the TEM images corresponds to 100 nm.

As expected, small NPLs with an edge length of 12.2 ± 1.9 nm are obtained. The stacking indicates a small size distribution and the sharp peaks in the absorption and photoluminescence spectra (Figure 20) show the high quality of this batch of seeds.

For the following size extension, three separate syntheses were done. Different amounts of Se-ODE were added to achieve the different sizes. The amount of added Se-ODE was 0.05 mmol for NPL B, 0.10 mmol for NPL C and 0.15 mmol for NPL D. The results of these three syntheses are shown in Figure 21, Figure 22 and Figure 23.

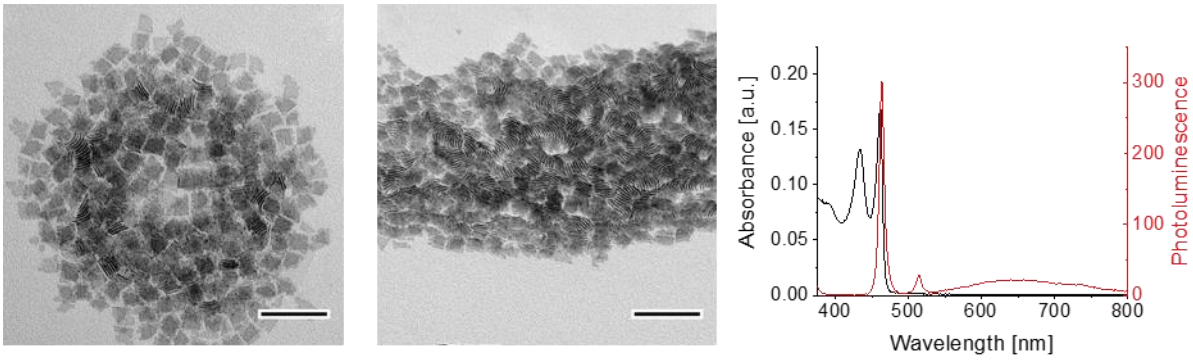

Figure 21: TEM images and spectral data of the smallest sized extended NPLs using 0.05 mmol Se. In the following, they are named with NPL B. The scalebar in the TEM images corresponds to 100 nm.

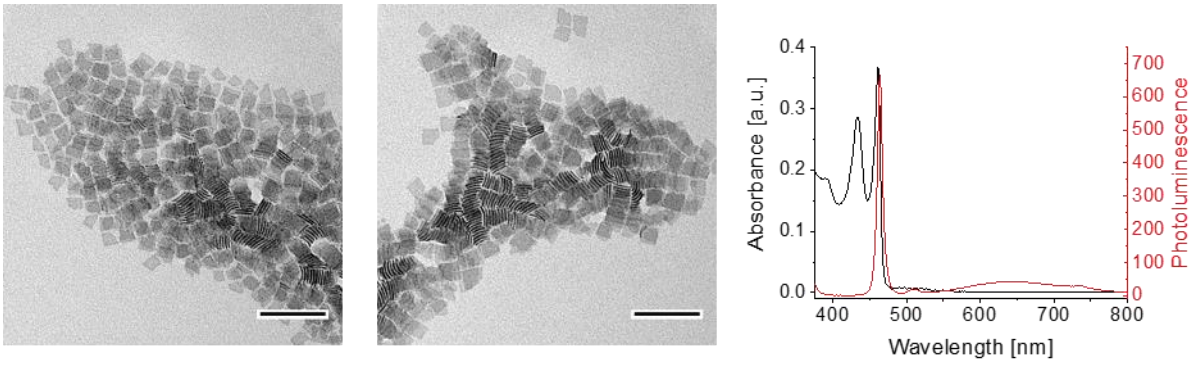

Figure 22: TEM images and spectral data of the middle sized extended NPLs using 0.10 mmol Se. In the following, they are named with NPL C. The scale bar in the TEM images corresponds to 100 nm.

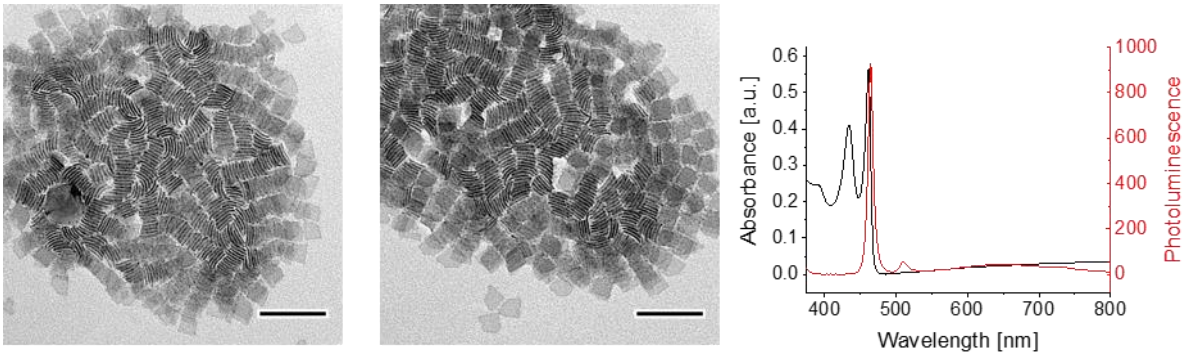

Figure 23: TEM images and spectral data of the largest sized extended NPLs using 0.15 mmol Se. In the following, they are named with NPL D. The scale bar in the TEM images corresponds to 100 nm.

Like in the experiments in section 4.1.3., the absorption spectra of the products (black line in Figure 21, Figure 22 and Figure 23) resulted in only three ML NPLs and no QDs nor other impurities. The photoluminescence spectra (red line in Figure 21, Figure 22 and Figure 23), show clear peaks at 462 nm and some trap states that increase with increasing the amount of Se-ODE. The increase of the trap states cannot be avoided completely.

For the batch NPL B, an anomalous event was observed where the temperature instead of staying at 105 °C increased quickly to 135 °C after degassing. Therefore, NPL B behaves differently from the other NPLs and cannot be used for the systematic energy transfer experiments in chapter 4.2.

The average size of the four NPLs in the stock solution can be found in Table 16. Surface areas is calculated under the assumption that the NPLs are quadratic.

Table 16: Edge length, and surface areas of the final NPLs.

Sample	NPL A	NPL B	NPL C	NPL D
Edge length / nm	12.24 ± 1.87	21.41 ± 3.66	24.47 ± 4.16	28.68 ± 4.01
Surface area / nm^2	149.8 ± 42.3	458.4 ±.143.3	598.8 ± 186.3	711.8 ± 103.2

4.1.4.2. Characterisation of the NPL stock solutions

After the successful synthesis of the NPLs, the NPLs must be characterised. This means to determine the quantum yield of the solutions, the concentration and the photoluminescence lifetime.

Quantum yield (QY)

The QYs of the NPLs are measured by a relative method. Therefore, a dye with known QY is used as reference. The dyes used are 9,10-diphenylanthracence (DPA), perylene and rhodamine 6G. To determine the QY of the NPLs, absorption and photoluminescence in different dilutions were measured for the NPLs and compared to the reference dyes. This was done with four different dilutions for each NPLs sample and each reference dye. For example, the photoluminescence spectra from 4 different dilutions of NPL A are shown in Figure 24 A. The corresponding absorption spectra are shown in Figure 24 B. For the reference dyes, only one photoluminescence spectrum is shown in Figure 24 C and the absorption spectrum is shown in Figure 24 D.

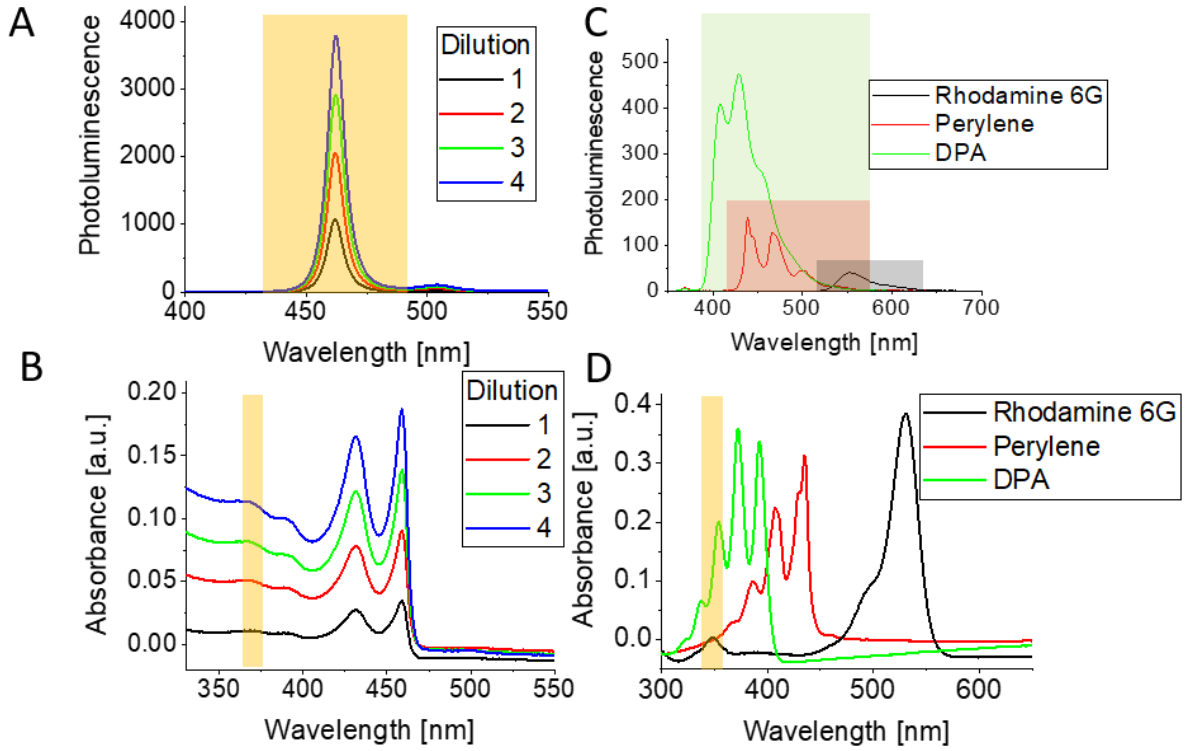

Figure 24: Determination of quantum yield. (A) Photoluminescence spectra of four different dilutions of NPL A. The yellow background represents the integrated area for the integrated photoluminescence. (B) Absorption spectra of the four dilutions of NPL A corresponding to the photoluminescence spectra in A. The yellow area represents the area of integration. (C) Photoluminescence spectra of the three used dyes and their area of integration showed with the different coloured backgrounds. (D) Absorption spectra of the three reference dyes and their area of integration showed with the yellow background.

To determine the QY, one must know how many photons are absorbed by the sample and how many come back as luminescence. To do this, the absorption in a range of 10 nm (FWHM of LED source) around the excitation wavelength (369 nm) is integrated for each sample. This area is marked by yellow areas in Figure 24 B and D. To determine the resulting photoluminescence, the whole peak of the photoluminescence must be integrated. This is shown by the yellow marking in Figure 24 A. For the dyes this is shown through their respective boxes in Figure 24 C. Once the integration values are quantified, the corresponding absorption and photoluminescence can be plotted (Figure 25).

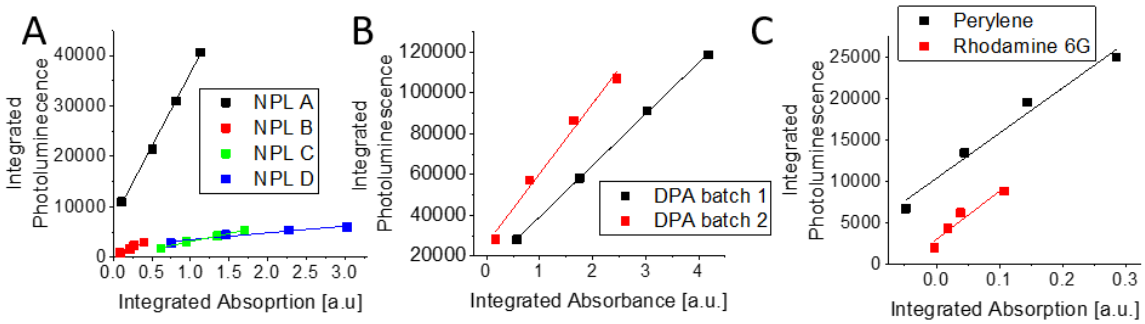

Figure 25: Plots shown the linear fits to determine the slope for the calculation of the quantum yield. (A) Plots for the slope of NPL A, NPL B, NPL C and NPL D. (B) Plots for the slope of the two different DPA batches. (C) Plots for the slope of perylene and rhodamine 6G. Remark that the integrated absorption is calculated smaller than zero for the lowest concentration of perylene. This arises from a baseline problem of the spectrometer for the low concentration of perylene.

As shown in the plots in Figure 25, there is a linear correlation between the absorption and photoluminescence at different dilutions. The data were fitted linearly to obtain slopes for each sample. The slopes for the dyes and their literature quantum yield is listed in Table 17. For the NPLs the slopes can be found in Table 18.

Table 17: Slope, literature quantum yield and used solvent for the different dyes, which are used.

Dye	DPA 1	DPA 2	Perylene	Rhodamine 6G
Slope	25277	34316	54731	58124
QY in Literature [41]	93%	93%	94%	95%
Solvents	cyclohexane	cyclohexane	cyclohexane	ethanol
n_D solvent	1.42623	1.42623	1.423623	1.3611

The quantum yield of the NPLs can be calculated by comparing the slope of the NPLs relative to the slope of the dye using the following equation:

$$\mathrm{QY_{NPL}} = \mathrm{QY_{Dye}} \cdot \frac{\mathrm{slope_{NPL}}}{\mathrm{slope_{dye}}} \cdot \left(\frac{\mathrm{n_{D,NPL}}}{\mathrm{n_{D,Dye}}}\right)^2 \tag{6}$$

Hereby n_D refers to the refractive index of the used solvents. The refractive indices of the solvents used to dissolve the dyes are listed in Table 17, while for the NPLs, hexane was used as the solvent (refractive index $\mathrm{n_{D,Hexane}} = 1.3272$). The resulting QYs for the NPLs measured relative to the different dyes are listed in Table 18.

Table 18: Slope and Quantum Yield for the final NPLs calculated with the different dyes.

Sample	NPL A	NPL B	NPL C	NPL D
Slope	29188	6921	3151	1346
QY DPA 1	99%	24%	11%	5%
QY DPA 2	73%	17%	8%	3%
QY perylene	46%	11%	5%	2%
QY Rhodamine 6G	48%	11%	5%	2%

The QYs obtained relative to DPA are inconsistent with the QYs obtained relative to perylene or rhodamine 6G. Therefore, the average QYs obtained from perylene and rhodamine 6G are taken as QYs of the NPLs. The size extended NPLs have a decreasing QY with increasing size, which agrees with observations reported in literature[11].

Concentration

The molar concentrations of NPLs of a certain size can be calculated from its absorption by comparing it to the number of Cd atoms present in the dispersion. The latter value can be obtained from inductively coupled plasma optical emission spectrometry (ICP-OES) and can be compared to the estimated number of Cd atoms present in a single NPL according to their crystal structure and size. According to experiments by Henry Halim, NPLs with an area of 121 nm^2 and an absorption of 9.355 a.u. have a concentration of $1.29 \cdot 10^{-6}\ \frac{\mathrm{mol}}{\mathrm{L}}$. This value is used as reference for the concentration calculation of differently sized NPLs. For four ML NPLs it is known that the absorption cross-section is linearly dependent to the area of the NPLs[11]. Assuming that this is also true for the three ML NPLs, the calculation is a simple proportional relation between the absorption of the NPLs in dispersion shown in Figure 26 and the concentration of the NPLs with respect of the size of the NPLs. This leads to equation 7.

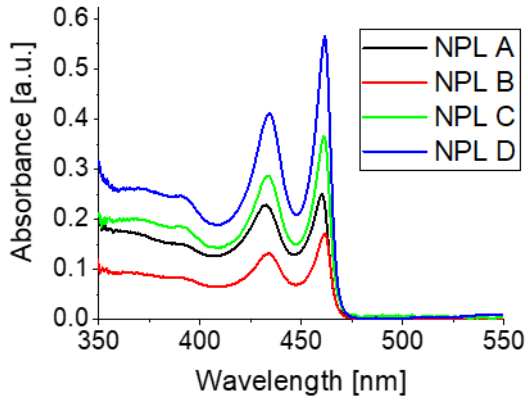

Figure 26: Absorption spectra of the stock solutions of NPL A, NPL B, NPL C and NPL D. 20 µL NPLs are diluted with 600 µL hexane.

$$\frac{c_{ref}}{ABS_{ref}} \cdot area_{ref} = \frac{c_{sample}}{ABS_{sample}} \cdot area_{sample} \tag{7}$$

If this equation is rearranged to c_{sample} the values for the concentration can be calculated. The results are shown in Table 19.

Table 19: Absorption and resulting concentration of the stock solutions of NPL A, NPL B, NPL C and NPL D.

Sample	Diluted Absorption / a.u.	Stock solution Absorption / a.u.	Area of a NPL / nm^2	Concentration of the NPL / 10^{-7} $\frac{\text{mol}}{\text{L}}$
NPL A	0.250	7.50	149.8 ± 42.3	8.4
NPL B	0.172	5.16	458.4 ±.143.3	1.9
NPL C	0.367	11.01	598.8 ± 186.3	3.1
NPL D	0.565	16.95	711.8 ± 103.2	4.0

The calculated concentrations based on equation 7 are plausible for NPL C and NPL D: 2 mL of the seed solution (NPL A) are used for each size extension and after the centrifugation, the resulting NPLs are re-dispersed in 5 mL hexane. Assuming a yield of 100% of the size extension, the concentration of NPL C and NPL D is expected as roughly $\frac{2}{5}$ of NPL A. Based on the measured absorption and size for NPL A, a concentration of $8.4 \cdot 10^{-7}$ $\frac{\text{mol}}{\text{L}}$ is calculated, as listed in Table 19. $\frac{2}{5}$ of this value is $3.4 \cdot 10^{-7}$ $\frac{\text{mol}}{\text{L}}$, which is near to the calculated concentration of NPL C and NPL D, see Table 19.

The same comparison doesn't work for NPL B. This confirms again, that for NPL B some mistakes were occurred during the synthesis, as described before.

With the calculation of the concentration of NPLs using equation 7, it is possible to adjust the amount of NPLs in the samples of the energy transfer experiments, see chapter 4.2.

Photoluminescence lifetime

For all four sizes of NPLs, the lifetimes of the photoluminescence of the NPLs are measured. The data and the fit are shown in Figure 27.

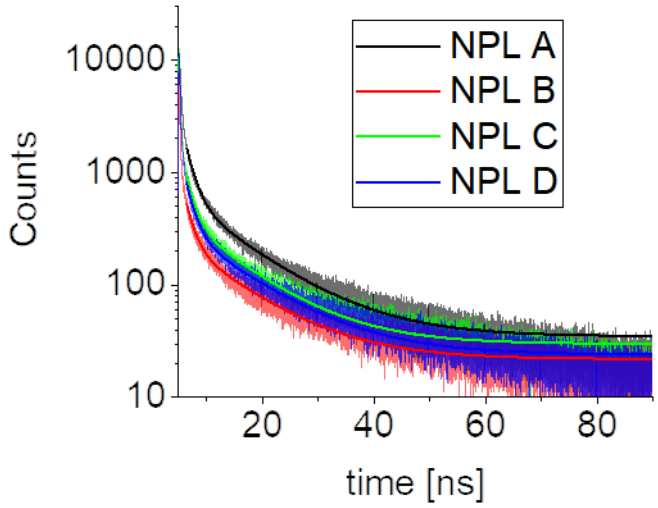

Figure 27: Determination of the lifetimes of the NPLs. Raw data (transparent line) and fit (solid line).

To fit the data a double exponential tail fit was applied. The equation is shown below:

$$I(t) = A_1 \cdot e^{-\frac{t}{\tau_1}} + A_2 \cdot e^{-\frac{t}{\tau_2}} \tag{8}$$

Hereby *A* is the amplitude, *t* the time and τ the lifetime.

The results of the fit are shown as solid line in Figure 27. The resulting lifetimes vary around 11 ns for τ_1 and around 1.5 ns for τ_2 for all NPLs, as listed in Table 20.

Table 20: Results of the fits for determination the photoluminescence lifetime of the NPLs.

Sample	NPL A	NPL B	NPL C	NPL D
τ_1 / ns	11.101	10.913	10.498	11.567
τ_2 / ns	1.575	1.432	1.377	1.492

The data in Table 20 show that the size of the NPLs does not influence the lifetimes τ_1 and τ_2 of the NPLs' luminescence. In other words, the lifetime of the exciton is independent from the size of the NPLs. The lifetime data is necessary to determine the FRET efficiency as discussed in section 4.2.6.

Summary of the values characterising NPL A – NPL D

All values characterising NPL A – NPL D are summarised in Table 21.

Table 21: Summarized values which characterised the NPLs used in the following energy transfer experiments.

Sample	NPL A	NPL B	NPL C	NPL D
Concentration of the NPL / 10^{-7} $\frac{\text{mol}}{\text{L}}$	8.4	1.9	3.1	4.0
QY	47%	11%	5%	2%
τ_1 / ns	11.101	10.913	10.498	11.567
τ_2 / ns	1.575	1.432	1.377	1.492
Edge length / nm	12.24 ± 1.87	21.41 ± 3.66	24.47 ± 4.16	28.68 ± 4.01
Surface area / nm2	149.8 ± 42.3	458.4 ±.143.3	598.8 ± 186.3	711.8 ± 103.2

4.2. Energy transfer Experiments

Introduction to the FRET experiments

In this chapter, the energy transfer between the photocatalyst dye Th-BT-Th-COOH and the NPLs is discussed. Absorption and photoluminescence spectra of the dye are shown in Figure 28 A. The dye was synthesised by Niklas Huber within our department[12]. We have chosen the combination of the three ML NPLs since there is a good overlap between the photoluminescence of the NPLs and the absorption of the dye (Figure 28 B). According to Förster's theory, this would be favourable for efficient energy transfer.

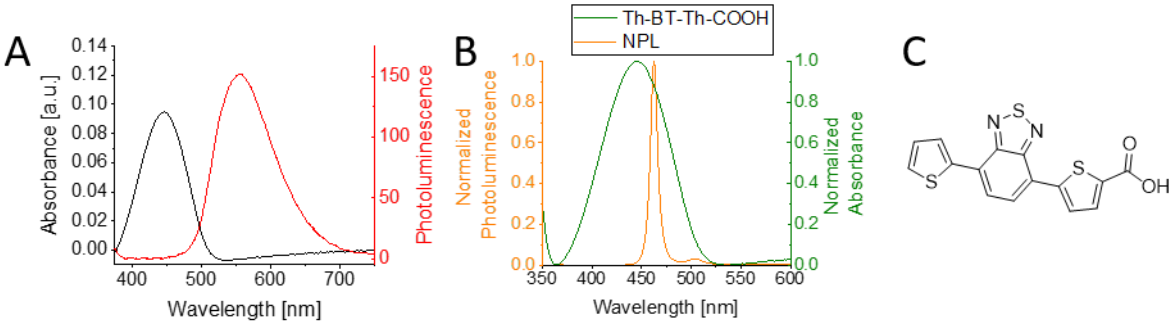

Figure 28: (A) Absorption and photoluminescence of the dye Th-BT-Th-COOH used for the energy transfer experiments. (B) Normalized photoluminescence spectra of the NPLs and normalized absorption spectra of the dye to show the spectral overlap according to the Förster theory. (C) Structure formula of Th-BT-Th-COOH.

In the following analysis only NPL A, NPL C und NPL D are used. NPL B shows a not reproducible behaviour if dye is added. Probably defects in the crystal structure resulting from the temperature problems during the synthesis (see section 4.1.4.1.) lead to this behaviour. To avoid inconsistent data in this study, the results from NPL B are not used in this work.

4.2.1. Adding dye versus direct mixing

In earlier works for each dye concentration a new mixture of NPLs and dye was prepared. This procedure burns a lot of NPLs' stock solution. To save NPLs' stock solution, the idea is, to start with the lowest dye concentration in the NPL-dye mixture and to add step by step more dye to this solution. If this way would lead to the same results as with the common method, a lot of NPLs' stock solution could be saved. In the further work, the common method is called "many cuvettes" and the new procedure is called "one cuvette".

To find out if both methods leads to the same results a comparison between both methods was done using NPL A. The results are shown in Figure 29.

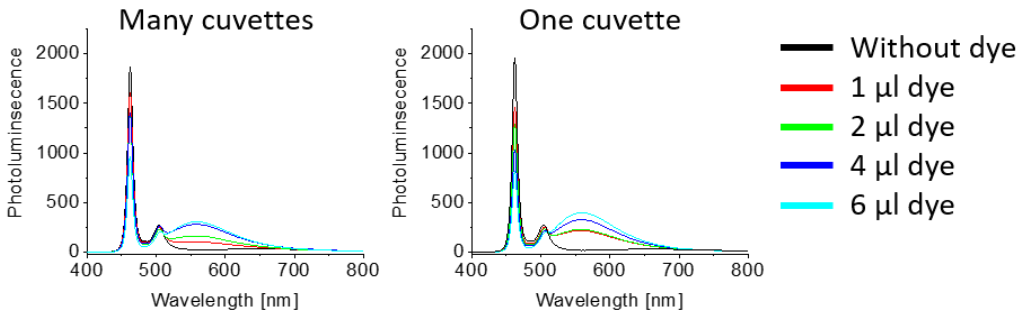

Figure 29: Comparison of the photoluminescence spectra resulting of different sample preparing strategies. (A) Making for every measured concentration of dye a new sample. (B) Using one cuvette and an amount of dye, measuring and adding more dye in the same cuvette. NPL A was used in the experiments.

As shown in Figure 29, both methods do not show a significant difference of behaviour for peaks corresponding to the NPLs at 462 nm nor the dye at 565 nm. For both methods the photoluminescence at 462 nm is decreased from around 2000 counts without dye (black line) to 750 counts after adding 6 µl of dye (turquoise line). Meanwhile the peak at 565 nm increases for both methods with a comparable maximum value of 300 counts (turquoise line). This shows that the "one cuvette method" is equivalent to the "many cuvettes method". Because the "one cuvette method" requires less material, it is used in the following experiments.

4.2.2. Kinetics of the nanoplatelet-dye binding

An ideal NPL-dye system would require that all dye molecules added to the NPL dispersion bind to the NPL surface, ensuring optimal conditions for FRET. To assess this, the photoluminescence for the NPLs at 462 nm and for the dye peak at 565 nm was measured over the time period of 10 min after dye addition. Each experiment was repeated 2 times (dotted lines and solid lines). The amount of dye added here was higher compared to the one in section 4.2.1. in order to have a higher photoluminescence signal at 565 nm. The results are shown in Figure 30.

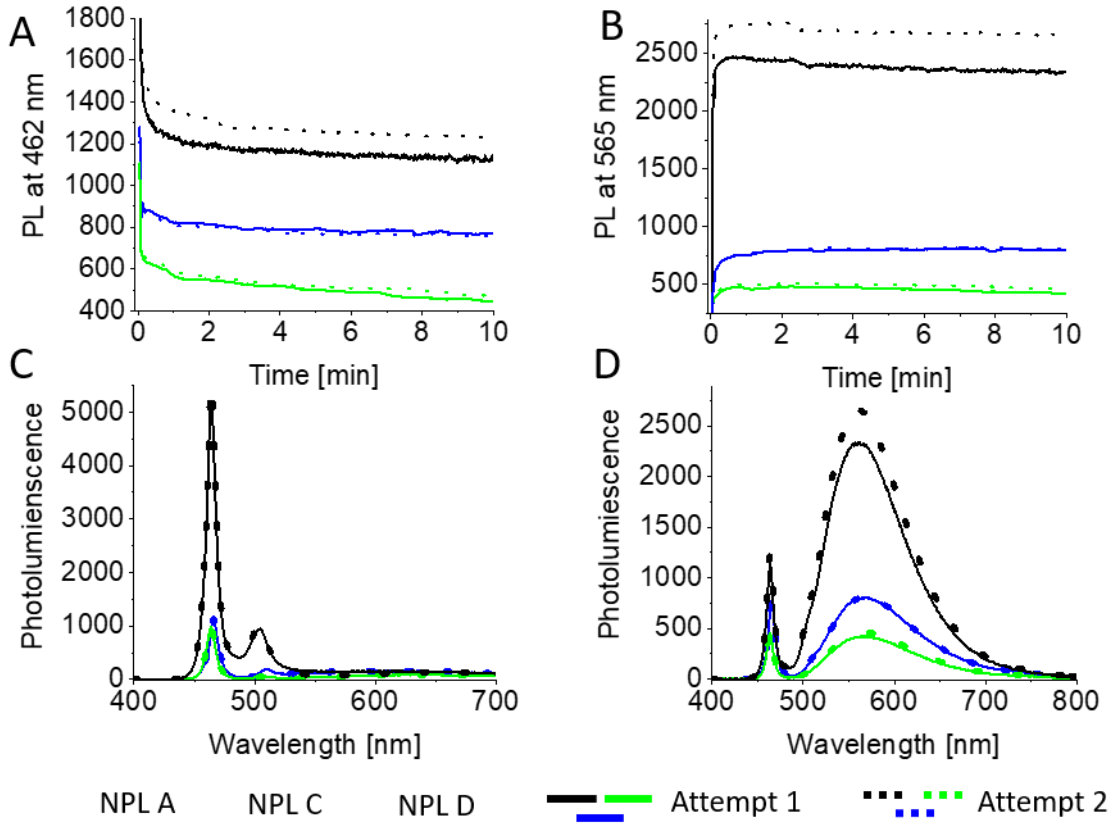

Figure 30: Results of experiments show the behaviour of the photoluminescence peak intensities over time after adding dye to the NPLs. The dotted line represents the reproduction of the experiment showed as solid line. (A) Photoluminescence behaviour of the Peak at 462 nm and (B) of the Peak at 565 nm over time. (C) Photoluminescence spectra of the sample before adding the dye and (D) after recording the time trace.

As it is shown in Figure 30 C (before the dye is added) and Figure 30 D (10 min after the dye is added), the photoluminescence decreases at 462 nm and increases at 565 nm. In Figure 30 A the behaviour of the photoluminescence peak intensity at 462 nm over time is shown. In all cases, the NPLs' photoluminescence peak rapidly decreases after addition of the dye. After approximately one minute the photoluminescence signal stays almost constant.

For the dye photoluminescence at 565 nm (Figure 30 B) a sharp rise is observed after adding the dye to the NPLs. The maximum value is reached after approximately one minute, which agrees with the data at 462 nm. After one minute, the photoluminescence values stay roughly the same.

Form the experimental data it can be concluded that the dye binds the surface of the NPLs and that this happens rapidly. To verify the assumption, that the dye binds to the surface of the NPLs, ITC (Isothermal titration calorimetry) measurements were performed. The results are shown in Figure 31.

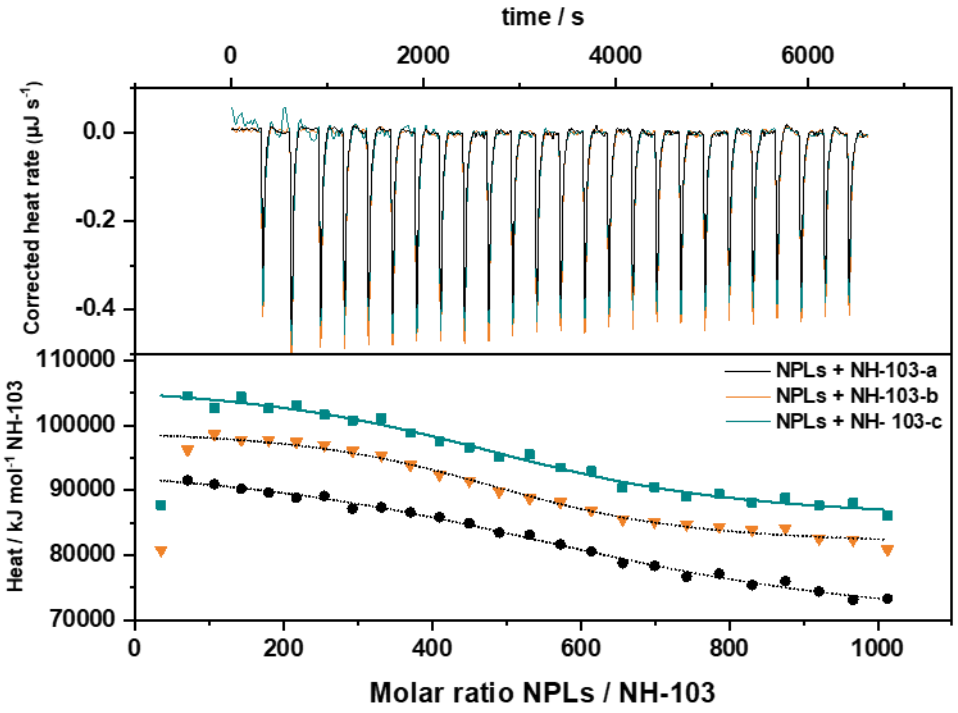

Figure 31: ITC results of the dye Th-BT-TH-COOH (here abbreviated with NH-103) with 4 ML NPLs. For this experiment, four ML NPLs with a lateral size of 480 nm² are used. Henry Halim prepared the samples of this experiment, Dr. Maria Martinez Negro did the experiment.

The data in Figure 31 show three titrations of the dye with four ML NPLs. Because of the similar chemical properties between three and four ML NPLs this does not make a huge difference for these experiments. Due to the poor solubility of the dye, the expected sigmoidal form of the data (Figure 31, bottom) is not pronounced. Nevertheless, it is possible to estimate the maximum surface coverage of a NPL with the dye n and the dissociation constant K_d for the dye on the NPL surface by fitting the data points. Since the surface area of the NPLs is known (960 nm²), the amount of dye per nm² at maximum coverage can be calculated. These values are presented in Table 22.

Table 22: Calculated results of the ITC measurements, shown in Figure 31. Calculation was done by Dr. Maria Martinez Negro.

	NPLs + dye - a	NPLs + dye - b	NPLs + dye - c	Average
K_d / 10^{-6}	2.95	1.90	1.19	2.0 ± 0.7
n	675.1	542.5	516.9	578 ± 69
Max. dye per nm²	0.703	0.565	0.538	0.602

The results of the ITC measurements in Table 22 show a very low dissociation constant K_d for the NPL-dye binding. Beside this, it is found, that the maximum coverage of the NPLs' surface is reached at ~0.6 dye/nm². The low dissociation constant is an indication, that the dye molecules which are

attached to the surface of the NPLs do not remove from there. Therefore, we can assume that all dye molecules will bind to the NPLs' surface until there is no free surface area available anymore. The measurements validate this assumption.

4.2.3. Energy transfer at constant concentration or constant absorption of nanoplatelets

In the following two sections, the energy transfer between the dye and the different sized NPLs is investigated in two different ways:

- The first way focuses on a constant concentration of the different sized NPLs. This is equivalent to constant molar ratio between NPLs and dye.
- In the second way, the absorption of the different sized NPLs is kept constant. This implicates a constant surface of the different sized NPLs.

Both ways are shown as scheme in Figure 32.

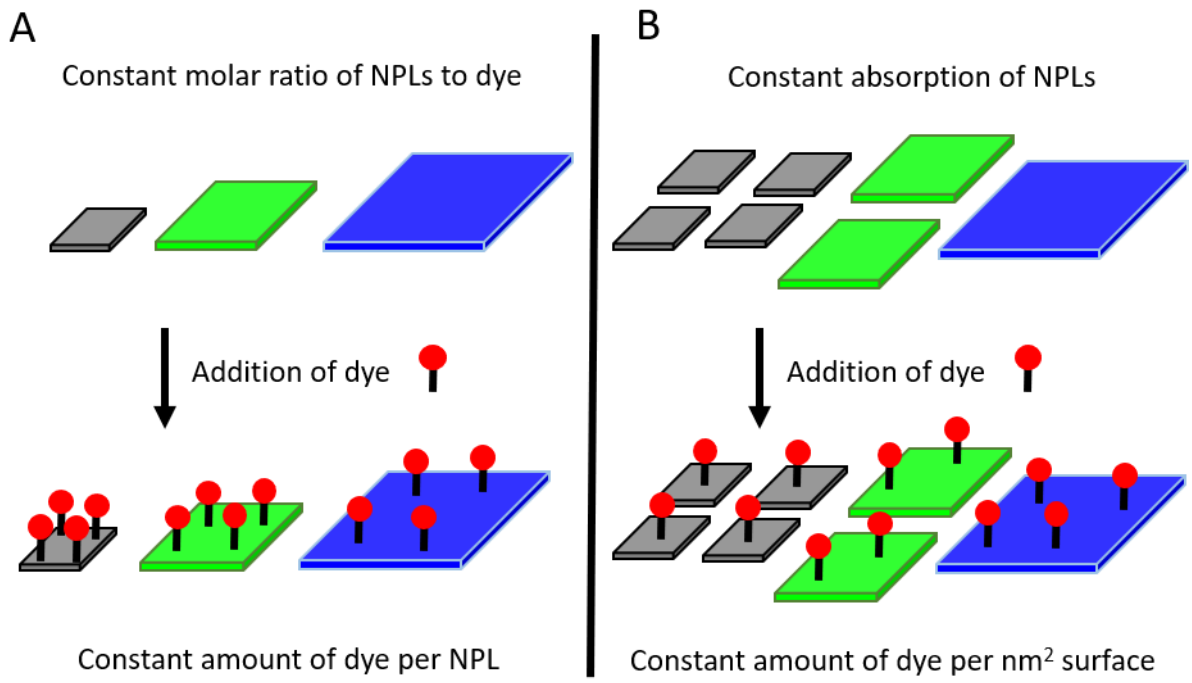

Figure 32: Scheme to show the two ways of energy transfer experiments. The smallest NPLs are black, the medium sized NPLs green and the large sized NPLs are blue. (A) Scheme using a constant molar ratio respectively a constant concentration of NPLs. (B) Scheme using a constant surface of NPLs, which leads directly to a constant absorption of the NPLs.

In the first way, the molar ratio between NPLs and dye respectively the concentration of NPLs is kept constant for all different sized NPLs, see the scheme in Figure 32 A. If dye is added to this samples with a constant concentration of NPLs, the amount of dye per NPL is kept constant for the different sized NPLs. Because different sized NPLs are used, the available surface and therefore the surface coverage differs between the samples of the NPLs and is highest for the smallest NPLs and lowest for the largest NPLs (see Figure 32 A).

In the second way, the number of absorbed photons for the different sized NPLs is kept constant. To ensure this, the absorption of the three different sized NPLs was fixed by adjusting the concentration of the NPLs in the samples. This resulted in constant available surface for all three NPLs because the absorption cross section is linearly correlated to the surface area of the NPLs, as mentioned in literature[4]. This is shown as scheme in Figure 32 B. Here the available surface of all NPLs is the same. For this reason, in these experiments the amount of dye per nm^2 on the surface of the NPLs is constant.

4.2.3.1. Experiments at constant concentration of NPLs

In Figure 33, the results of the experiments with constant concentration of NPLs is shown.

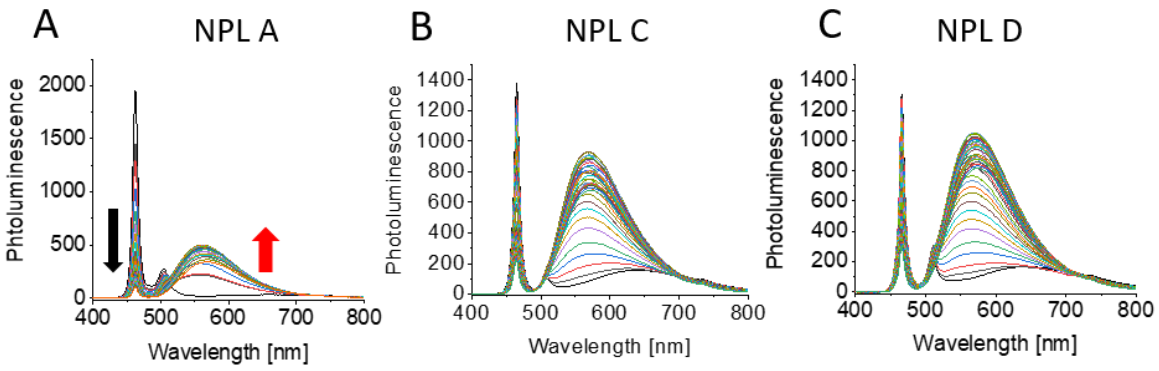

Figure 33: Series of photoluminescence spectra with increasing amount of added dye (Exp. con. 1). Photoluminescence spectra for (A) NPL A, (B) NPL C and (C) NPL D.

For all sizes of NPLs, the peak of the NPLs at 462 nm decreases with increasing amount of dye. The photoluminescence of the dye increases by increasing the dye as expected.

The maxima at 462 nm and at 565 nm are plotted against the amount of added dye solution. As an example, this is shown in Figure 34 for NPL batch A.

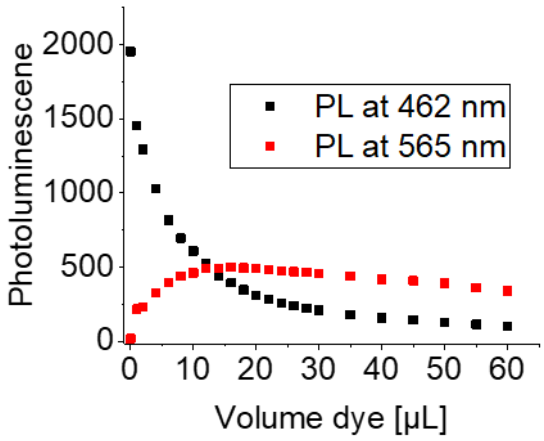

Figure 34: The maximum photoluminescence values of the peaks at 462 nm and 565 nm in the spectra in Figure 33 A plotted against the corresponding amount of volume dye added to a sample of NPL A.

The amount of dye per NPL can be calculated from the know concentration of NPLs and dye in the mixture. For the experiments shown in Figure 33, same ratios of dye per NPL were used. These samples were then compared with each other in terms of absorption and photoluminescence (Figure 35).

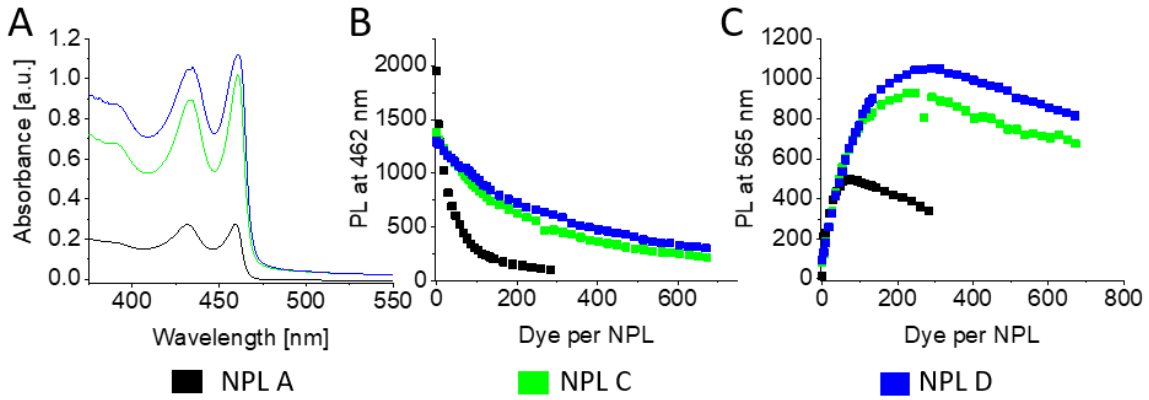

Figure 35: Comparison of the behaviour of the energy transfer using a constant concentration of NPLs (Exp. con. 1). (A) Absorption spectra of the samples. (B) Values for the photoluminescence at 462 nm while increasing amount of dye. (C) Values for the photoluminescence at 565 nm while increasing the amount of dye.

As expected, at constant NPLs' concentration, the absorption of the NPLs increases with the lateral size (Figure 35 A). This is related to the absorption cross section, which increases with the size of the NPLs[11]. The photoluminescence peak of the NPLs at 462 nm decreases with increasing the amount of dye as shown in Figure 35 B. However, the slopes of the photoluminescence decrease are different for the differently sized NPLs. For the smallest NPLs (NPL A, black dots) the decline is the steepest and for the largest NPLs (NPL D, blue dots) it is less steep. The measured values for the photoluminescence of the three NPLs without dye and (for instance) at 200 dye per NPL are listed in Table 23.

Table 23: photoluminescence values for the different sized NPLs without dye and with 200 dyes per NPL, data from Figure 35 B.

Sample	NPL A	NPL C	NPL D
Photoluminescence without dye	1953	1379	1303
Photoluminescence at 200 dye per NPL	148	630	724

The observation can be explained by the available surface for each sample. At the same particle concentration, the available surface area for NPL D is 4.8 times larger than the available surface area for NPL A. If we fix the dye:NPL ratio, then this leads to the result, where the probability of a dye to be near to an exciton is highest in the sample of NPL A. The behaviour of the photoluminescence at 462 nm can also be confirmed by looking at the behaviour of the dye photoluminescence at 565 nm (Figure 35 C). The increase of the dye's photoluminescence is greater by using the large NPLs (NPL D, blue dots) because more surface is available. For this reason, more dye is necessary to reach the same surface coverage as for the small NPLs and the same medium distance to an exciton. Concretely, for NPL C round four times more dye is necessary to have the same surface coverage as NPL A, for NPL D even round 5 times more dye is necessary to reach the same surface coverage as NPL A.

For differently sized NPLs, the maximum intensity for the dye emission changes. In addition, when larger NPLs are used, more dye per NPL is necessary to reach this maximum. This increase of the photoluminescence of the dye is contrary to the expectation, considering that the QY of the NPLs is relatively low when laterally larger (approx. 50% for NPL A and 10% for NPL C). In addition, the loss of NPL photoluminescence for the large NPLs is smaller than the gain of photoluminescence for the dye. This indicates that the FRET can occur efficiently even for NPLs with low QY.

It was also expected that the photoluminescence of the dye would reach a maximum and retain their intensity as more dye is added, i.e. when the total surface area is covered with dye, since the dye does

not absorb at the excitation wavelength (369 nm). However, the photoluminescence decreases after reaching a maximum. This behaviour suggests that self-quenching between the dyes also plays a role[42]. It can be observed that the self-quenching between the dyes starts at different dye:NPL ratios, depending on the size of the NPLs. For the large NPLs, the quenching occurs at higher amounts of dye per NPLs. This is expected because for large NPLs it should be possible to add more dye to the surface, before they are close enough to self-quench.

To continue the investigation, the data were verified by repeating the experiment under the same conditions. In addition to the experiment shown in Figure 35, the lifetime of the NPLs at 462 nm and of the dye at 565 nm was measured. The behaviour of the lifetimes is a second method to observe the energy transfer behaviour between NPLs and the dye.

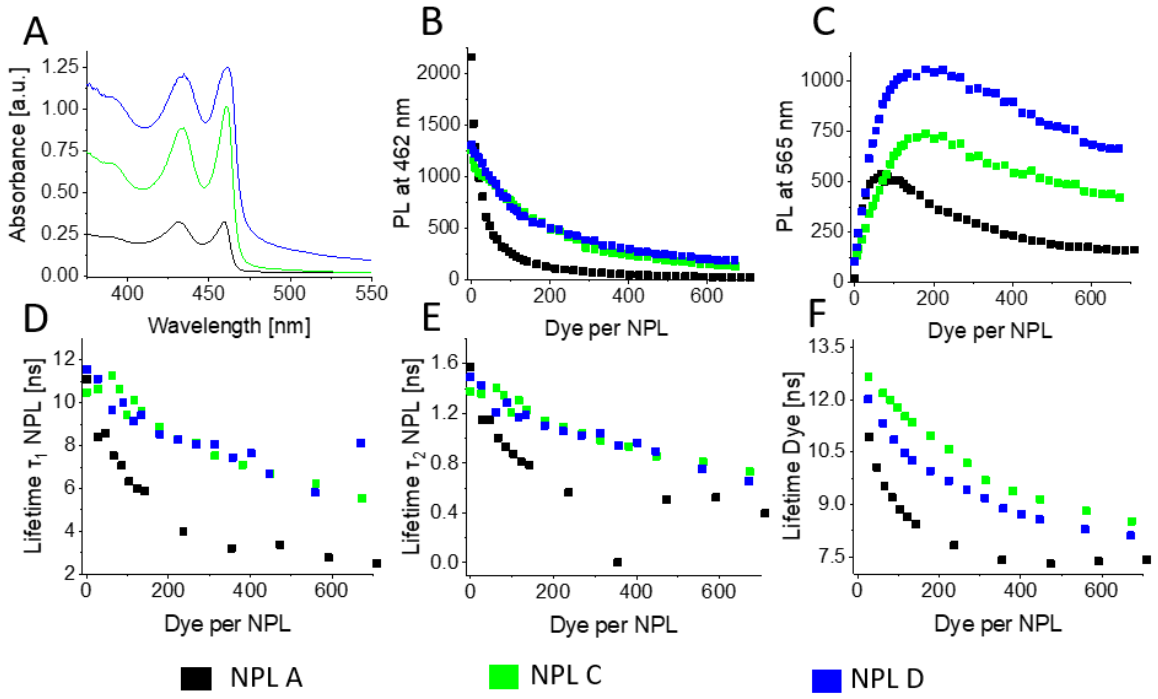

Figure 36: Reproduction of the experiments using a constant concentration of NPLs (Exp. con. 2). (A) Absorption spectra of the samples. (B) Values of the photoluminescence at 462 nm while increasing the amount of dye. (C) Values for the photoluminescence at 565 nm while increasing the amount of dye. (D) Lifetime τ_1 of the NPLs while increasing the amount of dye. (E) Lifetime τ_2 of the NPLs while increasing the amount of dye. (F) Lifetime of the dye while increasing the amount of dye.

The steady state absorption and photoluminescence results from this experiment (Figure 36) agrees with the results of the previous (Figure 35).

The lifetime of the NPLs at 462 nm and the dye at 565 nm are measured while increasing the amount of dye. To fit the data, equation 8 is used for the NPLs and the following equation 9 is used for the dye:

$$I(t) = A_1 \cdot e^{-\frac{t}{\tau}} \tag{9}$$

To show the behaviour of the lifetimes, they are plotted against the value of dye per NPL. For the NPLs, two lifetimes are obtained. *τ1* is shown in Figure 36 D and *τ2* in Figure 36 E. Both lifetimes show the same behaviour: the lifetimes get shorter when more dye is added. The decrease of the photoluminescence at 462 nm matches well with the decrease in lifetimes. The smallest NPLs have the steepest decrease (black dots, Figure 36 D and Figure 36 E), while NPL C and NPL D (green and blue

dots) show quite similar steepness in their decrease. The decrease in the lifetime and the photoluminescence is comparable and confirms the energy transfer behaviour.

However, the lifetime behaviour of the dye is different from their photoluminescence behaviour. After looking at the photoluminescence of the dye (Figure 36 C), it would be expected that the lifetime increases to a maximum and decreases when self-quenching starts to become significant. But the experimental data did not confirm this behaviour. In Figure 36 F is shown, that the lifetime of the dye decreass analogous to the lifetime of the NPLs. This behaviour is in opposite to the Förster theory and the experimental data of the photoluminescence of the dye. This behaviour will be discussed in detail in section 4.2.4.

4.2.3.2. Experiments at constant absorption

For further studies of the energy transfer behaviour, the absorption of the samples was fixed. Thus, in contrast to the experiment above, the total available surface is the same for all NPL samples. For reaching this, the concentrations of NPLs in the samples have to be adjusted. Here, the photoluminescence and lifetime data are plotted against the number of dye molecules per nm^2. The results of these experiments are shown in Figure 37.

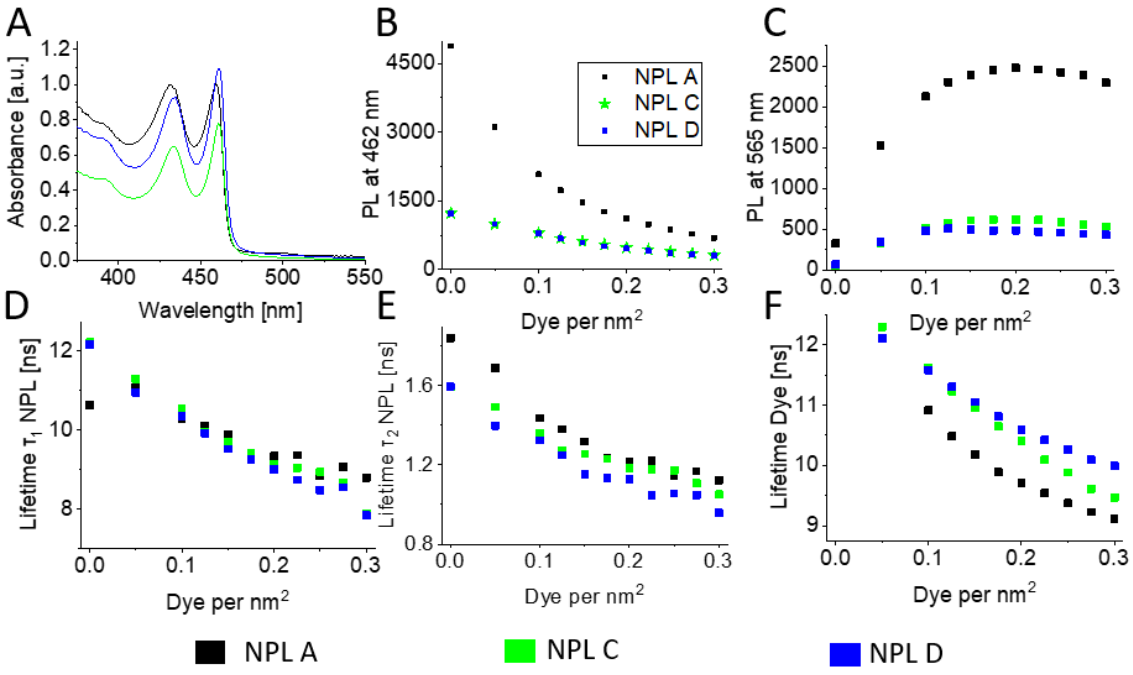

Figure 37: Experiments by constant absorption for the samples (Exp. abs.). (A) Absorption spectra of the samples. (B) Photoluminescence value of the NPLs at 462 nm. NPL C and NPL D have quite similar values. Therefore, the values for NPL C are painted as stars. (C) Photoluminescence value at 565 nm while increasing amount of dye. (D) Lifetime τ_1 of the NPLs while increasing the amount of dye. (E) Lifetime τ_2 of the NPLs while increasing the amount of dye. (F) Lifetime of the dye while increasing the amount of dye.

The absorption spectra (Figure 37 A) show similar absorption for all NPLs. NPL C (green line) shows slightly lower absorption, but this deviation is tolerable. From the photoluminescence data, shown in Figure 37 B, the slope of the smallest NPL A (black dots) appears to be the steepest. For NPL C and NPL D (green stars respectively blue dots) the values are very similar. This leads to the hypothesis that the energy transfer efficiency is highest for the smallest NPLs if the relation dye/nm² is the same. It is possible to confirm this result by looking at the photoluminescence behaviour of the dye in Figure 37 C.

For the photoluminescence of the dye, shown in Figure 37 C, the gain of the photoluminescence is the largest for the smallest NPL A. NPL A has the highest photoluminescent QY of all three samples. Because the amount of photons absorbed for all three different sized NPLs is equal, the number of photons, which can do energy transfer is the highest for the smallest NPLs. This assumes that the dark states in the NPLs decay 'too quickly' before being able to participate in FRET. Therefore, the probability of energy transfer is lower for the larger NPLs, because larger NPLs have a lower QY and contain more dark states.

In Figure 37 C the maximum value for the dye's photoluminescence can be observed at 0.2 dye per nm^2 which does not correspond to a full coverage of the NPLs' surface (0.6 dye per nm^2). The appearance of the maximum photoluminescence at a coverage of NPLs surface around 0.2 nm^2 points to self-quenching of the dye at high surface coverage and will be further discussed in chapter 4.2.5.

As in the experiment with constant concentration, the lifetimes are recorded to compare the lifetime behaviour with the photoluminescence behaviour. For the lifetimes of the NPLs (Figure 37 D and E) the lifetime decreases with increasing dye coverage from 0 to 0.3 dye per nm^2, which agrees with the energy transfer. The slopes for the decrease of lifetimes are all quite equal for the three NPLs. This contrasts the results from the steady state photoluminescence measurements of the NPLs, where only the slopes for NPL C and NPL D were equal, while the slope for NPL A is steeper. For the lifetime of the dye (Figure 37 F), the decrease is also quite equal for the three NPL sizes, only for NPL A the decrease is marginally steeper.

Once again, it can be observed that there is a difference in the behaviour between the lifetime and the photoluminescence of the dye. This difference will be the topic of section 4.2.4.

4.2.4. Different behaviour of the photoluminescence and the lifetime of the dye

As mentioned before, the behaviour of the photoluminescence of the dye and the lifetime of the dye does not match. Figure 38 shows the measured lifetime and photoluminescence of the dye for both experiments.

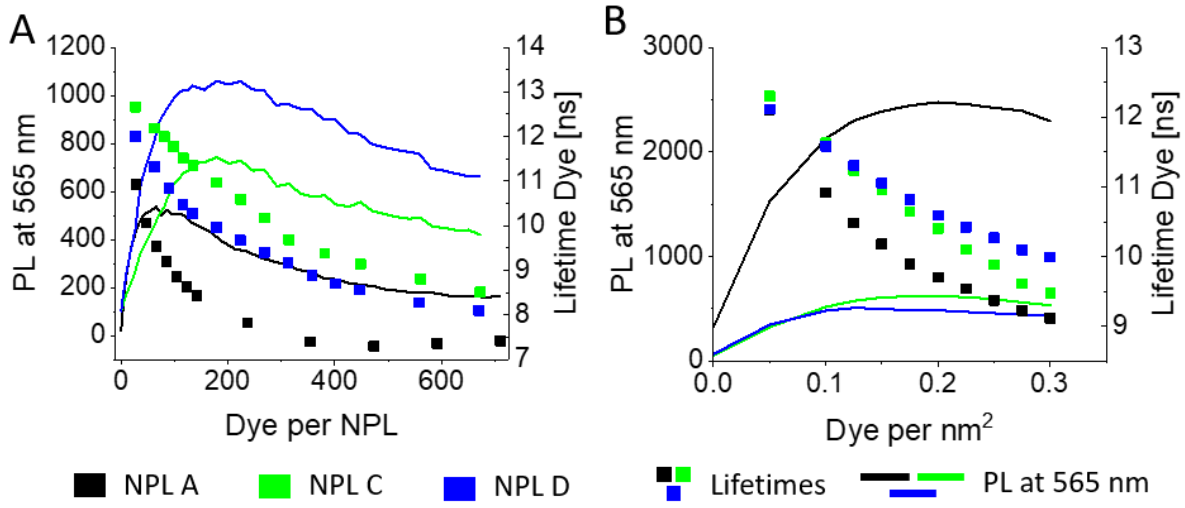

Figure 38: Difference in the behaviour for the photoluminescence and the lifetime of the dye. (A) Values for the photoluminescence of the dye at 565 nm (lines, left scale) and lifetimes (dots, right scale) while increasing the dye concentration. Data from the experiment Exp. con. 2, compare Figure 36 C and F. (B) Values for the photoluminescence of the dye at 565 nm (lines, left scale) and lifetimes (dots, right scale) while increasing the dye concentration. Data from the experiment Exp. abs., compare Figure 37 C and F.

Clearly, there is no apparent correlation between the two curves. It seems to be the case that the lifetime has a lower limit of $\tau = 7$ ns, but it does not correspond to the maximum photoluminescence. This is best visible for NPL A (black dots), but it is also visible for the other two NPLs samples (blue and green dots).

The lower limit of the lifetime found in Figure 38 A cannot be reproduced in Figure 38 B, because the amount of dye added in the experiment does not reach the amount needed to reach the minimum lifetime.

The decrease of lifetime at 565nm at high dye coverage tend to indicate quenching of the luminescence[34]. It is possible that quenching has a larger influence in the lifetime than the increase expected by FRET. So, in the lifetime, quenching dominates and a decrease of the lifetime with increasing amount of dye is observed. On the other hand, in the photoluminescence at 565 nm, a maximum is reached before it decreases again at higher dye concentrations (see Figure 38). However, the reason for the different behaviour of photoluminescence and lifetime needs further research.

4.2.5. Behaviour of the photoluminescence of the dye

In the previous section it was found that the photoluminescence of the dye reaches a maximum by roughly 0.2 dyes per nm^2. To compare the photoluminescence of the dye and analyse this maximum for all experiments, the dye photoluminescence values are plotted against the amount of dye per nm^2. This is shown in Figure 39.

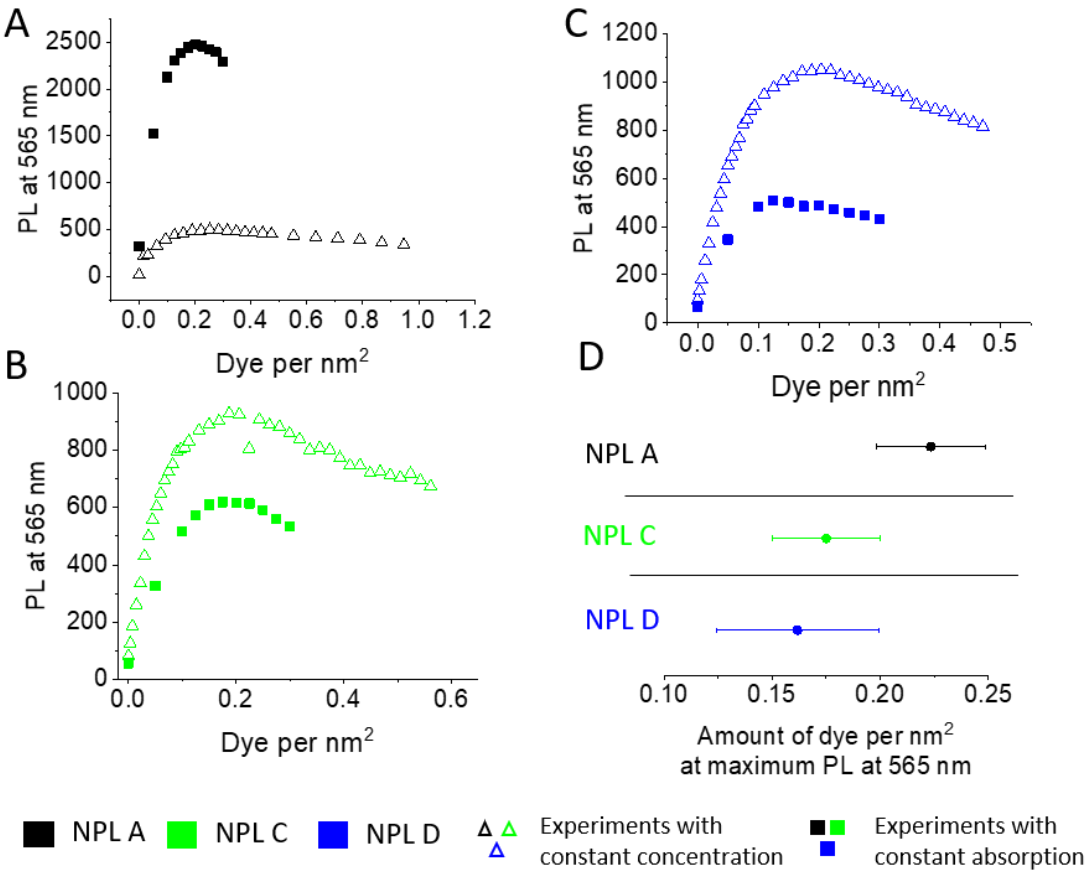

Figure 39: Comparison of the photoluminescence behaviour from the dye while increasing the concentration of dye in the different experiments. Triangles present experiment by constant concentration of NPLs and squares present the experiment by constant absorption. The photoluminescence value of the dye (A) from NPL A, (B) from NPL C and (C) from NPL D. (D) Comparison of the maximum value for the dye Photoluminescence corresponding to the packing rate of the surface of the NPLs for all sort of NPLs which are used.

For all types of experiments, the maximum photoluminescence is found roughly at a similar ratio of dye per nm^2. The number is slightly higher for the smaller NPLs, possibly due to the case where the dye binds to the side of the NPLs instead of the top. One thing to note is that the maximum photoluminescence of the dye also reaches maximum values in the same order of magnitude which shows the consistency of the results.

A possible reason why the photoluminescence of the dye decreases after the maximum point may be due to self-quenching and re-absorption[43]. As shown in Figure 28 A, the absorption and photoluminescence spectra of the dye have a small overlap. If the surface coverage is high, it is more likely that two dyes can be near each other. In this case, an energy transfer between the two dyes can happen, leading to self-quenching. Alternatively, the overlap of the absorption and photoluminescence spectra of the dye can lead to reabsorption of photons by the dye.

To show, that the energy transfer between the dyes seems to be the most plausible way for the self-quenching, the average distance of two dyes on the surface of the NPLs was calculated. Here, it was assumed that the distribution of the dyes is statistical.

The average amounts of dye per nm^2 at maximum photoluminescence at 565 nm (ave. dye coverage at max. PL) for each different sized NPL plotted in Figure 39 D are listed in Table 24. Using the surface area of the NPLs (see Table 16), the average space per dye can be calculated. The root of this space gives the average distance between two dyes on the surface of the NPLs. Both values are also listed in Table 24.

Table 24: Average amount of dye per nm^2 at maximum photoluminescence at 565 nm (ave. dye coverage at max. PL), the surface size of the NPLs, the average surface size per dye and the average distance between two dyes calculated for the NPL A, NPL C and NPL D.

Sample	NPL A	NPL C	NPL D
ave. dye coverage at max. PL	0.22	0.18	0.16
Surface size / nm^2	149.8	598.8	711.8
Surface size per dye / nm^2	4.54	5.5	6.25
average distance between two dyes	2.1	2.3	2.5

For the system of Th-BT-TH-COOH and NPLs, the Förster radius R_0 was calculated to be around 5 nm[44]. As shown in Figure 8, the efficiency of the energy transfer depends strongly of the distance between donor and acceptor. As shown in Table 24 the average distance between two dyes at maximum photoluminescence of the dye is smaller than the Förster radius of the dye. For the self-quenching of the dye, it is crucial that the average distance between two dyes is about 2 nm for improved interaction. Re-absorption is less dependent with regard to distance. Because of the dependence on the average distance between the dyes and the self-quenching, energy transfer seems to be the most plausible mechanism for the self-quenching. Therefore, covering the NPLs fully with dyes should be avoided in order to avoid self-quenching. If the surface is fully covered (0.6 dyes per nm^2) the average distance between two dyes is around 1.3 nm. This should lead to a high amount of quenching.

4.2.6. Energy transfer efficiency

To analyse the energy transfer, the FRET efficiency can be calculated. This can be done in two ways, either through the decrease of the photoluminescence of the NPLs or through the decrease of the lifetime of the NPLs. Both are done and shown in the following sections.

Energy transfer efficiency using photoluminescence of the NPLs

To calculate the energy transfer with the photoluminescence of the dye, the following equation can be used:

$$\text{FRET efficiency} = 1 - \frac{\text{PL}_{\text{with dye}}}{\text{PL}_{\text{without dye}}} \tag{10}$$

For the photoluminescence values, the maximum values at 462 nm are used. The values are plotted against the amount of dye per nm^2 and against the amount of dye per NPL (Figure 40).

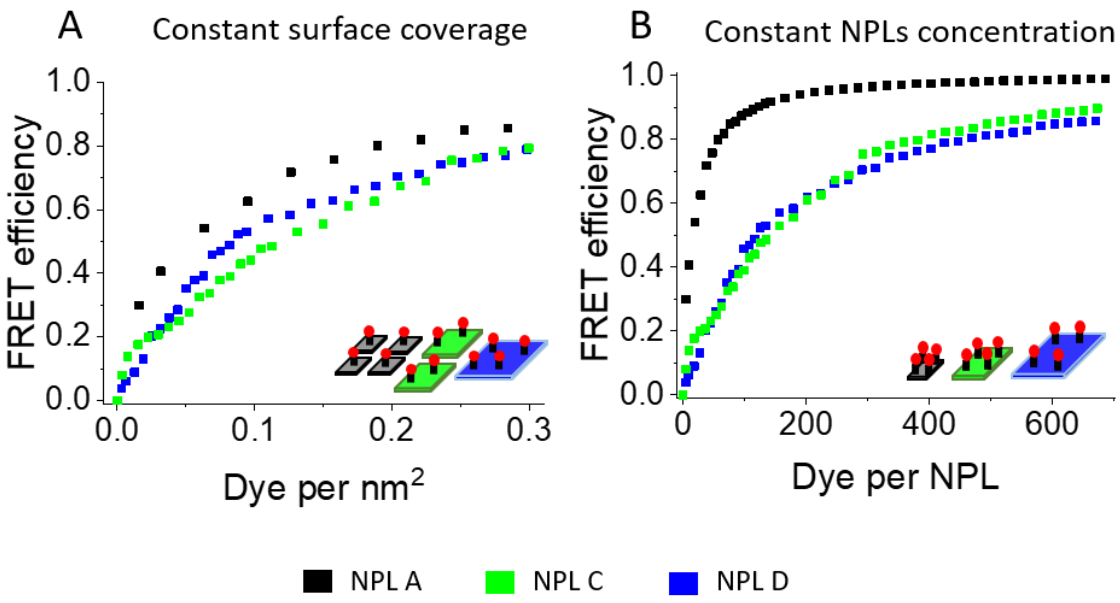

Figure 40: Energy transfer efficiency using the decrease of the NPLs photoluminescence at 462 nm. Data show the average of the experiments for each NPL. (A) Energy transfer rate plotted against the surface packing rate. The used method (constant surface) is integrated in the figure as scheme. (B) Energy transfer rate plotted against the number of dye molecules per NPL. The used method (constant concentration) is integrated in the figure as scheme.

The experiments show that the relation of the FRET efficiency is consistent for each NPL throughout the different experiments (details see Figure 46 in the appendix). Therefore in Figure 40 the average data for each NPL is shown.

It is visible that in case of constant surface (Figure 40 A) the relation of FRET efficiency versus surface coverage is consistent for the different sized NPLs. Only for the smallest NPL A (black), the values appear to be a little higher than for the other two samples, likely due to the higher QY.

In Figure 40 B (constant concentration of NPLs) the FRET efficiency is plotted against the amount of dye per NPL. Here, a clear difference between the different NPLs is found. For the smallest NPLs (NPL A, black) the energy transfer increases significantly faster than for the larger NPLs (NPL C and NPL D, green and blue respectively) and reaches higher final values in comparison to the larger NPLs. The explanation of this behaviour can be found by looking at the size of the Förster radius of the dye and the size of the exciton. An exciton in NPLs has typically a radius of 1 to 1.5 nm in NPLs[13]. This means, that if an exciton is generated, it is strongly localised. For FRET it is necessary that an acceptor molecule is in close proximity to transfer the energy non-radiatively via dipole-dipole interactions. Because of the relatively high degree of localisation of the exciton, the dye coverage on the NPL surface determines the average distance between the two dipoles. Thus, the dye coverage directly influences the FRET efficiency. If the size of the NPLs gets larger, more dyes per NPL are needed in order to achieve

the same coverage and the same probability for FRET. The data agree with this hypothesis, since the energy transfer behaviour gets worse when using larger NPLs.

Energy transfer efficiency using lifetime of the NPLs

To calculate the energy transfer efficiency, the lifetime of the NPLs can also be used. A double exponential function was necessary for a good fit and as a result, two values for the lifetimes are obtained. For the calculation of FRET efficiency, the weighted average was used, calculated with the following equation:

$$< \tau > = \frac{A_1 \tau_1}{A_1} + \frac{A_2 \tau_2}{A_2} \tag{11}$$

To calculate the FRET efficiency from the weighted lifetimes, the following equation was used:

$$\text{FRET efficiency} = 1 - \frac{< \tau >_{\text{with dye}}}{< \tau >_{\text{without dye}}} \tag{12}$$

The results of the FRET efficiency are plotted against the amount of dye per nm^2 and against the amount of dye per NPL. Because of the consistence of the data, in Figure 41 only the data from Exp. con. 2 are shown. For all experiments see Figure 47 in the appendix.

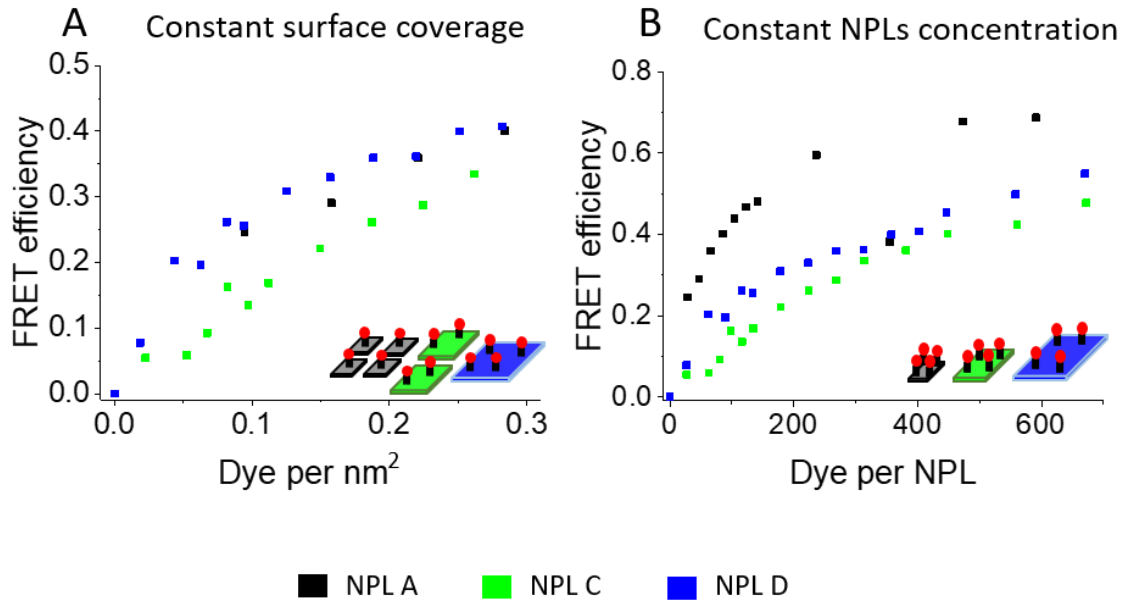

Figure 41: Energy transfer efficiency of Exp. con. 2 using the decrease of the amplitude weight NPLs lifetime, which was measured at 462 nm. (A) FRET efficiency plotted against number of dye/nm² and (B) against the number of dye / NPL.

From Figure 41 it results that the FRET efficiencies calculated from the lifetime of the NPLs increase with increasing the dye amount. The calculated maximum efficiencies in Figure 41 are lower than in Figure 40. For example, the maximum value for NPL A in Figure 40 B is close to 1, determined with the decrease of the photoluminescence at 462 nm, and in Figure 41 B it is only 0.7, determined with the decrease of the lifetime at 462 nm. This trend can be observed for all differently sized NPLs and all experiments (see Figure 46 and Figure 47 in the appendix).

Like in Figure 40, the FRET efficiency was plotted against constant surface coverage (Figure 41 A) and against the amount of dye per NPL (Figure 41 B). At the same surface coverage the FRET efficiency was found as not dependent on the size of NPLs (Figure 41 A). All NPLs show similar slopes and FRET

efficiencies. This results disagree with the results of Figure 40 A, where NPL A has the highest efficiency (see black squares in Figure 40 A).

If the FRET efficiency is plotted against the dye per NPL value, as shown in Figure 41 B, it is observable, that NPL A has the highest FRET efficiency for a constant amount of dye per NPLs. This agrees with the observation in Figure 40 B, where also NPL A has the highest FRET efficiency. So, it is again confirmed, that small NPLs have the highest energy transfer efficiency, if the number of dye molecules per NPL is constant.

Overall, the smaller NPLs lead to higher energy transfer efficiencies. This confirms the hypothesis that for efficient energy transfer from NPLs to dyes on the surface of the NPLs, the distance between the excitons of the NPLs and the dyes should be minimized, as predicted in Förster theory. Because the size of the exciton is small (1.5 nm[13]), less dye per NPL is required for smaller NPLs to have a dye near to that exciton. Having a small number of dyes per NPL reduces the probability of self-quenching between the dye molecules bound on the surface of the NPLs. The self-quenching was found to occur at surface coverage greater than 0.2 dyes/nm^2.

5. Comparison and Outlook

As shown in chapter 4.1., it is possible to synthesise size extended three ML NPLs with a high QY and a narrow size distribution. To achieve this, a seeded growth method was used. The three ML NPLs seeds were synthesised at low temperatures with bis(stearoyl)selenide. The synthesised NPLs have a narrow lateral size distribution and the desired optical properties, with a quantum yield around 50%.

The three ML NPLs were used in a second step to extend the size of the NPLs while maintaining the optical properties of the NPLs as much as possible. A less reactive selenium precursor Se-ODE was used to prevent further nucleation of new particles. The reaction temperature of the size extension was optimised to 190 °C. This is the ideal temperature to get the largest size extension under maintaining the sharp edges of the NPLs and minimizing the amount of trap states. Lower temperatures lead to smaller size extension and fraying, while higher temperatures lead to nucleation of new particles and destruction of the seeds. With this method, four stock solutions of differently sized three ML NPLs are prepared and characterised.

With the differently sized NPLs, FRET studies were conducted by adding different amounts of photocatalyst dye to the NPL dispersions. Form the kinetic measurements, it was shown that all the dyes added are binding to the NPLs surface. It was possible to systematically asses FRET by monitoring the changes in the photoluminescence and lifetime of NPLs.

Clear differences between the different sized NPLs in the energy transfer behaviour were found. Using a constant amount of dye per NPL, FRET is most effectively for the smallest NPLs because of the lowest average distance between the dyes and the excitons. For the energy transfer it is crucial to have a low distance between exciton and dye. The larger absorption cross section of larger NPLs doesn't compensate the higher distance between exciton and dye. Therefore, we conclude that the energy transfer efficiency depends mainly on the lateral size of the NPLs.

Beside this, it was found, that increasing the amount of dye on the surface of the NPLs lead to a maximum in the photoluminescence of the dye. At a surface coverage higher than 0.2 dye per nm^2 self-quenching between the dye molecules is favoured against the luminescence of the dye.

However, the differences between the lifetime and the photoluminescence of the dye was against the expectations of the experiments. This might be a result of the different influences of energy transfer and quenching to the lifetime and the photoluminescence. To get a better understanding of this phenomenon, further research is necessary.

The results of this study can be used to increase the efficiency of an organic photocatalyst. For the dye used in this study, catalytic activity was shown for a CH-functionalisation of election rich aromatic systems[12]. In further experiments it can be checked whether using a NPL-dye composite leads to a higher reaction rate or whether the same rate can be achieved by using less organic photocatalyst and more NPLs just as a sensitizer.

To improve the performance of the current system, improvements in the NPLs synthesis to obtain NPLs with higher QY and less trap states would be beneficial. Less trap states may be achieved by extending the reaction time of the NPLs and by lowering the speed of addition of the selenium precursor. Beside this, core-shell particles can used instead of the pure CdSe-NPLs to further decrease the number of trap states. In the future, different photocatalysts can also be studied to confirm these results and to increase their efficiency. One fundamental bottleneck is the self-quenching of dye molecules when they are bound at high concentrations on NPL surfaces. Future designs must consider this limitation and find ways to prevent the dye molecules from binding too close to each other on the surface of NPLs.

6. Appendix

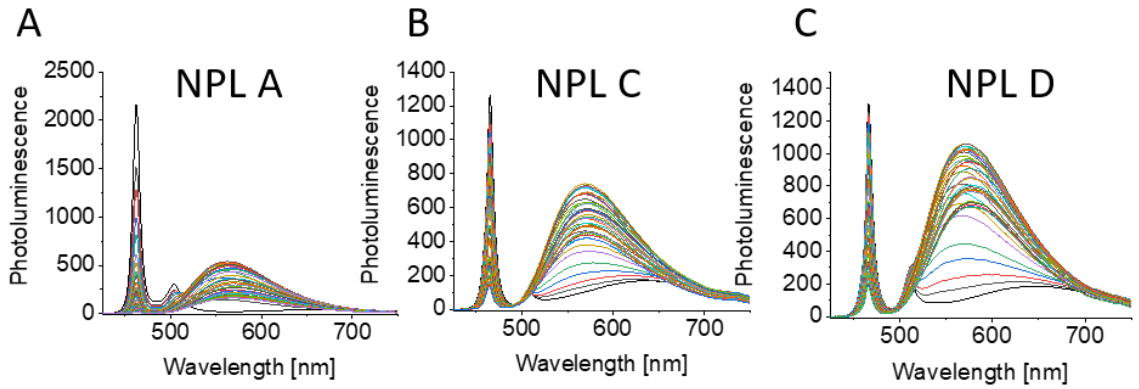

Figure 42: Photoluminescence spectra for the different amounts of dye from Exp. con. 2. Photoluminescence spectra for (A) NPL A, (B) NPL C, (C) NPL D.

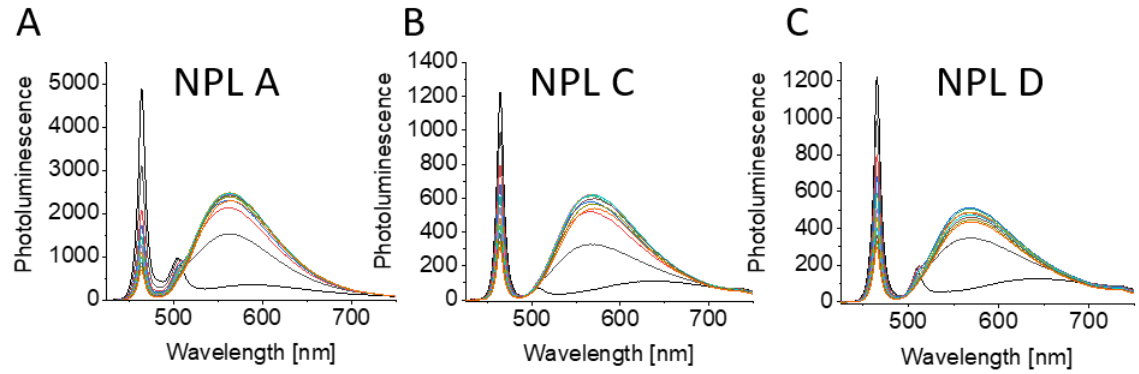

Figure 43: Photoluminescence spectra for the different amounts of dye from Exp. abs. Photoluminescence spectra for (A) NPL A, (B) NPL C, (C) NPL D.

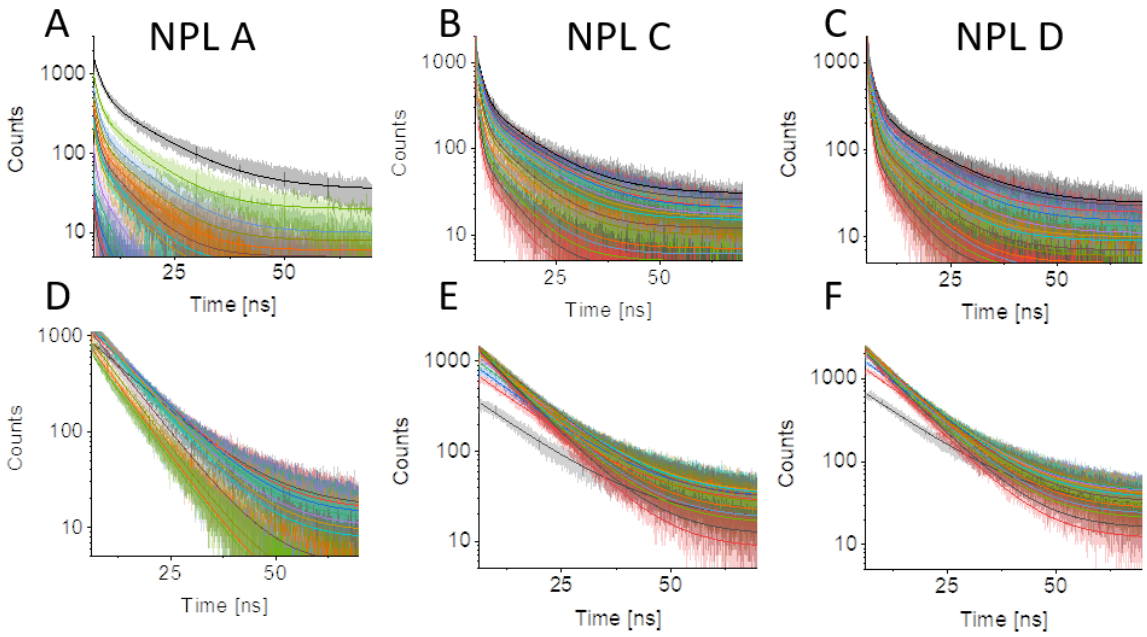

Figure 44: Results of the lifetime measurements of Exp. con. 2. Transparent line is the original data, solid line is the fit. (A) Lifetime of the NPLs using NPL A at 462 nm. (B) Lifetime of the NPLs using NPL C at 462 nm. (C) Lifetime of the NPLs using NPL D at 462 nm. (D) Lifetime of the dye using NPL A at 565 nm. (E) Lifetime of the dye using NPL C at 565 nm. (F) Lifetime of the dye using NPL D at 565 nm.

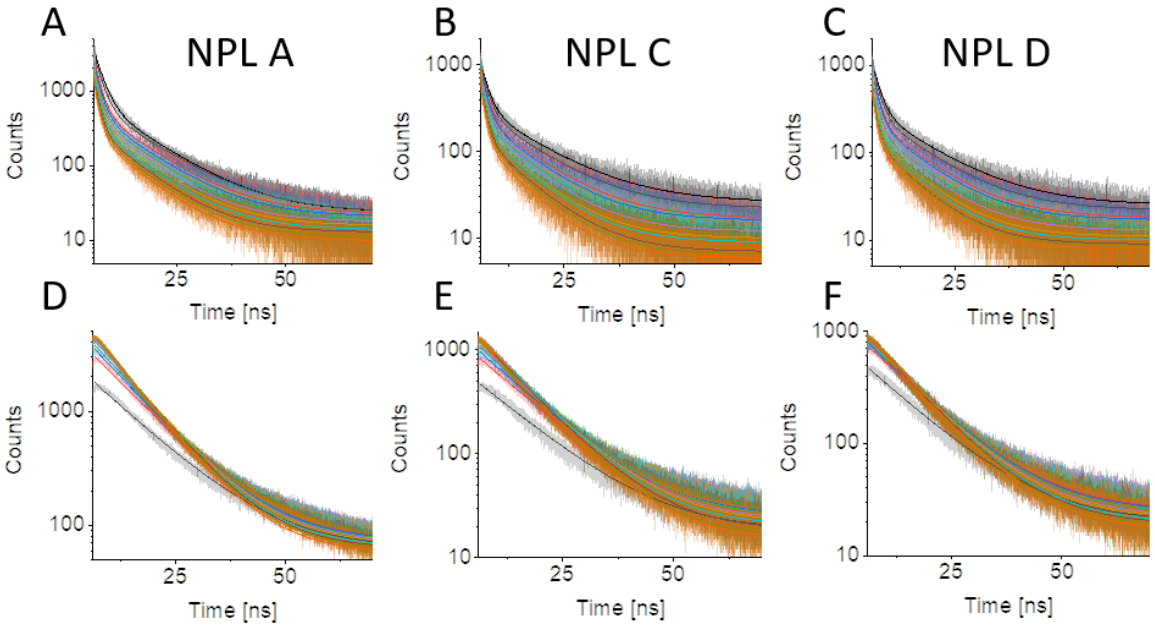

Figure 45: Results of the lifetime measurements of Exp. abs. Transparent line is the original data, solid line is the fit. (A) Lifetime of the NPLs using NPL A at 462 nm. (B) Lifetime of the NPLs using NPL C at 462 nm. (C) Lifetime of the NPLs using NPL D at 462 nm. (D) Lifetime of the dye using NPL A at 565 nm. (E) Lifetime of the dye using NPL C at 565 nm. (F) Lifetime of the dye using NPL D at 565 nm.

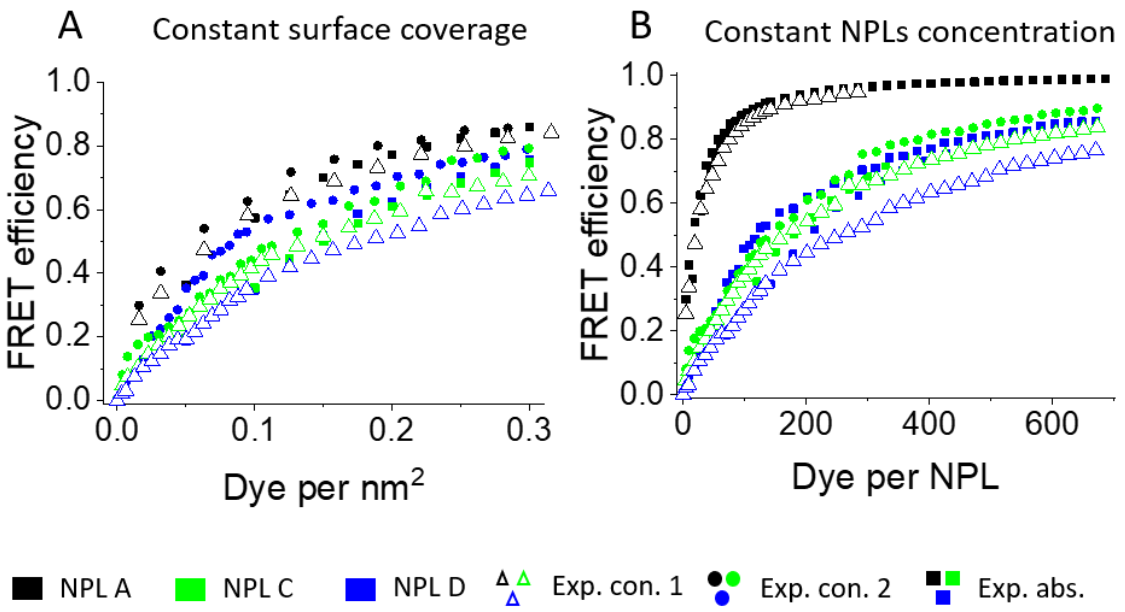

Figure 46: Energy transfer efficiency using the decrease of the NPLs photoluminescence at 462 nm. Triangles present experiment Exp. con. 1, circles present experiment Exp. con. 2 and squares present experiment Exp. abs. (A) Energy transfer rate plotted against the surface packing rate and (B) against the number of dye molecules per NPL.

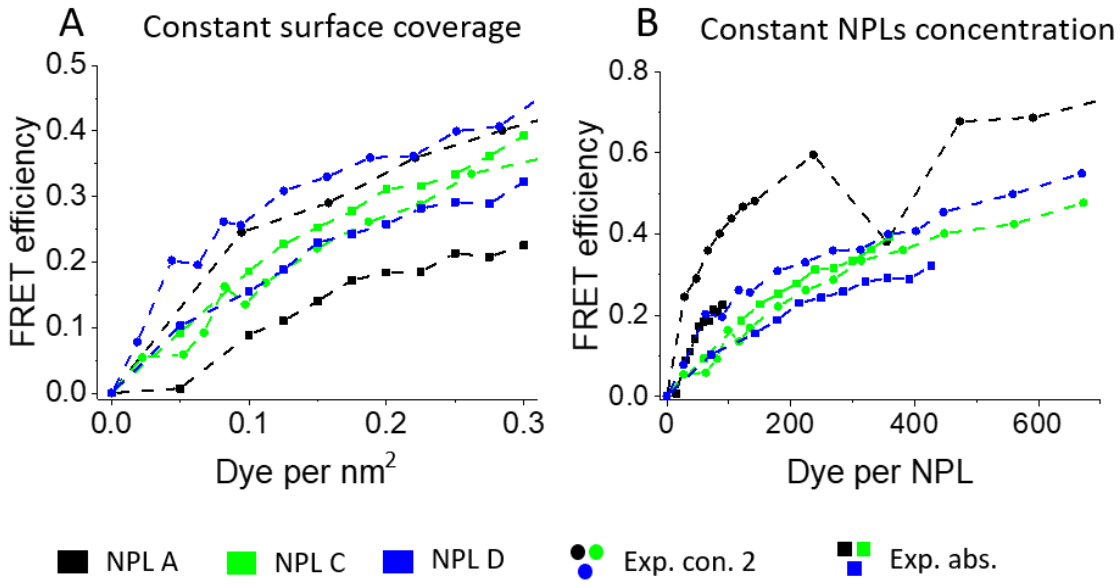

Figure 47: Energy transfer efficiency using the decrease of the amplitude weight NPLs Lifetime, which was measured at 462 nm. Circles present experiment Exp. con 2. and squares present experiment Exp. abs. The dotted line is only a guide for the eyes. (A) FRET efficiency plotted against number of dye/nm² and (B) against the number of dye / NPL

7. Acknowledgements

I would like to thank Prof. Dr. Katharina Landfester for giving me the opportunity to do my experimental work and write my thesis in her department.

In addition, I would like to thank Dr. Andreas Riedinger for helping me with this project, his excellent supervision and his detailed knowledge about nanoplatelets and energy transfer.

Besides, I am thankful for the support of Henry Halim. He taught me the synthesis of the nanoplatelets and helped me a lot with my practical work. I really appreciated the discussions with him that helped me to reach the completion of this thesis.

I also express my thanks to Rebecca Momper and the whole group of Dr. Riedinger for the good working atmosphere in the lab and the fruitful discussions for this project.

A special thank goes to Niklas Huber, who synthesised and provided the dye, Angelika Mannhart who synthesised the bis(steaoryl)selenide, Paul Kolpakov who synthesised the cadmium myristate and Dr. Maria Martinez Negro who did the ITC experiments.

Furthermore, I thank the whole department of physical chemistry of polymers for all their advice and the warm welcome.

At the end, I would like to thank my family and friends for their support during my studies, especially during the time preparing this thesis.

8. References

[1] V. Parmon, A. V. Emeline, N. Serpone, *International Journal of Photoenergy* **2002**, *4*, 91 - 131.
[2] N. V. Tkachenko, *Optical Spectroscopy*, Elsevier, **2006**.
[3] I. Sandrine, D. Benoit, *Journal of the American Chemical Society* **2008**, 16504 - 16505.
[4] A. Yeltik, S. Delikanli, M. Olutas, Y. Kelestemur, B. Guzelturk, H. V. Demir, *The Journal of Physical Chemistry C* **2015**, *119*, 26768-26775.
[5] C. A. Laetherdale, W.-K. Woo, F. V. Mikulec, M. G. Bawendi, *The Journal of Physical Chemistry B* **2002**, *106*, 7619 - 7622.
[6] T. Ren, P. K. Mandal, W. Erker, Z. Liu, Y. Avlasevich, L. Puhl, K. Müllen, T. Basché, *Journal of the American Chemical Society* **2008**, *130*, 17242 - 17243.
[7] C. Xia, W. Wang, L. Du, F. T. Rabouw, D. J. van den Heuvel, H. C. Gerritsen, H. Mattoussi, C. de Mello Donega, *The Journal of Physical Chemistry C* **2019**, *124*, 1717-1731.
[8] M. Stanisavljevic, S. Krizkova, M. Vaculovicova, R. Kizek, V. Adam, *Biosensensors and Bioelectronics* **2015**, *74*, 562-574.
[9] B. T. Diroll, I. Fedin, P. Darancet, D. V. Talapin, R. D. Schaller, *Journal of the American Chemical Society* **2016**, *138*, 11109-11112.
[10] T. Foerster, *Annalen der Physik* **1948**, *437*, 55 - 75.
[11] M. Olutas, B. Guzelturk, Y. Kelestemur, A. Yeltik, S. Delikanli, H. V. Demir, *ACS Nano* **2015**, *9*, 5041-5050.
[12] L. Wang, W. Huang, R. Li, D. Gehrig, P. W. M. Blom, K. Landfester, K. A. I. Zhang, *Angewandte Chemie* **2016**, *128*, 9935-9940.
[13] A. Brumberg, S. M. Harvey, J. P. Philbin, B. T. Diroll, B. Lee, S. A. Crooker, M. R. Wasielewski, E. Rabani, R. D. Schaller, *ACS Nano* **2019**, *13*, 8589-8596.
[14] H. de Waard, H. W. Frijlink, W. L. Hinrichs, *Pharmaceutical Research* **2011**, *28*, 1220-1223.
[15] V. K. La Mer, *Industrial and Enginering Chemistry* **1952**, *44*, 1270 - 1277.
[16] T. Sugimoto, *Journal of Colloid and Interface Science* **2007**, *309*, 106-118.
[17] S. G. Kwon, T. Hyeon, *Small* **2011**, *7*, 2685-2702.
[18] N. T. Thanh, N. Maclean, S. Mahiddine, *Chemical Reviews* **2014**, *114*, 7610-7630.
[19] A. Riedinger, A. S. Mule, P. N. Knusel, F. D. Ott, A. A. Rossinelli, D. J. Norris, *Chemical Communications* **2018**, *54*, 11789-11792.
[20] L. Scarabelli, A. Sanchez-Iglesias, J. Perez-Juste, L. M. Liz-Marzan, *The Journal of Physical Chemistry Letters* **2015**, *6*, 4270-4279.
[21] V. I. Klimov, *Semiconductor and metal nanocrystals synthesis and electronic and optical properties*, Marcel Dekker, **2004**.
[22] A. Riedinger, F. D. Ott, A. Mule, S. Mazzotti, P. N. Knusel, S. J. P. Kress, F. Prins, S. C. Erwin, D. J. Norris, *Nature Materials* **2017**, *16*, 743-748.
[23] N. Blachnik, *CdSe Nanokristalle*, Universität Mainz, **2015**.
[24] H. Halim, **2018**, talk, CdSe Nanoplatelets for Triplet - Triplet Annihilation Upconversion
[25] P. A. Cox, *Structure and bonding*, Oxford University Press, **1987**.
[26] S. Ithurria, G. Bousquet, B. Dubertret, *Journal of the American Chemical Society* **2011**, *133*, 3070-3077.
[27] Y. H. Liu, V. L. Wayman, P. C. Gibbons, R. A. Loomis, W. E. Buhro, *Nano Letters* **2010**, *10*, 352-357.
[28] S. Ithurria, M. D. Tessier, B. Mahler, R. P. Lobo, B. Dubertret, A. L. Efros, *Nature Materials* **2011**, *10*, 936-941.
[29] S. Jana, T. N. Phan, C. Bouet, M. D. Tessier, P. Davidson, B. Dubertret, B. Abecassis, *Langmuir* **2015**, *31*, 10532-10539.
[30] B. Guzelturk, O. Erdem, M. Olutas, Y. Kelestemur, H. V. Demir, *ACS Nano* **2014**, *8*, 12524 - 12533.
[31] A. M. Mooney, **2012**, URL: https://commons.wikimedia.org/wiki/File:FRET_Jablonski_diagram.svg
[32] T. W. J. Gadella, *Fret and Flim Techniques*, Elsevier Science, **2009**.

[33] M. Khrenova, I. Topol, J. Collins, A. Nemukhin, *Biophysical Journal* **2015**, *108*, 126-132.
[34] P. W. Atkins, J. d. Paula, *Physikalische Chemie, Vol. 5*, Wiley-VCH, **2013**.
[35] G. Hinze, *Zeitaufgeloeste Fluoreszenzmessung*, Universität Mainz, **2018**.
[36] C. Bouet, B. Mahler, B. Nadal, B. Abecassis, M. D. Tessier, S. Ithurria, X. Xu, B. Dubertret, *Chemistry of Materials* **2013**, *25*, 639-645.
[37] M. D. Tessier, P. Spinicelli, D. Dupont, G. Patriarche, S. Ithurria, B. Dubertret, *Nano Letters* **2014**, *14*, 207-213.
[38] S. Yadav, A. Singh, L. Thulasidharan, S. Sapra, *The Journal of Physical Chemistry C* **2017**, *122*, 820-829.
[39] C. She, I. Fedin, D. S. Dolzhinikov, P. D. Dahlber, G. S. Engel, R. D. Schaller, D. V. Talapin, *ACS Nano* **2015**, *9*, 9475 - 9485.
[40] E. Lhuilier, S. Pedetti, S. Ithurria, H. Heuclin, B. Nadal, A. Robin, G. Patriarche, N. Lequeux, B. Dubertret, *ACS Nano* **2014**, *8*, 3813 - 3820.
[41] A. M. Brouwer, *Pure and Applied Chemistry* **2011**, *83*, 2213-2228.
[42] E. M. Conroy, J. J. Li, H. Kim, W. R. Algar, *The Journal of Physical Chemistry C* **2016**, *120*, 17817-17828.
[43] M. Ghosh, S. Nath, A. Hajra, S. Sinha, *Journal of Luminescence* **2013**, *141*, 87-92.
[44] H. Halim, **2019**, talk, Photocatalyst - long report

Selbstständigkeitserklärung

Ich, David Trieb, Matrikelnummer 2706704, versichere, dass ich meine Masterarbeit selbstständig verfasst und keine anderen als die angegebenen schriftlichen und elektronischen Quellen sowie andere Hilfsmittel benutzt habe. Alle Ausführungen, die anderen Schriften wörtlich oder sinngemäß entnommen wurden, habe ich kenntlich gemacht.

Mainz, den 17.02.2020